uOttawa

L'Université canadienne
Canada's university

FACULTÉ DES ÉTUDES SUPÉRIEURES ET POSTOCTORALES

uOttawa

L'Université canadienne
Canada's university

FACULTY OF GRADUATE AND POSDOCTORAL STUDIES

Genille M. Gimbel
AUTEUR DE LA THÈSE / AUTHOR OF THESIS

M.A.Sc. (Human Kinetics)
GRADE / DEGREE

Department of Human Kinetics
FACULTÉ, ÉCOLE, DÉPARTEMENT / FACULTY, SCHOOL, DEPARTMENT

Characterization of the impact mechanics of polymeric foams subjected to quasi-static and dynamic compressive loading of various impact energies

TITRE DE LA THÈSE / TITLE OF THESIS

Blaine Hoshizaki
DIRECTEUR (DIRECTRICE) DE LA THÈSE / THESIS SUPERVISOR

CO-DIRECTEUR (CO-DIRECTRICE) DE LA THÈSE / THESIS CO-SUPERVISOR

EXAMINATEURS (EXAMINATRICES) DE LA THÈSE / THESIS EXAMINERS

Gordon Robertson

Yves Lajoie

Gary W. Slater
Le Doyen de la Faculté des études supérieures et postdoctorales / Dean of the Faculty of Graduate and Postdoctoral Studies

Characterization of the impact mechanics of polymeric foams subjected to quasi-static and dynamic compressive loading of various impact energies

Genille M. Gimbel

Thesis submitted to the
Faculty of Graduate and Postdoctoral Studies
in partial fulfillment of the requirements for the MSc degree in Biophysical Sciences

School of Human Kinetics
Faculty of Health Science
University of Ottawa

Your file Votre référence
ISBN: 978-0-494-50882-4
Our file Notre référence
ISBN: 978-0-494-50882-4

ABSTRACT

Impact mass and inbound velocity are important parameters defined in helmet standards, which represent the total energy transferred during a hit to the head. The purpose of this study was to determine the influence that impact mass and inbound velocity had on energy attenuation characteristics of polymeric materials used in helmet design. Materials consisted of three densities of expanded polystyrene, expanded polypropylene, and vinyl nitrile foam. Each sample was impacted once at 25 different levels of energy using a monorail drop test. Significant main effects were observed for impact mass, inbound velocity, and material density on peak linear acceleration and impulse ($p<0.05$). Using peak linear accelerations as the determinant for risk of injury, head mass and inbound velocity played a significant role in helmet material performance.

ACKNOWLEDGMENTS

I would like to take this opportunity to thank my research supervisor, Dr. Thomas Blaine Hoshizaki for his guidance and sound advice. His enthusiasm and passion for research has been an inspiration and I am truly grateful to have had the opportunity to work beside him. As well, a sincere thank you goes to my colleagues, Philippe Rousseau, Leslie Lamb, and Natalie Coulson for their support, advice, and positive moral. As well, thank you to our research coordinator, Andrew Post, for his assistance and guidance.

I would also like to thank Dr. Gordon Robertson, my committee member, for his feedback and help during the analysis part of my study. As well, thank you to Dr. Yves Lajoie, for being my committee member and providing me with feedback. I would also like to extend my gratitude's to Andre Noel, product engineer at Polymos Inc for donating the materials necessary to conduct this study. Thank you to Joe Lenny for also donating materials used in this study and to Xenith Inc. for in part supporting the Neurotrauma Impact Science Lab.

TABLE OF CONTENTS

LIST OF FIGURES

LIST OF TABLES

CHAPTER 1. INTRODUCTION

1.1 PROBLEM STATEMENT

Safety standards which govern helmet design have changed marginally throughout the last two decades despite the significant advancements in scientific research regarding brain injury mechanisms (Hoshizaki & Brien, 2004). Helmet standards make a quantifiable judgment regarding the protection capabilities of a helmet and may be jeopardizing the safety of young children by ignoring critical physiological and biomechanical distinctions between children and adults. This study investigated the biomechanical differences between children and adults that influence the risk of head injury. For example, children's helmets are presently tested using an adult-weighted headform of around five kilograms and are impacted using velocities representative of adult anatomy (Becker, 1998). Thus, the overall momentum (mass times velocity) reproduced in standard testing is exaggerated while testing children's helmets, which may diminish their protective abilities and place children at an increased risk of injury. Research involving the effects of impact mass and inbound velocity on the energy attenuation of helmet materials is needed to improve the impact protection capabilities of children helmets.

1.2 OVERVIEW

Sports related head and neck injuries are responsible for some of the most catastrophic athletic injuries seen. In 2003-2004, sports and recreational activities were the third leading cause of traumatic head injury admissions in Canadian hospitals. In particular, twenty-eight percent of all children admitted in the emergency ward for traumatic head injuries were due to such activities (Canadian Institute for Health Information, 2006). The outcome of these head injuries can be devastating, often leading to significant lifelong physical, social, emotional, and economical consequences. Avoidance, education, and protective head gear are the best intervention strategies for preventing or minimizing these sport-related head injuries (McIntosh, McCrory, & Finch, 2006).

An impact to the head is characterized by a sudden onset of high forces over a short duration (Barth, Freeman, Broshek, et al., 2001). High forces acting upon the head result in head injuries, where the severity of injury is directly related to the magnitude of the impacting force (Newman, 2006). The intracranial response to a head impact varies according to the overall size (mass and geometry) of the human head. It has been demonstrated that maximal effective stress, maximal shear stress, and frontal and occipital pressures in the brain increase significantly with increasing head size, given the same acceleration pulse (Kleiven & Holst, 2002). The relationship between force, acceleration, and mass is best explained using Newton's Second Law of Motion, where resultant force is the product of mass and acceleration ($\Sigma F = m \times a$). Given the same impacting force a smaller head mass would result in greater accelerations being transmitted to the brain, thus a greater chance of serious injury (Newman, 2006).

Nearly all helmet standards implement a quantifiable pass/fail criteria based on peak linear acceleration (g), where acceleration is measured from a simulated helmeted head impact and is used to define injury thresholds (Goldsmith & Plunkett, 2004). Acceleration is expressed in gravitational units (g), where one g is equal to the acceleration of gravity, 9.81 meters per second squared (m/s^2) (CAN/CSA-D113.2-M89). The goal of the helmet is to distribute and dissipate the impact forces below the injury threshold, thereby minimizing the kinetic energy or acceleration transmitted through to the head (Avalle, Belingardi, & Montanini, 2001). Unfortunately, these tolerance levels are generally set between 250 and 300 g's for all individuals, regardless of age, weight, or sex (Goldsmith & Plunkett, 2004). Children's brains have a lower degree of calcification and greater water content; therefore, kinetic energy is more easily transferred from an impact to the brain placing children at an increased risk of injury (Avalle et al., 2001; Stevenson, 1998). Subsequently, injury threshold limits as low as 150 g's or lower have been suggested to be more appropriate for children (Becker, 2000).

In addition to unreasonably high threshold limits, many helmet standards test a child's helmet by strapping it to a five kilogram (kg) headform mass and dropping it from a predefined inbound velocity, where the parameters have been defined based on the average mass and falling momentum (mass × velocity) of an adult head during impacts (Becker, 1998). The head mass of children under the age of five years; however, ranges from approximately 2.8 to 3.9 kg (Heh & Stadnik, 1997). Newton's first law, the Law of Inertia states that a body's momentum is the product of its mass and linear velocity ($p = mv$), which indicates that a lower body mass and inbound velocity would significantly decrease the body's resistance to change momentum (Gordon. Dooley, & Wood, 2006).

Foams incorporated in helmets function within a prescribed energy range, where an inbound momentum that is too low or too high can cause the material to fail. For example, if the liner density is too low for a given impact energy the material compresses too quickly and fails, whereas if the density is too high, the material fails to compress and absorb energy causing the forces to exceed the critical head injury threshold (Avalle et al., 2001). If helmet standards used a headform weight that better represent a young child's head and reduced the allowable peak g's, helmets may need to be designed with a lower density liner to lessen the impact forces transmitted to the head (Heh & Stadnik, 1997; Stevenson, 1998). The effect of impact momentum on energy transfer evidently plays a significant role in the risk of injury (Newman, Beusenberg, Shewchenko, et al., 2004) and protective materials need to be designed with this in mind (Martin, Liptai, Yerby, et al., 1994).

Overall, it is the helmet properties, the mass of the human head, and the impact momentum which determines the level of energy transmitted to the brain during impact (Becker, 1998). Enhancing ones understanding of these factors will help improve the design of helmets and level of head protection offered to children.

1.3 OBJECTIVES

1. To determine the effects of impact mass on the energy attenuation mechanics (peak linear acceleration and impulse) across material densities for expanded polystyrene, expanded polypropylene, and vinyl nitrile.
2. To determine the effects of inbound velocity on the energy attenuation mechanics (peak linear acceleration and impulse) of expanded polystyrene, expanded polypropylene, and vinyl nitrile.
3. To determine the effects of material density on the energy attenuation mechanics (peak linear acceleration and impulse) of expanded polystyrene, expanded polypropylene, and vinyl nitrile.

1.4 EXPERIMENTAL HYPOTHESES

1. Changes in impact mass will have a significant effect on peak linear acceleration.
2. Changes in impact mass will have a significant effect on impulse.
3. Changes in inbound velocity will have a significant effect on peak linear acceleration.
4. Changes in inbound velocity will have a significant effect on impulse.
5. Changes in material density will have a significant effect on peak linear acceleration.
6. Changes in material density will have a significant effect on impulse.

1.5 INDEPENDENT VARIABLES

1. Impact mass (kg): 3.59 kg, 4.09 kg, 4.59 kg, 5.09 kg, and 5.59 kg
2. Inbound velocity (m/s): 1.0 m/s, 1.5 m/s, 2.0 m/s, 2.5 m/s, and 3.0 m/s for vinyl nitrile; 1.0 m/s, 2.0 m/s, 3.0 m/s, 4.0 m/s, and 5.0 m/s for expanded polystyrene and expanded poly propylene.
3. Material density (kg/m^3): Expanded polystyrene (EPS) 62.95, 83.46, and 100.12 kg/m^3;

   Expanded polypropylene (EPP) 44.53, 83.94, 117.09 kg/m^3;

   Vinyl nitrile (VN) 602, 600, and 740; equivalent to 97.32, 111.62, and 127.17 kg/m^3, respectively.

1.6 DEPENDENT VARIABLES

1. Peak linear acceleration (measured in g's)
2. Impulse (measured in Newton seconds (N·s))

1.7 SIGNIFICANCE

Considering helmet liners as the primary shock absorbing component of the helmet (Mills & Gilchrist, 1991), understanding the energy absorption capabilities of these open and closed cell foams will allow better understanding of the performance of helmets for different head masses and impact energies. Since foam materials function within a prescribed energy range, it is presumed that child helmet liners could be improved significantly if appropriate testing parameters were considered in their design. If the above hypotheses are proven significant, than conclusions may be made that helmet standards need to modify their testing procedures to use more fitting parameters to function within the range of impact energies for the intended age group. Helmets can thus be designed more suitably for the unique requirements of children and adults, which will ultimately decrease the risk of brain injuries during impacts to the head and reduce the amount of sport-related concussions and brain injuries world-wide.

1.8 LIMITATIONS

All foam samples were not moulded into their test sizes due to product availability limitations. When the foam samples were drilled from the manufactured sheets, it may interfere with the foam cell properties at their outer edges/walls and influence their impact performance.

1.9 DELIMITATIONS

The headform composition was kept constant throughout all dynamic impact tests. In reality, the composition of ones brain changes significantly from birth until adulthood; however, the headforms used for this study are in accordance to the BS EN 960:1995 standard for testing headforms, which has been adopted by many international helmet testing standards (ISO TC 83/SC 5N, 2006). The headforms were not biofidelic and thus, conclusions regarding the internal forces within biological tissues were not possible.

The dimensions of the sample significantly affect the energy absorption mechanics of the material. The thickness of 2.54 cm was kept constant throughout the study, as well as the diameter of 5 cm. This diameter was chosen because larger diameters were not compressing before exceeding the force thresholds of the equipment. Thus, conclusions made from this study were in reference to these dimensions only.

In addition, all impacts were in the crown position. Different impact positions have different geometrical shapes, which varies the impact footprints and subsequently the results. Thus, all results were in reference to the crown position only.

1.10 ASSUMPTIONS

1. Polymeric foam plasticity initiated at the beginning of the stress plateau (Zhang, Kikuchi, Yees, & Nusholtz, 1998).
2. The 0.2% offset was the most appropriate value for approximating compressive yield.
3. The impact drop mass and force plate acted as a completely rigid body.
4. The internal properties of each foam sample (ie. air cells, cell walls) were evenly distributed throughout each material.

CHAPTER 2. REVIEW OF LITERATURE

2.1 HELMETS AND HEAD PROTECTION

The overall goal of a helmet is to manage the severity of an impact and limit the shock transmitted through the helmet to the head (Becker, 1998). Helmets reduce the deceleration of the skull during collisions to help minimize the movement of the brain. This is primarily done through the management of the impact by crushing the soft material (foam liner) incorporated inside the helmet (Becker, 1998; Mills & Gilchrist, 2003). For helmets to function effectively, the head must slow to a complete stop before the material/liner inside the helmet has been crushed to its minimum thickness. Generally, low density polymeric foams are used as they have "excellent impact energy absorbing capabilities" (Zhang et al., 1998, p. 370). Helmets function by spreading the impact forces over a larger area and preventing direct contact between the skull and the impacting object, which protects against abrasions (Camacho, Nightingale, & Myers, 2001; Hui & Yu, 2002; Ivarsson, Viano, Lövsund et al., 2003; Towner, Dowswell, Burkes et al., 2006). As well, helmets aid in increasing the impact duration time, thereby decreasing the peak force transmitted to the head (Hch & Stadnik, 1997).

Helmets generally consist of an outer shell, inner liner, comfort padding/foam, and a chin strap (Liu, Chang, Chin-Ming et al., 2003). Hockey helmets, shown in figure 1(a), consist of a tough plastic outer shell that can withstand severe impacts at low temperatures. They are built with a polypropylene or vinyl nitrile foam liner for absorbing and distributing shock and a nylon chin strap that holds the helmet securely to the head. Football helmets, shown in figure 1(b), are built much the same way as hockey helmets; with a tough thermoplastic shell and polymer (vinyl nitrile) foam lining. For hockey and football helmets, a faceguard is attached to the shell and a chinstrap which holds the helmet to the head

(Newman et al., 2004). Bicycle helmets, shown in figure 1(c) are designed with an approximately 0.3 mm thick microshell, which plays minimal roles in attenuating energy upon impacts and also consist of a polymer lining (expanded polystyrene foam), comfort padding, and a chip strap (Hui & Yu, 2002).

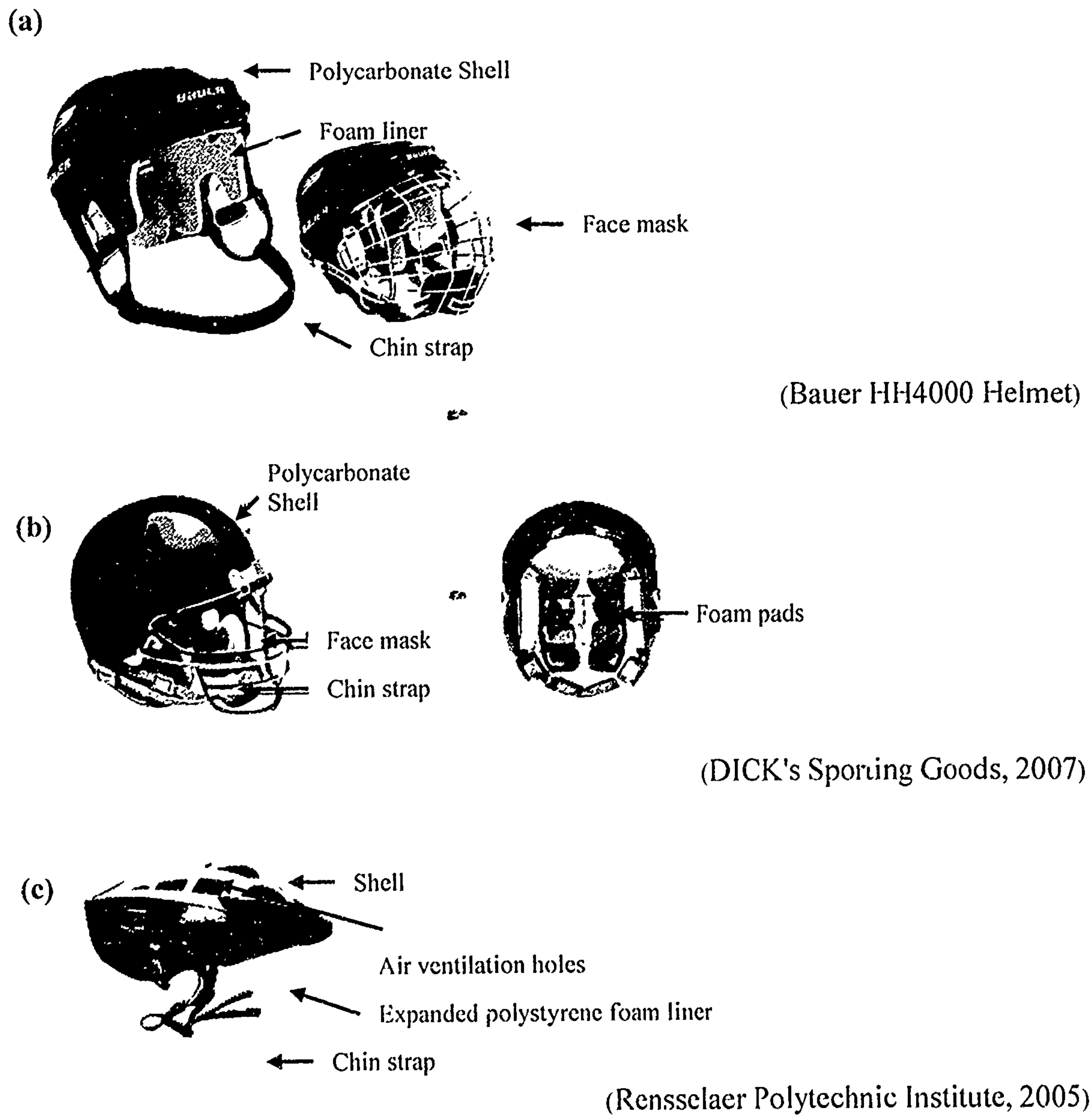

Figure 1 Main features of an ice hockey helmet (a), football helmet (b), and bicycle helmet (c).

2.2 SINGLE VERSES MULTIPLE IMPACT HELMETS

Helmet liners are generally made of either expanded polystyrene (EPS), expanded polyethylene (EPE), expanded polypropylene (EPP), vinyl nitrile (VN), or cross-linked polyethylene foams (Hoshizaki & Brien, 2004). EPS is an example of nonrecoverable foam, popularly used in single impact/crash helmets. EPS is the choice for most bike helmets because it performs well in hard impacts and is light, cheap, reliable to manufacture, and easy to ventilate (Hoshizaki & Brien, 2004; Landro, Sala, & Olivieri, 2002). To make EPS liners, polystyrene beads are formed in a mould, which is subsequently injected with steam to glue the beads into the desired shape. All foams have a microstructure which can be represented as a "stacking of randomly distributed cells of various shapes and sizes," (Shulmeister, Van der Burge, Van der Giessen, et al., 1998, p.125). Nonrecoverable foams absorb energy by crushing the walls of the foam cell during impact and therefore are only functional for one hard impact (Hoshizaki & Brien, 2004).

On the other hand, recoverable foams, such as EPP, EPE, VN, and cross-linked foams used in helmets designed for multiple impacts, dissipate energy by pushing air out of their cells and do not require damaging the structure of a cell wall to do so. These liners are moulded using the same process as EPS and recover after head impacts; however, they are generally less efficient energy absorbers than nonrecoverable foams (Ivarsson et al., 2003). EPP and VN foams are commonly used in hockey helmets and VN foams in football helmets.

2.3 MECHANISM OF HEAD INJURY

Fortunately, through advances in medical research the understanding of head injury mechanisms has improved significantly in recent years. Knowing how head impacts affect the brain improves our knowledge regarding how helmets should function and subsequently allows for advancements in helmet design.

Traumatic brain injuries (TBI's) include mild to severe concussions, which can be defined as "a complex pathophysiological process affecting the brain, induced by traumatic biomechanical forces" (Patel, Shivdasani, & Baker, 2005). Head trauma begins with positive pressure, which occurs at the site of the impact (coup site) and ends in negative pressure from the brain striking the skull at the opposite side of the impact (contrecoup site) (King, Ruan, Zhou et al., 1995). Shear strain within the brain results from this movement inside the skull after it has been significantly impacted. The greater the angular accelerations applied to the head the greater the axons are stretched inside the brain, which results in rupturing of the bridging veins. Harder impacts would cause greater damage to the bridging veins, which results in decreased blood drainage from the brain to the dural sinus (King et al., 1995). Rupture of these veins can result in subdural hematomas, causing significant injury to the individual. In addition, significant impacts can cause stretching of the neurons, which are responsible for processing and sending signals for thinking and moving (Ommaya, Goldsmith, & Thibault, 2002).

There are two main mechanisms for TBI's in children and adults (Goldsmith & Plunkett, 2004). The first is described as impulsive loading and the second as impact loading. Impulsive loading occurs when a body is struck by some external object that causes the head to move. This is similar to "whiplash", where an unsupported head rotates around the cervical spine causing shear strain and subsequent damage to the bridging veins between the brain and skull as they rotate at different rates (Goldsmith & Plunkett, 2004; King et al., 1995). The second mechanism, impact loading results when two solid objects collide at a velocity sufficient enough to cause significant effects. This second mechanism is of more interest for the current study as this relates to the current testing techniques for helmets. The impact of a head against a solid surface or object always results in accelerations to the brain. These accelerations are used to define injury thresholds, which are used by current federally mandated standards for testing helmets (Goldsmith & Plunkett, 2004).

Nearly all head impacts result in both translational and rotational acceleration. Translational accelerations generate pressure gradients in the direction of the motion and are proportional to the magnitude of acceleration; however, rotational acceleration causes differential displacements between the layers of the brain resulting in shearing of the tissues and subsequent damage to blood vessels. Deceleration/accelerations are the key issues when discussing the forces applied to the brain. Deceleration is simply the negative of acceleration, which occurs when the velocity of the impact is slowing down (Barth et al., 2001). A brief explanation of acceleration is the change in velocity over time. Basically, the quicker the change in the head's velocity the greater the force applied to the structures of the brain, causing increased damage. Using the players mass and the accelerations during impact allows for an estimate of the level of force involved. To obtain precise calculations of force would actually involve the consideration of all vectors (direction and magnitude of force) involved in the impact, which is the goal of future research (Barth et al., 2001). In summary, the magnitude of the impact force, the location of the impact, and the resultant head and brain accelerations account for brain injury (McIntosh & McCrory, 2000).

In the literature, there have been notable differences regarding the mechanism for head injuries in different age groups, especially young children, which suggest that unique standards and subsequent helmet designs are needed for distinct age groups (Heh & Stadnik, 1997).

2.3.1 HEAD INJURY THRESHOLDS

The aim of a shock absorber (or helmet) is to minimize the peak force of the impact below a set limit/threshold. All head injuries are the result of some force acting upon it, where force and acceleration are interlinked. This is demonstrated through Newton's Second Law of Motion: $\Sigma Force = mass \times acceleration$, which aids in the calculation of the stresses on neural fibres under various impact conditions (Barth et al., 2001; Newman, 2006). Acceleration is a vector quantity representing the rate of change of linear velocity with time. Many current international helmet standards use peak linear accelerations as determinants for injury, with set tolerance levels between 250 and 300g for both adults and children, which have been argued to be too high for children (Stevenson, 1998).

Acceleration can be measured using a piezoelectric acceleration transducer located at the center of mass of a testing headform (NOCSAE *001-06m06*, 2006). Peak acceleration alone however, is generally not the best indicator for injury as it neglects the role that impact duration plays (Gadd, 1966). Consequently, some standards use the Gadd Severity Index (GSI) or Head Injury Criterion (HIC) as pre-determined injury thresholds (Becker, 1998; Camacho et al., 2001, Ivarsson et al., 2003., Myers & Nightingale, 1997).

2.3.2 GADD SEVERITY INDEX

The GSI and HIC are based on the Wayne State Tolerance Curve (WSTC) (Gadd, 1966). The WSTC was developed at Wayne State University, which conducted the first study to examine the relationship between acceleration level and impact duration by relating them to the risk of a serious head injury. Unfortunately, factors such as age, weight, sex, or size were not accounted for in this curve even though it has been applied to all individuals, including small children (Goldsmith & Plunkett, 2004). Nevertheless, the WSTC revealed that as impact duration increased, the tolerable intensity decreased, which concluded that acceleration or force alone was not the most appropriate criterion for determining injury thresholds (Gadd, 1966).

In 1966 Charles W. Gadd had proposed plotting the WSTC on a log-log scale to present the tolerance curve as a straight line (McHenry, 2004). The inverse of the slope corresponded mathematically to a power weighing factor, from which a numerical value could be used to define an injury threshold, now known as the GSI (Gadd, 1966). Gadd had established a GSI value of 1000 as the threshold for a serious internal head injury. It was recognized however, that this value would change as knowledge regarding injury mechanisms advanced, which helps explain why different standards have varying GSI values. The GSI is calculated by raising the acceleration vector (a(t)) in gravitational units (g's) to a power of 2.5 and integrating it with respect to the impact time in seconds:

$$GSI = \int_{T}^{0} a(t)^{2.5} dt$$

(CAN/CSA-D113.2-M89, 1996)

Where:

a = acceleration (g's) at the head's centre of gravity
n = weighting factor greater than 1
t = time (seconds)

The exponential weighting factor of 2.5 is based on the slope of the WSTC. This value was originally designed to predict frontal head injuries; however, it continues to be used today for several impact locations. The figure below displays the log-log plot of the WSTC with the original curve.

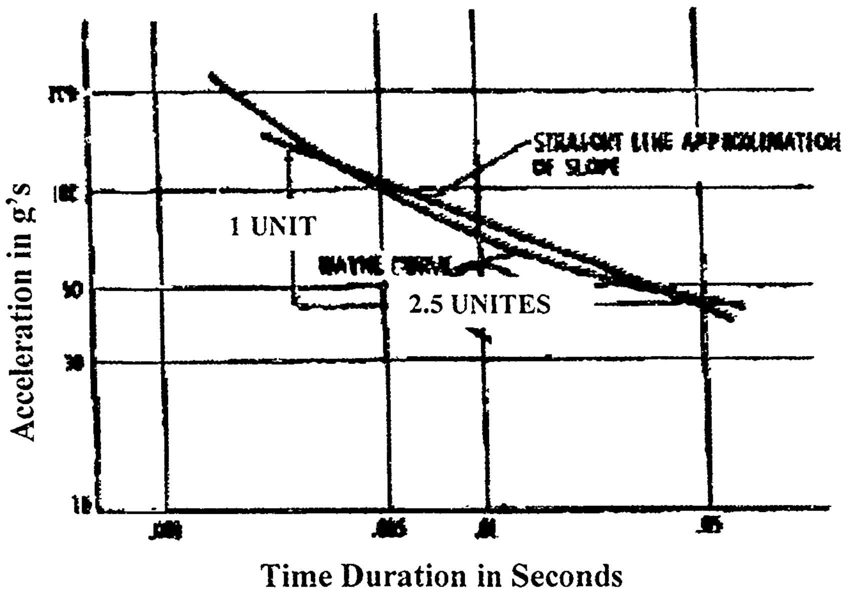

Figure 2 The log-log plot of WSTC showing Gadd's straight line approximation of the slope over the time duration of an automotive interior head impact (Gadd, 1966, p.169).

The straight line in the figure above is the GSI line. The slope or steepness of this line is shown by the ratio of 1 unit (rise) to 2.5 units (run). The acceleration threshold displayed in the vertical axis decreases at a slower rate than the impact duration increases, indicating that the acceleration magnitude was more important than time duration by the weighting exponent, 2.5. As pointed out by Richard G. Snyder, the GSI line is only applicable within reason. For example, if you were to extend the GSI line infinitely it would appear that a constant force of 1 g for 16 seconds would cause permanent injures. Given that humans are exposed to 1 g all of our lives, it is quickly evident that this line is only appropriate for short impact durations (Snyder, 1976).

The HIC is a refinement of the GSI, which is based on the resultant translational (linear) accelerations and is represented by the formula:

$$HIC = \left[\left(\frac{1}{t_2 - t_1}\right)\int_{t_1}^{t_2} a(t)dt\right]^{2.5}(t_2 - t_1).$$

(Ivarsson et al., 2003; Myers, 1997; CAN/CSA-D113.2-M89, 1996)

In this formula, 'a(t)' and 't' are the same as in the GSI; 't_1 and t_2' are also measured in seconds and represent two points during the impact which maximize HIC. The GSI and HIC criterions are generally more complex to measure; however, with advancing computer technology they have been receiving more attention (Becker, 2000).

2.3.3 IMPULSE

The term impulse can be used to further explain the relationship between force and time, where the area under the curve of a force time graph can be used to show impulse (Gordon et al., 2006). The following formula can be used to calculate impulse:

$$I = \int F dt$$ (Gordon et al., 2006)

Where,

F = Force
t = Impact duration

The duration of an impact can been used to determine the risk of injury, where a very short impact duration would result in more serious injury for a given impulse (Townsend, 2002). This relationship can be demonstrated in the figure below.

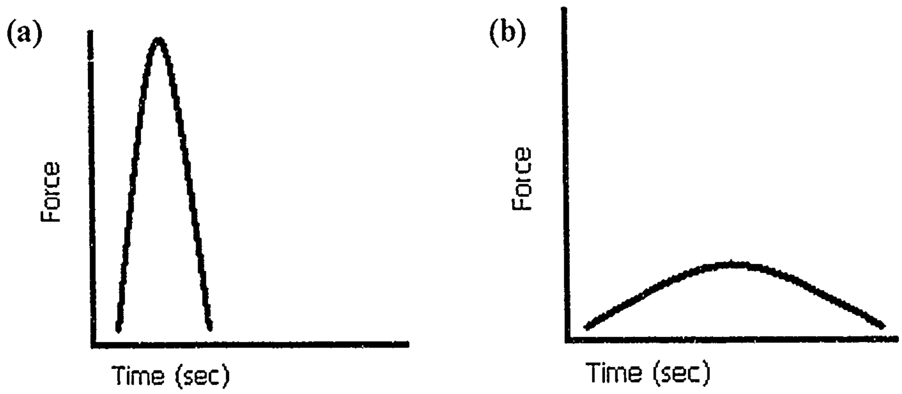

Figure 3 Force time graphs used to represent impulse (area under the curve) for two scenarios: (a) short time duration and (b) long time duration (Townsend, 2002).

For a given force, figure 3 (a) displays the results of an impact in which the force was transmitted in only a few milliseconds. Figure 3 (b) displays the results of the same impact when a padded surface is used to attenuate the impact energy. The resulting damage from figure 3 (b) would be less since the force is spread over greater time duration as noted by the significantly lower peak force. Thus, regardless of having similar impact energy the risk of injury is significantly greater in figure 3 (a) than figure 3 (b).

The GSI is similar to impulse, but uses accelerations opposed to force and a weighting factor to emphasize the contributions that time and acceleration have on the risk of obtaining a head injury.

2.3.1 LIMITATIONS TO HEAD INJURY THRESHOLDS

As mentioned, knowing the exact forces which occur in the head during impacts is rather difficult to calculate since head injury mechanisms involve impact and non-impact (impulsive loading) injuries, as well as linear and angular accelerations (Barth et al., 2001). The GSI and HIC neglect the contribution of the angular acceleration of the head, which many argue diminishes the value of these models for predicting the risk of injury (Curnow, 2003; Newman, 2006; Zhang, Yang, & King, 2004). It is known that translational and rotational accelerations occur simultaneously in most head impacts; however, they are much harder to test (Goldsmith & Plunkett, 2004).

As well, these formulas do not account for the complex motion of the brain within a deformable skull. Current injury thresholds are based on tests conducted on flat surfaces with linear impacts using animal concussion tests and cadaver skulls (Zhang et al., 2004). Thus, it is argued that the current injury threshold levels are not representative of real life collisions

(Curnow, 2003: Goldsmith & Plunkett, 2004; Zhang et al., 2004). However, GSI continues to be used as an acceptable reference for predicting head injury risk in both automotive and athletic related head impacts.

If head injury thresholds were lowered, helmets would have to be redesigned to pass such limits. There have been considerable debates regarding injury thresholds in adults, which lead into the next discussion regarding injury thresholds in children.

2.3.2 HEAD INJURY THRESHOLDS IN CHILDREN

The biomechanical response of a child's brain to head injury was traditionally thought to be that of a miniature adult. However, recent studies have noted many distinctions between a child and an adult head and have suggested that different threshold levels should be employed for children. For example, children have smaller head sizes and more resilient brain tissue than adults (Depreitere, Van, Maene et al., 2004; Gefen, Gefen, Zhu et al., 2003; Goldsmith & Plunkett, 2004). Head size grows rapidly between ages zero and four and it isn't until the age of 20 that the bone plates of the skull fully close (Arbogast, Margulies, Patlak et al., 2003). A child's brain has higher water, which increases swelling pressure and osmotic intracellular pressure; subsequently, making their brains stiffer than an adult. This increase in pressure increases the intracranial strain during head impacts and therefore the risk of head injury. The mean and long-term shear moduli decrease with age as a result of this decrease in water content of the brain as axons become increasingly myelinated with growth (Gefen et al., 2003).

As well, child neck muscles are considerably weaker than adults and ligaments tend to be stretched more during impacts to the head. Their blood vessels are less likely to tear under twisting or squeezing stress, but require less force to deform or stretch thereby resulting in greater risk for long lasting damage (Arbogast, Margulies, Patlak, et al., 2003;

Depreitere et al., 2004; Johnson & Young, 2005). Lower head injury threshold levels have therefore been postulated for young children. For example, one study concluded that a peak acceleration of 110 g's or HIC value of 600 corresponded best to a 25% irreversible injury for individuals under 6 years old. This study modeled pedestrian-automobile impacts using 6-year-old child dummies (Goldsmith & Plunkett, 2004).

Linear and angular velocity, which are directly related to the falling height of the individual, are often used as an indirect method to gauge the degree of potential trauma or stresses generated by an impact (Ommaya et al., 2002). A child's falling distance is much lower than an adult and therefore generates lower impact forces; however, the consequences can be quite serious for both groups. A toddler falling from 0.91 m would result in an impact velocity of 4.24 m/s; whereas, an adult falling from 1.82 m would have a contact speed of 6 m/s. Both situations produce forces which exceed skull fracture tolerances in children and adults (Ommaya et al., 2002). Figure four shows the level of stress necessary to fracture the skull of an adult, a young child, and an infant, in addition to the corresponding skull thickness for each group.

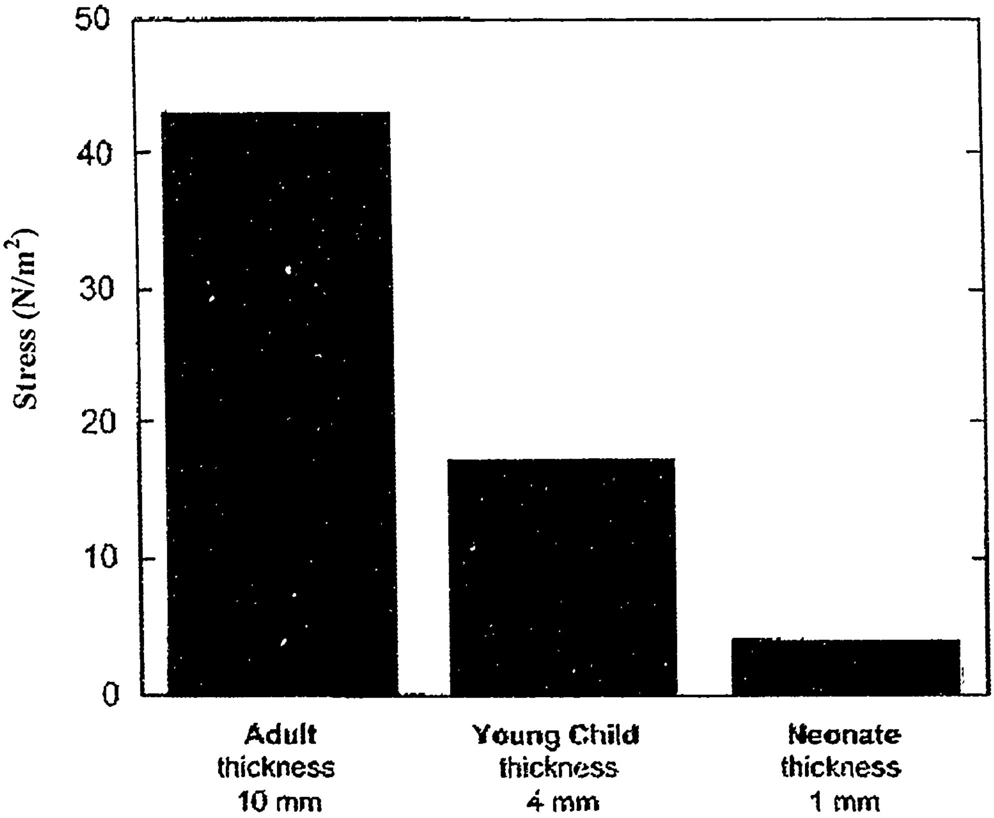

Figure 4 Skull failure stress (N/m^2) in an adult, young child, and neonate (Ommaya et al., 2002, p. 224).

As skull thickness increases with age, the moduli of the bones increase, which can subsequently withstand greater forces before fracturing. Figure five compares the risk of head injury for an adult, young child, and neonate by observing the magnitude of rotational accelerations required to cause concussion and diffuse axonal injuries (DAI). It is noticed that as head mass decreases from and adult to a neonate, the threshold values for concussion and DAI increase respectively when using rotation accelerations as the determinant for injury. Ommaya et al. (2002), state that a rotational acceleration of 10000 rads/s^2 would be required to produce a concussion for a neonate; whereas, an adult would only require a rotational acceleration of 4500 rads/s^2 to cause concussion. These accelerations produce a velocity gradient within the brain and result in shear stresses that can rupture neurons and bridging veins.

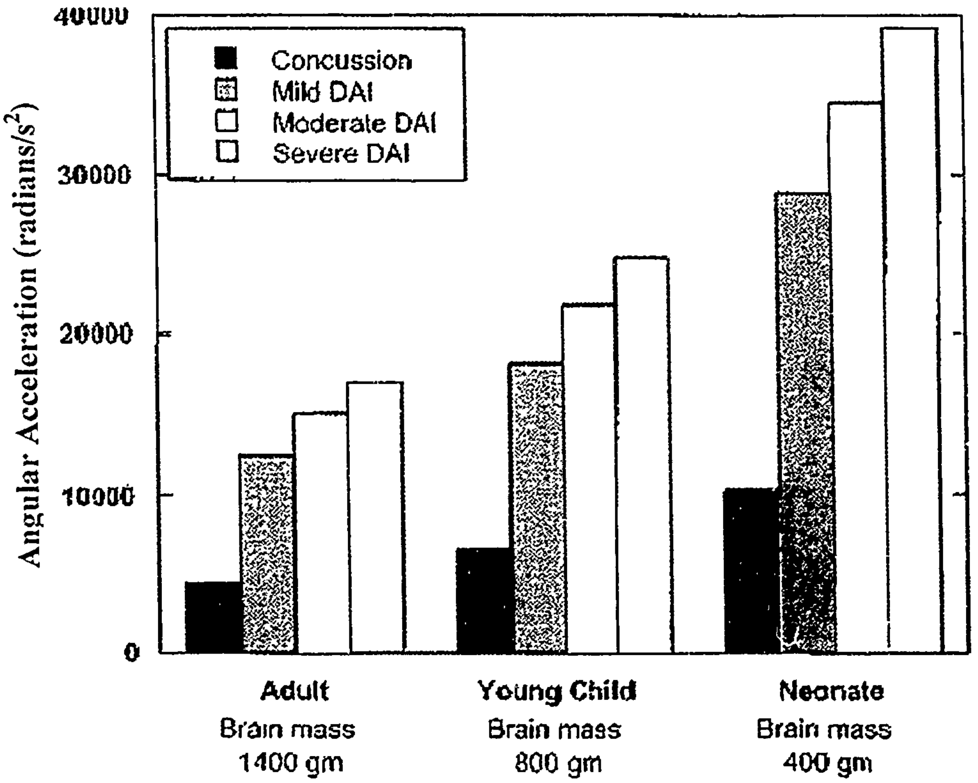

Figure 5 Brain injury tolerance scaling in the adult, young child and neonate (Ommaya et al., 2002, pg. 228).

HIC values have been shown to decrease with increasing head size for a given acceleration pulse, which shows that head mass can vary the intracranial response during an impact (Arbogast et al., 2003; Johnson & Young, 2005; Kleiven & Holst 2002; Newman et al., 2004). The figure below shows that there was a significant non-linear relationship between head mass and maximal shear stress, maximal frontal pressure, maximal occipital pressure, and HIC (Kleiven et al., 2002).

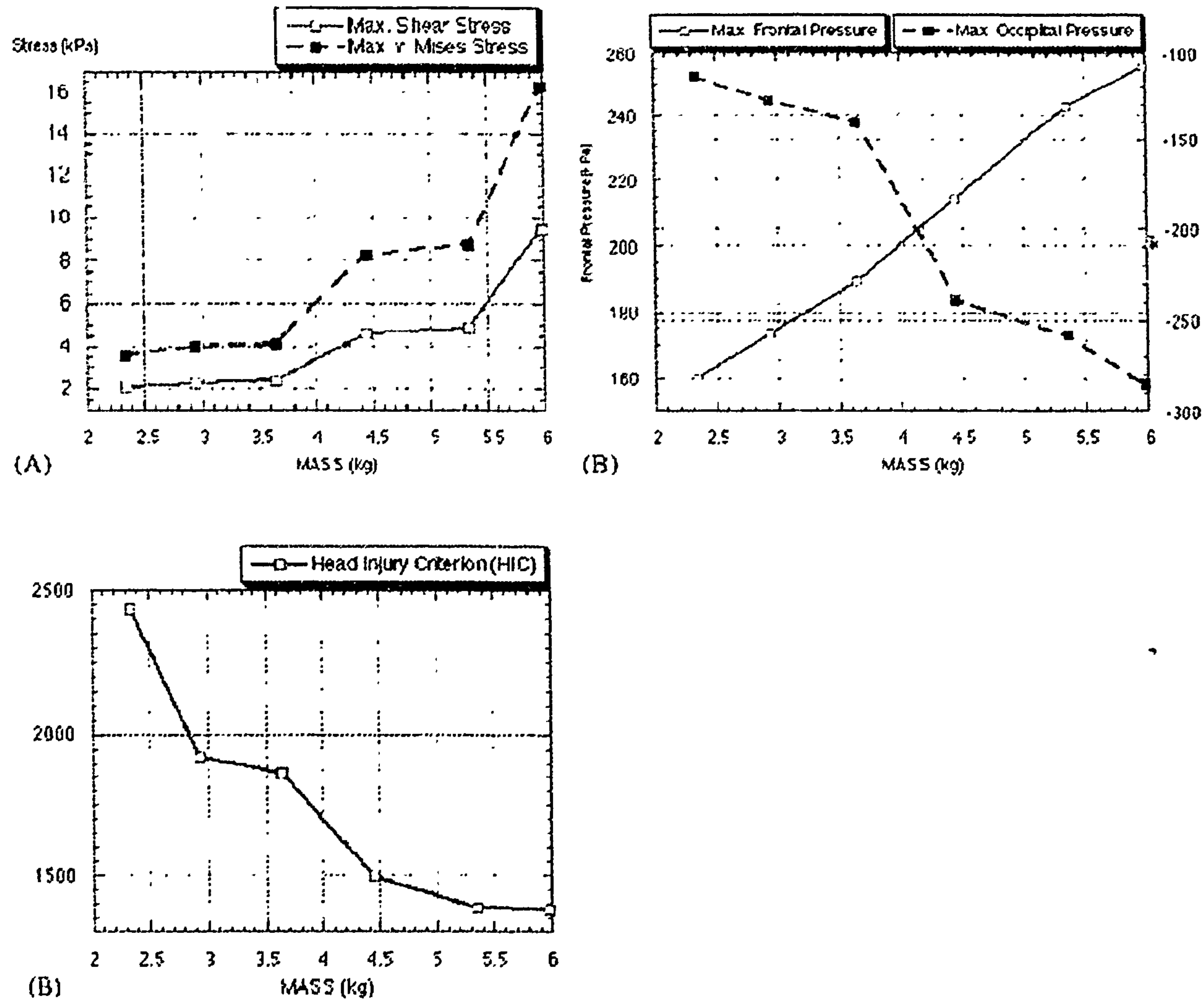

(C)

Figure 6 The dependence of the intracranial stress (A), pressure (B), and HIC (C) on head mass using the same acceleration impulse during a frontal impact (Kleiven et al., 2002, p. 157).

Overall, the HIC value decreased with increasing head size, whereas the maximal intracranial stresses increased. These data show that head mass had a significant effect on the risk of obtaining a brain injury during an impact to the head.

Johnson & Young (2005) and Newman et al. (2004) have concluded that the duration of an impact (total length of the acceleration pulse) increased with increasing impact mass size, where increase in both impact duration and mass were linked to increases in peak force or impulse. This is contrary to an impact of a given impulse being mitigated over a longer duration as such a situation would result in decreased peak forces, which is the goal of a helmet. These studies are showing that when the overall impulse increased (not mitigated), the risk of injury increased.

Increases in inbound velocity were also shown to be linearly correlated with increases in peak force, but inbound velocity was not correlated to the duration of the acceleration pulse (Johnson & Young, 2005; Newman et al., 2004). When time duration and acceleration are graphed, the shape is able to predict the velocity change (Δv), where Δv is the product of the average accelerations and the time duration. A higher velocity change or longer impact duration means higher injury probability. Since higher head mass is linked to longer duration, individuals with larger heads are at risk for a greater peak force during impact (Newman, 2006).

The aforementioned research supports the need for helmets to function distinctively for smaller and larger head masses and for varying impact velocities. It can be implied that testing headforms, which are currently designed with the same materials, should be designed using the unique physiological parameters of younger age groups in addition to mass specifications. Although the present study will not be investigating injury thresholds or the mechanism of injury, there is an evident need to understand the effect of head size (impact mass) and inbound velocity on the performance of helmet liners.

2.4 STANDARDS

Impact protection is the primary consideration of almost every helmet standard. Standards consist of prescribed helmet testing techniques, which attempt to reproduce head impacts to measure the outcomes of these impacts on the brain. Each test is basically a one dimensional measure of the exchange of momentum between a helmeted headform and an impactor (Becker, 2000). The mass of the headform and the inbound velocity are important parameters, which are defined based on the specific standard. The headforms certified by the

International Standards Organization are primarily made of a magnesium or aluminum alloy and are not biofidelic. Thus, they do not recreate the dynamic impact characteristics of a human head when contacting a surface. The unique physiological and biomechanical protection requirements for children, adults, and elderly are therefore ignored (Hoshizaki & Brien, 2004). Nevertheless, impacting helmets using these headforms has been accepted internationally in dozens of standards.

Each helmet standard specifies the headform's size, material property, and configuration; as well as, the impact locations on the helmets, drop height, impactor surfaces, and impact severity levels (Becker, 2000). Impact surfaces, also known as the anvil, can be flat, spherical, or sharp (CAN/CSA-D113.2-M89, 1996). Almost every standard includes a flat impact surface as part of their testing protocol. The other shapes cause more focused shock to the helmet surface and the test required using these shapes is generally from lower drop height to meet the maximum acceleration/criterion threshold (Becker 1998). Drop height can also be determined by the velocity measured just before the impact, which would increase as the drop height increased. These parameters account for the impact severity, which presently vary across standards. There are limited objective measures for prescribing impact severities for helmet tests and further research is needed to define injury threshold levels (Becker, 1998).

The performance of a helmet is evaluated based on acceleration outputs measured by an accelerometer placed at the center of mass of the headform. Most helmet standards implement a pass-fail criterion based on peak linear acceleration. Other measures include the duration of the impact and the time to peak linear acceleration (Becker, 1998). Some standards use the Gadd Severity Index (GSI) or Head Injury Criterion, (HIC) as defined earlier. Even if the same criterion types are used, standards differ on the criterion limit (injury threshold).

Most helmet criteria are based on the needs of adult males. Younger people (mentioned previously) and older people; however, have different needs and thus require unique helmet designs (Mills & Gilchrist, 2003). In the article, Paediatric Bicycle Injuries, published by Cass and Gray in 1989, it was stated that separate standards may need to be implemented for helmets for children under the age of six (Cass & Gray, 1989). This argument remains pertinent today, 18 years later, as many international helmet standards are still neglecting the significant physiological and biomechanical differences for this demographic group.

2.4.1 CANADIAN STANDARDS ASSOCIATION

The Canadian Standards Association (CSA) has recognized that injury tolerance levels for children and adults are different and are one of the only standards in North America to incorporate variable impact mass and velocity in their testing protocols (Bicycle Helmet Safety Institute, 2006). Their new helmet standards for children, five years and younger, significantly lowered the peak g limits from 300g's to 200g's on a standard helmet drop test using a flat anvil. In addition, they have set the drop height from 2 metres to 1.5 metres onto a flat anvil, as well as a 1.0 metre drop height on a cylindrical anvil with a threshold reading of less than 150g's (CAN/CSA-D113.2-M89, 1996).

In addition to lowering the drop height and threshold levels, the standard has also decreased the test headform masses for children less than 5 years of age. The CSA requires that the mass of the headform and support assembly for headforms A and E must be 3.1 kg +/- 3% and 4.1 kg +/-3% (CAN/CSA-D113.2-M89, 1996), opposed to the Consumer Product

Safety Commission and Snell Memorial Foundation requirements of 5.0 kg (Stevenson, 1998). This reduction in head mass and drop height decreases the overall energy in the drop test. Thus, the landing needs to be softer for the head, which is done by decreasing the density of the foam. American approved helmets would most likely not pass the CSA standards (Becker, 1998).

2.4.2 SNELL FOUNDATION

Criticisms by both the Snell Memorial Foundation and Consumer Product Safety Commission (CPSC) have been made regarding this change and have refused to change their standards using more child-like parameters. The Snell Foundation basically stated that the new parameters set forth are too drastic and that there is not enough research justifying the need for this change (Becker, 1998).

Edward Becker, the executive director of the Snell Memorial Foundation, agreed that the height at which the cyclist falls is an important element in the design of any bicycle helmet. He explained that the shock transmitted to the head is related to acceleration, which is the transition from the falling velocity just before impact to the rebound velocity just after the impact (Becker, 1998). As mentioned, the velocity at which a head impact occurs is referred to as the inbound velocity, which is shown to be an important element when designing sport and age specific head gear. Thus, an argument could be made that children helmets need to be tested from child-like drop heights, not the standard adult drop heights that are currently being used. However, Becker argued that bicycle helmets are already proving to be effective in preventing head injuries and therefore should not be tampered with (Becker, 1998). This was supported by epidemiology studies that compared the percentages of head injuries occurring from helmeted and non-helmeted bicycle users and showed that

85% of all cycling fatalities caused by head injuries could be prevented by using a helmet (Noakes, 1995).

Currently, the Snell Foundation helmet standards for bicycling, horseback riding, motorcycling, and other sports use five headform's with geometries described in the International Standards Organization (ISO) Draft Standard ISO DIS 6220-1983. The mass however, is kept constant at 5 kg for all of the ISO headform shapes. As the geometry decreases, the impact footprint decreases creating a more localized and severe impact. In addition, helmets are tested from a drop height of 1.5 metres using a guided free fall drop apparatus and must pass a maximum peak acceleration threshold of 300 g's (Snell Memorial Foundation, 2000). There are no specifications regarding lower drop heights or lower threshold levels for children.

2.4.3 CONSUMER PRODUCT SAFETY COMMISSION

The United States Consumer Product Safety Commission's (CPSC) is a standard that is very similar to the Snell-90 and the American Standards for Testing Material (ASTM) standards for helmets. All helmets sold in the US have to meet this requirement (Towner et al., 2006). The CPSC standard for bicycle helmets establishes performance requirements for two categories of helmets, the first applies to young children, 1-5 years, and the other applies to older children and adults, 5 years and older (Stevenson, 1998). The only requirement set forth by the CPSC standard that differentiates these two categories is head coverage. Helmets intended for young children are subject to impact testing over greater surface area to ensure these users are protected from impacts falling lower on the brow, sides, and back of the head (Stevenson, 1998).

Similar to Snell standards, the CPSC standard continues to use 300 g's as the acceptable peak g's for impact testing for helmets for young children and adults. In addition, this standard uses adult-weight headforms to test child helmets instead of more representative head weights. In 1995, it was proposed that the standard should adjust the headform drop mass to 3.9 kg and peak acceleration value to 250g's for children; however, this proposal was refused. Basically, they said more research is needed to be put forth regarding the benefits of these changes before the standards would be adjusted (Stevenson, 1998).

2.4.4 NATIONAL OPERATING COMMITTEE ON STANDARDS FOR ATHLETIC EQUIPMENT

NOCSAE, the National Operating Committee on Standards for Athletic Equipment, is an internationally recognized standard that has regulated procedures and performance requirements for testing protective headgear. In particle, NOCSAE sets standards specific for football, softball, baseball, hockey, lacrosse, and polo helmets. These testing standards define the impact velocities, testing methods, peak accelerations, and maximum Severity Indexes. Angular accelerations are ignored in the NOCSAE drop test method and only linear accelerations are considered for impact thresholds (NOCSAE *001-06m07*, 2007).

There are three headform sizes used for testing helmets: small, medium, and large. These sizes are defined based on the headform weight (including the mounting surface) and 14 anthropometric measurements of the head, such as the head breadth, maximum brow width, and ear hole to ear hole measurements (NOCSAE *001-06m07*, 2007). As noted in the figure below, the mass of the small, medium, and large headforms are 4.12 kg, 4.85 kg, and 5.83 kg respectively, which includes the mass of the support assembly.

POINTS OF MEASURE	HEADFORM SIZES 6 5/8	7 1/4	7 5/8
1 Head Breadth	5.63 (143)	5.98 (152)	6.46 (164)
2 Maximum brow width (frontal diameter)	4.65 (118)	5.20 (132)	5.52 (140)
3 Ear hole to ear hole (bitragion diameter)	5.24 (133)	5.51 (140)	6.06 (154)
4 Maximum jaw width (bigonial diameter)	4.13 (105)	4.65 (118)	5.08 (129)
5 Head length (glabella landmark to back of head)	7.09 (180)	7.87 (200)	8.15 (207)
6 Outside eye corner (external canthus) to back of head	6.22 (158)	6.81 (173)	7.32 (186)
7 Ear hole (tragion) to back of head	3.50 (89)	3.86 (98)	4.25 (108)
8 Ear hole to outside corner of eye (tragion to ext. canthus)	2.72 (69)	2.95 (75)	3.07 (78)
9 Ear hole to top of head (tragion to vertex)	4.72 (120)	5.24 (133)	5.67 (144)
10 Eye pupil to top of head	4.13 (105)	4.53 (115)	4.96 (126)
11 Ear hole ‡ to jaw angle (tragion to gonion)	3.31 (84)	3.03 (77)	2.84 (72)
12 Bottom of nose to point of chin (subnasal to menton)	2.56 (65)	2.80 (71)	3.03 (77)
13 Top of nose to point of chin (nasion to menton)	4.45 (113)	4.88 (124)	5.39 (137)
14 Head circumference	21.02 (534)	22.68 (576)	24.17 (614)
15 Head weight including mounting interface	9.08 lb (4.12 kg)	10.7 lb (4.85 kg)	13.32lb(6.04 kg)

† The anthropometric measurements are based upon references 2.3 and 2.4.
‡ The right ear of each headform shall be removed flush with the skin surface.

Figure 7 The physical properties of the NOCSAE headforms, sizes 6 5/8, 7 1/4, and 7 5/8 (NOCSAE 001-06m07).

If a helmet happens to be smaller than the smallest NOCSAE headform then testing of that size is not required so long as at least two headform sizes and two other helmet models were tested and passed. Thus, helmets are not being tested for children with head masses lower than the 4.01 kg headforms (NOCSAE *001-06m07*, 2007). There were no specifications regarding children's helmets found in any NOCSAE documents.

The Standard Performance Specification for Newly Manufactured Football Helmets and Hockey helmets state that the peak severity index, or GSI, of any impact is to be no greater than 1200 SI (NOCSAE *001-06m07*, 2007; NOCSAE *002-98m05*, 2006). Again, no unique specifications were mentioned for individuals of younger age groups.

2.4.4 INTERNATIONAL STANDARDS ORGANIZATION

The International Standards Organization (ISO) produces industrial and commercial standards world-wide. In 1960, ISO formed a technical subcommittee to work solely on protective headgear (Becker, 1998). ISO technical subcommittees collaborate with various international organizations, both governmental and non-governmental, while preparing standards.

The ISO/EN 10256, Head and Face Protection for Use in Ice Hockey standard, was created to help decrease the frequency and severity of head injuries caused during play (ISO TC 83/SC 5N, 2006). The headforms used in this standard and for the present research study are required to conform to geometrical specifications from the BS EN 960:1995 standard titled, Headforms for Use in the Testing of Protective Helmets. Contrary to the Snell Memorial Foundation and the CPSC, this standard requires that the headform and support assembly have a combined mass of 3.1 kg, 4.1 kg, 4.7 kg, and 5.6 kg for headform sizes A, E, J, and, M respectively. The helmet however, is impacted at a velocity of 4.5 +/- 2 m/s for all tests regardless of headform size or impact location (ISO TC 83/SC 5N, 2006). Both mass and velocity requirements are similar to the ASTM Standard Performance Specifications for Ice Hockey Helmets standard (ASTM International, F 1045-06, 2006).

The ISO hockey helmet standard identifies the impact locations to be used during impact testing.

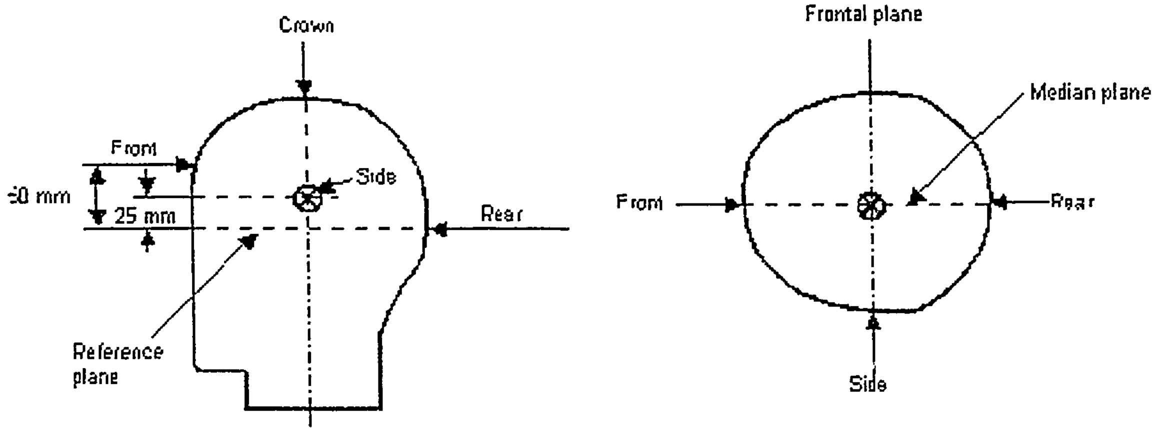

Figure 8 An ISO headform indicating the frontal, side, crown, and rear impact locations, as well as the frontal plane, median plane, and reference line (ISO TC 83/SC 5N, 2006).

The impact locations are perpendicular to the surface of the headform for all impact sites. As noted in figure 8, the reference plane is parallel to the basic plane of the human head, which is located at the upper borders of the ear canal and the inferior margins of the orbits of the eyes, and is a function of the size of the headform. The median plane, which divides the headform into right and left halves, passes through the middle of the headform from front to back. Perpendicular to the median and reference planes is the frontal plane, which passes through the top of the headform (ISO TC 83/SC 5N, 2006).

From these different planes, the frontal, side, rear, and crown impact locations can be identified. The crown, which will be used in the present study, is found at the top of the headform where the central vertical axis meets. The frontal position is located 50 mm above the anterior intersection of the reference plane and falls on the median plane. The side impact location is found along the median plane, 25 mm upwards from the reference plane and the rear impact site is located at the posterior intersection of the median and reference planes (ISO TC 83/SC 5N, 2006).

2.5 MATERIAL CHARACTERISTICS

2.5.1 DENSITY AND THICKNESS

The main structural features of foam are in relation to relative density and proportion of open and closed air cells (Landro et al., 2002; Shulmeister et al., 1998). In closed-cell foams, most cells share a thin membrane wall, which is bounded by struts. Vinyl nitrile used in football helmets are an example of closed cell foams designed for multiple impacts. Removal of these cell walls, using chemicals or reticulation, produces open-cell foams (for example EPS) that are classified according to their relative density (Shulmeister et al., 1998).

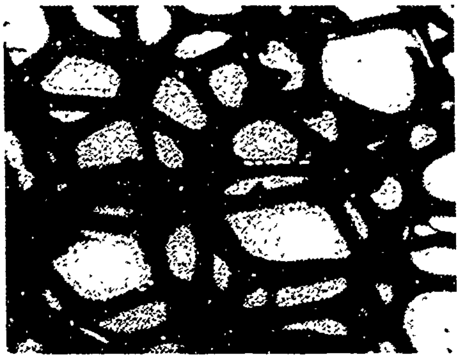

Figure 9 Image of low-density open-cell foam. (Shulmeister et al., 1998)

In low density foams, as demonstrated in figure 9, the solid material is distributed rather evenly along thinly spaced struts. Conversely, high density foams show more than 10% in the solid phases concentrated at the vertices (Shulmeister et al., 1998).

The goal when choosing a foam liner is to optimize the density and thickness to protect against the widest range of impact conditions possible for a specific sport. As well, it is to dissipate the kinetic energy of the impacting mass while keeping the maximum force (or acceleration) below injury threshold levels (Avalle et al., 2001). Foam density is a measurement of mass per unit volume, which is measured in pounds per cubic foot (pcf), or in metric terms, kilograms per cubic metre (kg/m^3). Lower density foam usually results in a softer liner, which may help improve the protection for lower-severity impacts. On the other hand, denser foams resist harder impacts better before compressing to their limits and transferring impact energy to the head (Landro et al., 2002).

There is a linear relationship between density and tensile strength for EPS, where a high-density EPS is able to absorb larger amounts of energy compared to low-density EPS, but transfers higher accelerations and forces localized at the impact point. A quasi-static relationship exists between foam stiffness and density when strut bending is the dominant deformation mechanism (Shulmeister et al., 1998). In addition to density, increasing the thickness of the liner increases the ability of the material to attenuate energy. However, liners can only be so thick before imposing further detrimental risks, such as increased angular accelerations imparted to the brain during impacts. Also, as thickness increases the aerodynamic performance of the helmet decreases, as well as it becoming aesthetically unacceptable (Landro et al., 2002). Once the acceptable thickness and maximum crushing are prescribed, the optimal EPS density can be defined for a given amount of energy to be absorbed (Landro et al., 2002).

2.5.2 MECHANISMS FOR ENERGY ABSORPTION

Stress-strain curves, commonly used in material engineering, provide an important graphical measure of a material's mechanical properties (Roylance, 2001). Below is an example of a stress-strain curve displaying three general phases foam experiences during quasi-static compression (Avalle et al., 2001; Ivarsson et al., 2003; Viot et al., 2005).

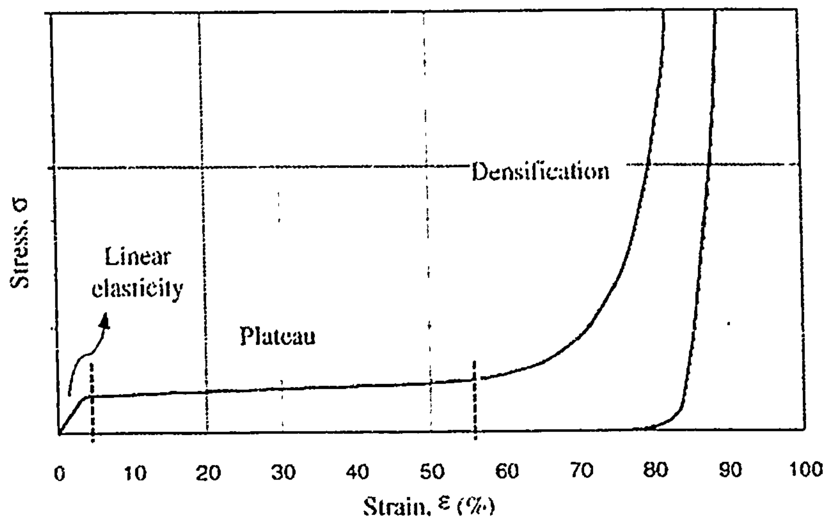

Figure 10 Typical foam stress-strain curve from a quasi-static compression (Avalle et al., 2001).

This curve is a graph derived from measuring the load (stress) versus the extension or compression (strain) of a sample of material. The first phase of the curve is the linear elastic phase, which is controlled by the bending of the cell edges, compression of gas trapped into the cells, and the stretching of the cell walls (Avalle et al., 2001; Landro et al., 2002). This initial slope of the stress-strain curve is equal to the Young's modulus of the foam. The second phase is the plateau or functional phase, which is when the cells collapse and absorb the bulk of the impact energy. A flatter force curve indicates higher energy absorption efficiency (Yu-Hallada, Kuczynski, & Weierstall, 1998). Once the cells have almost completely collapsed the opposing cell walls come in contact and the foam bottoms out, which is the final phase of a stress-strain curve (Avalle et al., 2001; Landro et al., 2002; Viot et al., 2005). Densification causes the stress to increase steeply. This final phase depends on the foam density and the strain rate, where an increase in either will increase the plateau stress (Viot et al., 2005).

Ivarsson, Viano, Lövsund, and Parnaik demonstrated the dynamic stress-strain characteristics for seven foams commonly used in upper vehicle components; such as the front and rear headers, the side rails, the roof, etc (Ivarsson et al., 2003).

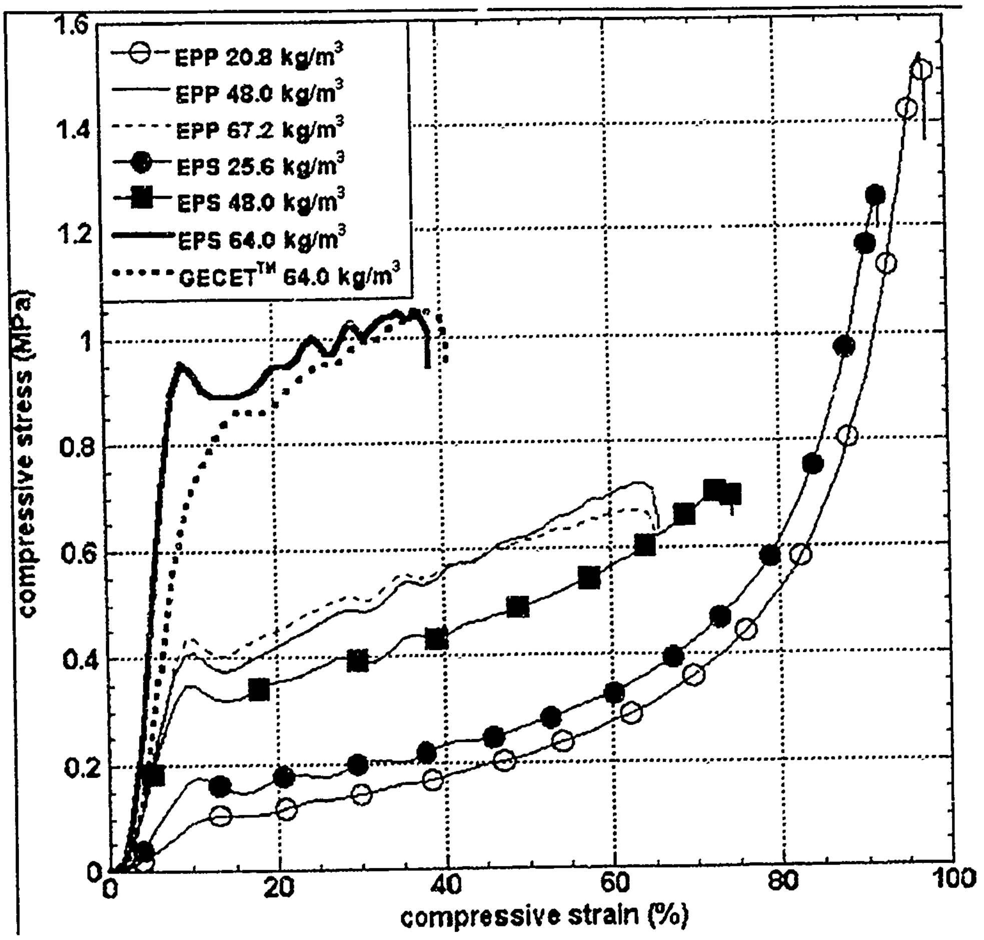

Figure 11 Dynamic stress-strain characteristics for seven foams commonly used in upper vehicle components (Ivarsson et al., 2003).

In this figure, there are three stages of the stress-strain curve for seven foams subjected to drop weight testing: EPP 20.8 kg/m^3, EPP 48.0 kg/m^3, EPP 67.2 kg/m^3, EPS 25.6 kg/m3, EPS 48.0 kg/m^3, EPS 64.0 kg/m^3, GECET™ 64.0 kg/m3. The samples were 102 mm by 21 mm in size and were compressed using a cylindrical drop mass of 6.8 kg with a diameter of 178 mm. The weight was dropped from a height of 2274 mm or 6.7 m/s and an accelerometer attached to the drop mass was able to record accelerations. As shown in figure 11, the lower density EPS of 25.6 kg/m^3 succumbed to significantly greater compressive strain compared to the higher density EPS of 64 kg/m^3, but bottomed out at lower stress values (Ivarsson et al., 2003). Researchers have found that an increase in density correlates to a higher plateau stress, which indicates that higher density foam is more resilient (Ivarsson et al., 2003; Viot et al., 2005). For helmet liner application, when the foam is too dense, as shown in the EPS 64 kg/m^3 curve, the force would exceed the threshold/critical level before enough energy would been absorbed to collapse the foam cells and dissipate energy (Song, Chen, Dou et al., 2005).

The above study on upper vehicle components utilized a Hybrid III head-neck model, weighing 6.8 kg, and measured sagittal plane linear and angular head accelerations (Ivarsson et al., 2003). Although their study was able to show how various density foams react under such impacts at three impact speeds (5, 7, and 10m/s), further analysis is needed before generalizing these results to individuals with significantly different head-neck masses.

Comparisons between strain-rate behaviour using quasi-static compression and dynamic loading demonstrated that the elastic responses were completely different between the two testing techniques (Viot et al., 2005). It has been suggested that air-bubbles inside foam cells are released during quasi-static compression; whereas, they are trapped during dynamic loading. This enables the foam to spring back more forcefully and thus does not compress as flat as the quasi-static (Viot et al., 2005). This effect is noted in figure 12 below.

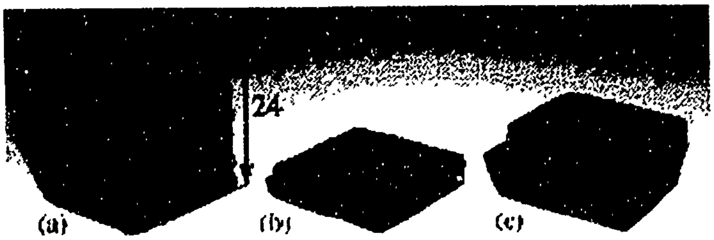

Figure 12 Effect of the strain rate on polypropylene foam sample (24×24×24 mm^3) after compression: picture of sample before test (a), after quasi-static compression (b), and after dynamic loading (c) (Viot et al., 2005).

McIntosh, McCrory, and Finch recently examined the energy attenuation performance of polyethylene foam that could be incorporated into headgear by investigating the effects of foam thickness, density, and drop height (McIntosh et al., 2006). They tested 10 mm, 12 mm, 14 mm, and 16 mm thick samples of 50 kg/m^3 and 67 kg/m^3 densities from drop heights of 0.2 m-0.8 m (in 0.1 m increments). They found the thickest foam resulted in improved impact energy attenuation for all drop heights. No significant differences were found between the two densities of foam; however, if more densities were used it was speculated that differences in performance would naturally occur. This study did not take into account the effects of mass and therefore is only applicable to individuals with a 5 kg head mass (McIntosh et al., 2006). As well, it failed to show a difference between material densities, which is contrary to the predicted outcomes of the present study.

Subhash, Liu, and Gao (2006) investigated the effects of bulk density for polymeric structural foams under uniaxial quasi-static and high strain rate loading conditions. Their primary interest was to understand impact and energy absorption characteristics of polymers used for automotive impact protection. Contrary to McIntosh et al. (2006), significant differences were found between the Young's Modulus, yield strength, ultimate strength, and the strain to failure for epoxy based polymeric foams of 0.83, 0.90, 1.21, and 1.46 g/cm^3. The graph below displays these differences.

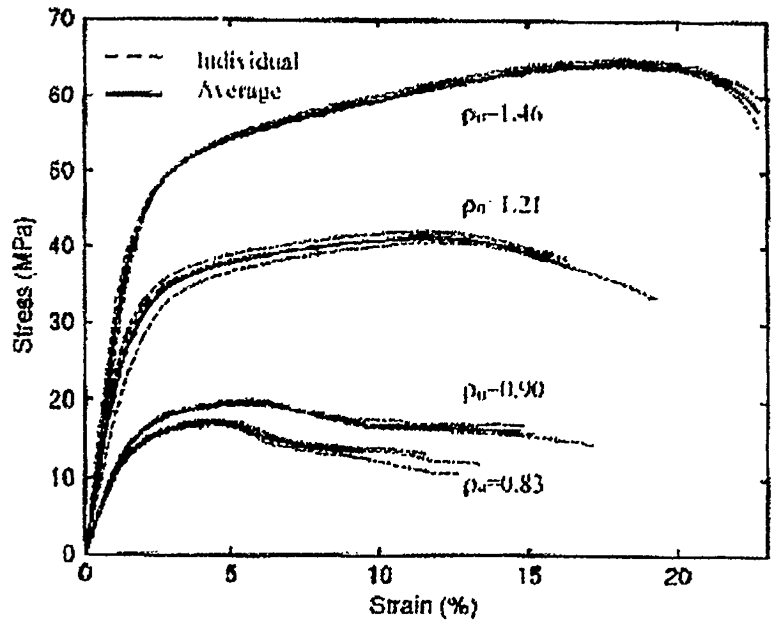

Figure 13 Stress strain curves for three types of epoxy based polymeric foams of various densities subjected to quasi-static uniaxial loading at a strain rate of 1.5×10^{-3}/s (Subhash, Liu, & Gao, 2006).

The above figure displays the quasi-static stress strain response of three foam samples at four different densities. A servohydraulic compressive testing machine was used at a strain rate of 1.5×10^{-3}mm/s and the average of each foam sample was indicated by a black solid line (Subhash et al., 2006). It was concluded that the higher the initial density of foam, the higher the Young's modulus, yield stress, ultimate strength, and strain to failure were. Actually, these properties increased nearly linearly with increasing density. The authors attribute this difference primarily to the porosity of the foams, where porosity and bulk density are inversely related. Porosity, expressed as a percentage, is a measure of the empty spaces within a material. More empty space increases the size of the material without increasing the mass, thus creating a lower density material (Subhash et al., 2006). The percentage of porosity was calculated as follows:

$$\% \text{ Porosity} = \left(1 - \rho_0/\rho_s\right) \times 100$$

(Subhash et al., 2006)

Where,

ρ_0 = bulk density

ρ_s = solid material density

Bulk density differs from solid material density in that it refers to the density of the samples when injected with steam. Thus, the relative mass is the same as the solid material but the volume it occupies is much larger as it includes the air cells or spaces within the sample (Subhash et al., 2006). It was stated that high-density (low porosity) foams have smaller sized pores, but thicker walls and exhibit large inelastic strain compared to low density foams. The lower density foams with larger pores and thinner walls have been shown to crack macroscopically at much lower stress rates and more quickly compared to high density foams, thereby explaining the major differences seen between the low and high density foams during quasi-static compressions. In high density foams, the deformation of the sample occurs more gradually and failure results more from hardening of the material and shear strain (Subhash et al., 2006).

During dynamic testing of the same materials above, Subhash, Liu, and Gao (2006) found that with increasing foam density, the ultimate strength was significantly greater than during quasi-static loading. The low-density foam failed at much lower strain rates, which was again attributed to the large and thin cell walls. This shows that foams are strain rate dependent; having greater strength at higher dynamic strain rates compared to the quasi-static loading rates (Subhash et al., 2006).

Martin, Liptai, Yerby, and Williams (1994) conducted a study to predict the effects of mass on impact acceleration by dropping 2.69 and 7.40 kg weights from 31.8 cm onto three deformable surfaces. They chose these masses to approximate the masses of a large head and a child's head. Impact force was measured with a force plate and was divided by the drop mass to obtain accelerations ($a = F/m$). The calculated accelerations were than used to measure impact severity. The equation below was used to represent the ratio between two masses, m_1 and m_2, and the average acceleration, a_1 and a_2 produced for a given drop height and impact surface.

$$a_1/a_2 = (m_1/m_2)+1/(p+1)$$

(Martin et al., 1994)

It was stated that for a given acceleration-time curve, the mean and peak accelerations are proportional to one another. The variable 'p' in the above equation was used as a constant (not given) to represent a load deformation characteristic of the impact surfaces. It was found that the small mass produced significantly greater peak accelerations than the larger mass. However, peak forces produced by the larger mass were consistently greater than those produced by the smaller mass, regardless of the surface (Martin et al., 1994). The accelerations resulting from the impact forces were stated to be responsible for shear stresses and strains produced in the brain that cause concussion and diffuse axonal injury.

2.5.2 EFFECTS OF MATERIAL SIZE

The dimensions of the polymer sample are an important consideration in dynamic impact testing as this variable will significantly affect the results. The relationship between the forces applied to the sample and the subsequent indentation of the material is dependent upon the materials stiffness (Todd, Smith, & Vongpaseuth, 1998). It has been shown that the compressive propert'es of open cell foams .ary as the cross-sectional area changes in size relative to the indenter. Material samples with cross sectional areas smaller than the indenter exhibit lower stiffness characteristics compared to samples larger than the indenter. When the sample is larger than the indenter it is suggested that the shear forces created during compression between the material and the sides of the indenter is included in the total stress calculations (Todd et al., 1998). The figure below demonstrates this phenomenon.

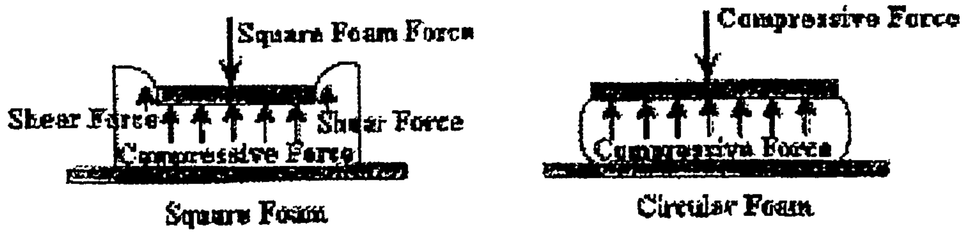

Figure 14 Compressive response of two foam samples subjected to compressive forces, where the sample on the left has a cross sectional area larger than the indenter and the sample on the right has a cross sectional area smaller than the indenter (Todd et al., 1998, p.223).

It has therefore been recommended that researchers choose the size of their testing material similar to the intended application. For example, if research is being conducted on seat cushions, than the indenter should be smaller than the sample as most buttocks would sit within the cushion, thereby generating shear forces between the two. An indenter with curved sides should also be taken into consideration if the application involves rounded edges, such as a buttock, or in the interest of the present study, a human head (Todd et al., 1998).

2.6 SUMMARY

Current helmet designs are limited in their protective capabilities by ignoring research defining differences between injury mechanisms and thresholds in children and adults. Two primary differences exist between helmet standards: impact energy (determined by impact velocity and headform weight) and pass/fail criteria (injury thresholds) (Thom, 2007). Arguments have been made regarding these differences in children and adults. The purpose of the current study was not to discover these differences, rather to identify the effects of two variables, impact mass and inbound velocity, that have largely been ignored in previous helmet testing.

As mentioned, American helmet standards, such as the CPSC and SNELL foundation, are testing helmets with headforms of variable sizes, but with a constant mass (Becker, 2000). Since human beings, especially those of much younger ages, have a considerable range of head masses it was of interest to understand what effect this plays on the energy attenuation abilities of helmets. Some standards, such as the Canadian Standards Association have recognized this concern and in fact recently adjusted their helmet standards for children and use lighter headforms for testing (Becker, 2000; CAN/CSA-D113.2-M89, 19[illegible]). Further research is needed to understand the effect that mass has on energy transfer and the risk of head injury (Becker, 2000; Newman, 2006).

It is argued that since a padded surface absorbs energy from impacts through crushing, the mechanical properties of the pad needs to be adjusted to match the mass as well as the velocity of the impacting object (Martin et al., 1994). A heavier object would deform a pad more severely than a lighter object, as well as it would take a longer period of time to completely stop the object. Hence, if a pad (or helmet liner) is too stiff or the impact mass is too light, the deformation of the material upon impact would be too small to be effective (Martin et al., 1994).

Many experimental studies have been conducted to characterize the impact properties of polymeric foams; however, it is argued that the results of these studies are "scattered and not sufficiently general" (Avalle et al., 2001, p.457). An accurate understanding of the energy absorption capacity of polymeric foams under dynamic testing is necessary for effective helmet design. Quasi-static testing is necessary to quantify each material, such as foam strain-rate sensitivity, and understand the influence of certain design parameters (Avalle et al., 2001). Overall, since foam material functions within a prescribed energy range, it is presumed that current helmet liners could be improved significantly if smaller parameters were considered in their design.

CHAPTER 3. METHODOLOGY

3.1 MATERIALS

The three material types, expanded polystyrene, expanded polypropylene, and vinyl nitrile, used in this study represent materials used in bicycle, hockey, and football helmet designs. Their structures are unique and consequently they are used for different purposes. As mentioned previously, EPS is used in single impact helmets and EPP and VN is used for multiple impact helmets. The three materials subsequently can not be compared to one another; however, it is of interest to see whether the trends observed from the study were similar across material types. Since many helmets combine more than one material type, it is useful to know if they react similarly throughout various impact energies.

Three densities were chosen to represent an average range of the most common helmet liner density for bicycling, hockey, and football. According to the product manager at Easton Bell Sports, bicycle helmets are generally moulded at 70.5 kilograms per cubic metre (kg/m^3). The product engineer at Polymos Inc. suggested and supplied an appropriate range of densities for expanded polystyrene and expanded polypropylene based on his knowledge regarding bicycle and hockey helmet design. Manufacturers are reluctant to provide exact specifications regarding material structure; however, a range about the approximated average demonstrated the objective of the present study.

Three types of foam materials were used for this study:

1. Expanded polystyrene (EPS), in three nominal densities (62.95, 83.46, 100.12 kg/m^3)
2. Expanded polypropylene (EPP), in three nominal densities (44.53, 83.94, 117.09 kg/m^3);
3. Vinyl nitrile (VN 602, VN 600, VN 740), equivalent to 97.32, 111.62, and 127.17 kg/m^3, respectively.

3.1.2 MATERIAL PREPARATION

The dimensions of foam samples were measured using a digital micrometer and recorded to minimize any variations in the foam samples. The thicknesses of 20 randomly selected samples of each material density were recorded as an average of three measurements taken at three different contact points. The average thickness and standard deviation for each material was 2.572 cm and 0.0458 cm respectively. Results for each density are presented in table B3 in appendix B.

For the dynamic drop tests, a hole saw with a diameter of 5.0 cm was used to cut all material samples. Material thickness was kept constant at 2.54 cm, which compares to the thickness of the dynamic air chambers. As well, all samples were tested under ambient conditions. The average temperature and humidity in the lab during testing was 23.7 (+/-1.11°) degrees and 45.57% (+/-3.82%).

The diameter of the samples used during the quasi-static compressive testing was 5.0 cm and the thickness was kept constant at 2.54 cm, which is similar to the dynamic samples. These dimensions fit in accordance with the International Standard (ISO) 3388/1, which states that the dimensions of a compression specimen must have a minimum thickness of 10 mm and a minimum diameter/thickness ratio of 2:1 (ISO 3388/1, 1986).

3.1.3 MATERIAL VALIDATION

The density of EPS and EPP is demonstrated using the specification sheets provided by Polymos Inc, which are presented in appendix B. For VN 602, 600, and 740, the density was quantified using density = mass/volume (d =m/V) (Gillette, Neidig, & Spencer, 1999) and weighed using a Denver Instruments SI603 scale. The volume of the materials was determined by measuring the diameter and depth of the cylindrical samples. For each measurement, three trials were averaged. The average mass was converted into kilograms and the average weight was converted into cubic metres to determine density.

3.2 COMPRESSION TESTING

3.2.1 GENERAL DESCRIPTION: INSTRON

Material compression testing was conducted using a universal electromechanical material testing machine called the Instron 5560 Series Dual Column System. The Instron 5560 Series is a universal testing machine used for evaluating mechanical characteristics of material specimens subjected to tension and compression stress (Instron, 1997).

In the present study, the compression test determined the load-deformation characteristics of each foam sample used in the present study at very low strain rates. Each sample was compressed and the deformation at various loads was stored and measured using the computer software program provided by Instron. The force was measured from a load cell and displayed on a computer, where the compressive stress and strain were calculated and plotted as a stress-strain curve. The elastic modulus, yield load, yield stress, and yield strain strength were determined from this curve. All three yield values were reported to account for readers who may relate to one value more than the other.

Testing procedures were programmed and controlled by a computer to ensure high accuracy and repeatability of results. The 5560 Series has a maximum load of 50 kN, a 500 Hz data acquisition rate, and a load accuracy of 0.4% of the indicated load (Instron, 1997).

3.2.2 PROCEDURE

The foam samples were positioned flat between a support surface and a compression plate. The foam was positioned such that the compression plate overlapped the sample in all directions as specified by the ISO 3386/1 standard. The load was then applied perpendicular to the tangential face of the foam specimen. The compression plate was set to compress the sample at a uniform relative rate of 100 mm/min until a compression of 80% of the initial sample thickness was achieved (ISO 3386/1, 1986). The machine recorded the amount of force used during compression to an accuracy of +/- 0.1%, as well as the thickness of the sample to a precision of +/- 0.2 mm. This procedure was repeated three more times and results were averaged. All testing was conducted at ambient conditions.

3.3 DYNAMIC IMPACT TESTING

3.3.1 GENERAL DESCRIPTION: MONORAIL

To test the dynamic energy absorption characteristics of the materials a monorail helmet impactor was used. The monorail is designed to simulate a free falling human head and is often used in helmet testing standards. Below is an image of the monorail and its various components.

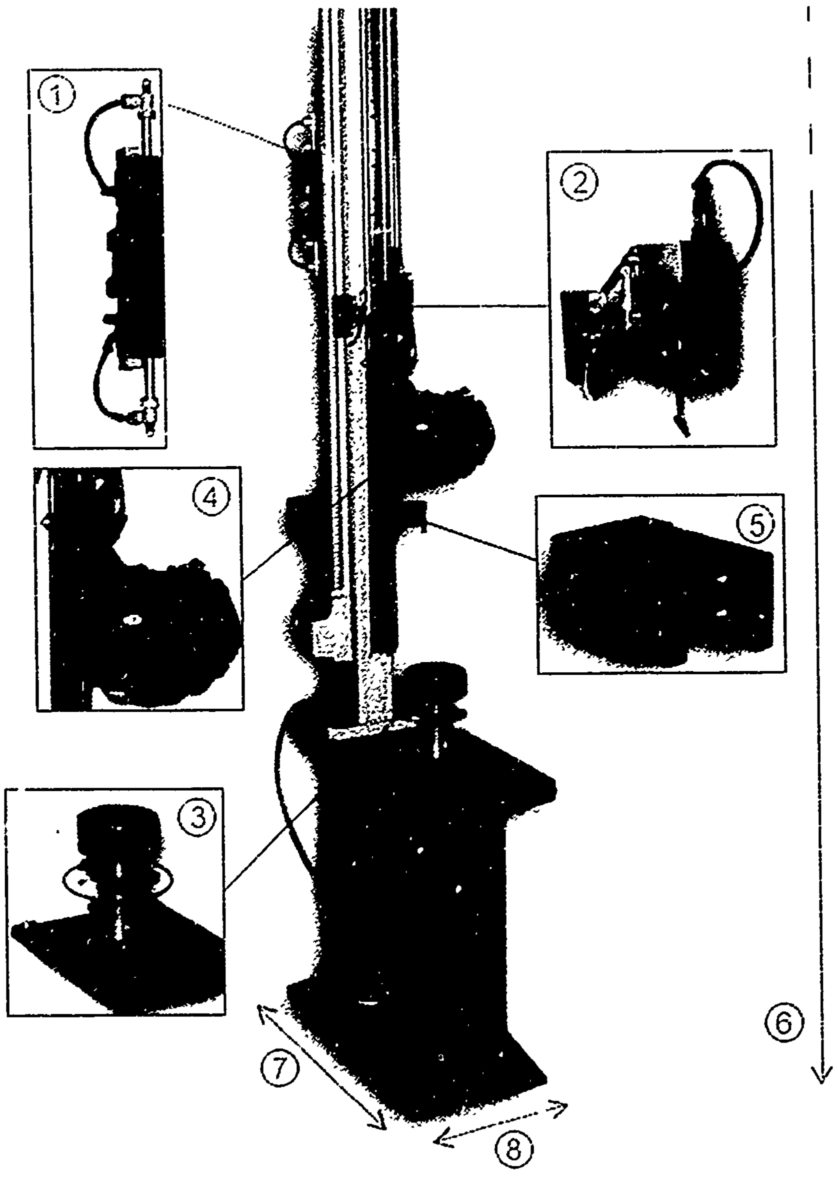

1. Tri-axial headform catch
2. Drop carriage
3. Anvil quick release support clamp
4. Half magnesium headform K1A
5. Time gate
6. Linear impactor track
7. The depth of the base: 63.5 cm
8. The width of the base: 31.8 cm

Figure 15 The lower half of a monorail helmet impactor and its various components (Cadex, 2006b).

The monorail consists of a carriage assembly upon which various types of headforms can be attached by way of a universal ball. For the purpose of this study, a half EN 960 magnesium K1A headform used for uni-axial impacts was used. On the magnesium headform is a socket-like opening that the universal ball can be secured (see figure 16). Four studs on the impactor were used to position the ball on the headform's center of gravity, where additional weights were mounted when needed.

Figure 16 The half magnesium headforms K1A displaying the socket-like opening (a) used for uni-axial impact tests and the five most commonly used headform sizes: A, E, J, M, and O (b) (Cadex, 2006a).

The above half headforms were designed to meet the ISO/DIS 6220 Standards and are composed of 100% pure magnesium with an additive of 0.3% to 0.7% zirconium (Cadex, 2006a). The detailed diagram of these headforms can be found in appendix A.

An anvil, composed of 6061T6 aluminum red anodice 2.54 cm thick by 19.1 cm in diameter, is mounted with a quick release device to the base of the system (see 3 from figure 15) (Cadex, 2006b). The quick release device is used to securely hold the impact anvil to the base of the monorail and can be put on and taken off without any mechanical tools. A metal plate was fixed to the anvil upon which a PCB model 203B force ring rested. On top of the force ring was a 1.1 cm by 16 cm diameter steel cylindrical anvil that the testing samples rested on. This set-up is shown below displaying various components of the system.

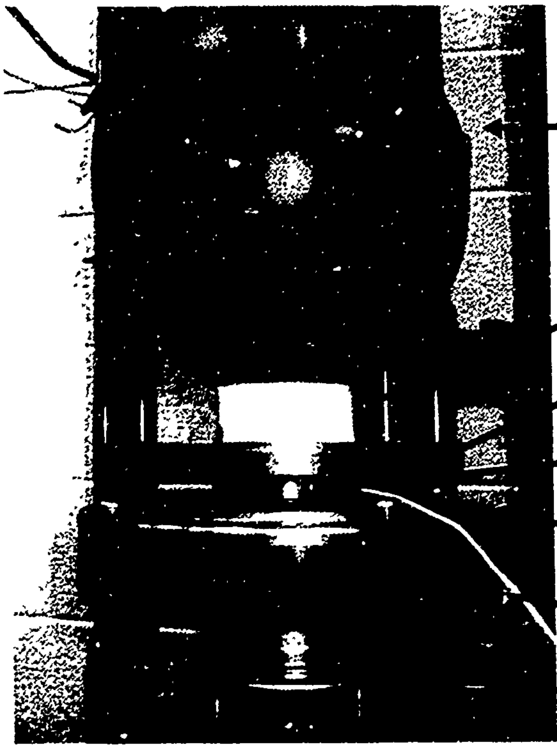

Figure 17 Half magnesium headform impacting VN 740, 2.54 cm thick with 6 cm diameter.

The base of the machine is 67.3 cm high, 30.5 cm wide, and 38.1 cm deep and is fixed to the floor using 6 concrete bolts. The 6 metre vertical track is also bolted to the wall and to the ceiling to prevent any movement of the system and eliminate background noises and vibrations. A computer software program, Photron Motion Tools, was used for acquiring and recording test data.

3.3.2 HEADFORM WEIGHTS

HEADFORM	A	E	J	M	0
Serial number #	4811	4824	4801	4770	4781
Headform Weight	1806	2464	3109	3201	3356
Split Ring Clamp	421	421	421	421	421
4 Bolts for Clamp	83	83	83	83	83
Total Flying Arm	677	677	677	677	677
Accelerometer Kits	11	11	11	11	11
Aluminum Ball Arm	589	589	589	589	589
TOTAL mass	**3587** g	**4245** g	**4890** g	**4982** g	**5137** g

Figure 18 Headform and support assembly weights in grams (g).

The smallest headform model A was used and calibrated 0.500 kg weights were added to the headform to represent a range in head masses, while keeping the geometrical configuration constant. The 0.500 kg weights were positioned over the center of gravity of the headform and attached using four metal bolts. The radius of the headforms decrease with decreasing head mass, similar to what would occur in a real human head. It is however, important to manipulate one variable at a time, thus the circumference of the headform and impact foot print were kept constant.

In addition, all impacts were conducted in the crown position. The geometrical shape of the headforms vary with differing head positions, thus one location had to be chosen. The crown position represents an impact on the top of the head and is easy to accurately position on the ball and arm support assembly. As well, this position allows for a flat opening for the 0.5 kg weights to be added over the headforms center of gravity. Figure 19 displays the weights added to the headform.

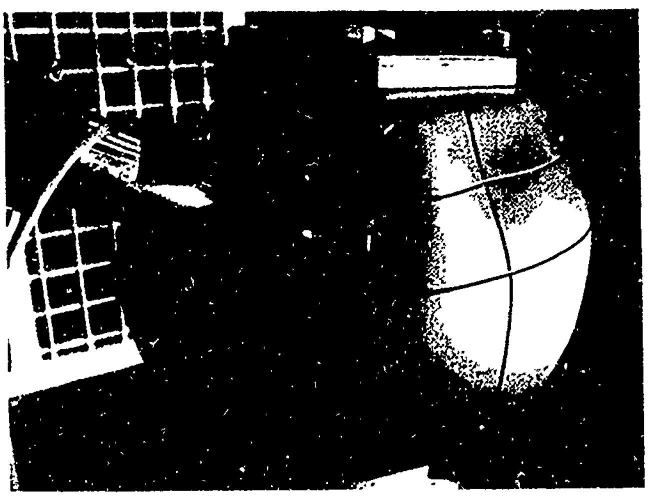

Figure 19 A half ISO Magnesium headform, size A, with four 0.5 kg weights attached over the headforms center of gravity.

3.3.3 FORCE SENSOR

The PCB 203B force sensor collected at 20000 hertz and was impacted directly above the vertical axis. This produced a signal on impact which was conditioned by a model 484B series PCB signal conditioner and passed on by BNC to an A/D board to a computer through a National Instruments PCI 6023E NiDaq card (Post, 2006). The force signal was collected by a computer using Photron Motion Tools Suite and analyzed using both Photron Motion Tools Suite and BioProc2. From this computer software program, force signals were graphed over time and impulse was calculated.

3.3.4 HIGH SPEED CAMERA

A Fastcam 512 PCI high speed camera was used to video all impacts at 2000 frames per second. The camera was set up orthogonal in front of the impact site and was connected directly to the computer. Photron Motion Tools Suite recorded the force data synchronized with video for each dynamic impact trial. Two spot lights were directed at the impact location to enhance the video image clarity and a TTL (transistor-to-transistor logic) trigger was used to synchronize the digital imaging with the data acquired from the force sensor. This was done by pressing a button immediately preceding the impact.

3.3.2 PROCEDURE

The monorail and all supporting equipment were warmed-up prior to testing. The signal conditioner, in particular, was warmed up 10-15 minutes prior to data collection to thermally stabilize the systems components, which was indicated by the metre on the signal conditioner by reading "green". A twin-wire cable attached the signal condition to the force sensor.

A new foam sample was used for each dynamic impact condition on the monorail and the EPP, VN, and EPS samples were impacted once per impact condition. Thus, a total of 25 conditions (5 inbound velocities × 5 drop masses) were tested for each material and 5 sets were conducted for reliability and validity purposes. Inbound velocity was calculated by manual video digitization, where the video data was filmed at 2000 frames per second.

3.4 MONORAIL CALIBRATION

3.4.1 FORCE SENSOR

The force ring was preconditioned by preloading it to a fixed output as specified in the ICP Force Sensor Operation Manual (Model 203B ICP. Dynamic Force Sensor Installation and Operating Manual). On November 16th, 2006 a traceable calibration graph from the National Institute of Standards and Technology (NIST) was provided with the force sensor. During this calibration, the sensor was preloaded to 4000 pounds (lbs) using a 081A13 beryllium copper mounting stud. At 4000 lbs, the output read was 0.952 volts (V) (Coleman, 2006). The test data produced were as follows:

Table 1 Test data indicating the input (lbs) and output (V) from the calibration certificate for the ICP 203B Force Sensor conducted in 2006 provided by PCB Piezotronics (Coleman, 2006).

INPUT (LBS)	OUTPUT (V)
4000	0.952
8000	1.911
12,000	2.869
16,000	3.831
20,000	4.809

To prepare the force sensor for data collection, a copper beryllium stud was used to preload the sensor which was centered within a plate located on top of the sensor. The plate allowed for the bolt to pass through and not "shunt" any force (Model 203B ICP). A digital voltmeter (DVM) was connected to the PCB signal conditioner and zeroed. The DVM was then used to monitor the sensor output voltage to ensure the desired preload value was achieved. The PCB signal conditioner was on DC coupling to have slower signal decay, which allowed for a more precise preloading value to be achieved. The force plate was tightened until a pre-load value of 0.952 volts and an input of 4000 pounds was indicated (Model 203B ICP).

After preloading, the force sensor was further validated by placing a known mass on top of the plate. By comparing the force value exported to the computer to the vertical force of the known weight, the accuracy of the force sensor was determined. The force registered force was the same as the known applied force, so the system was considered calibrated.

3.5 DESIGN

An observational, fully crossed design (see tables 2, 3, 4) was used for all data collection. There was no effect on order of treatments; therefore, it was not necessary to randomize trials since each impact condition was completely independent from the other.

Table 2 Cross-sectional research design for expanded polystyrene.

	A1	A2	A3	
B1	A1B1C1	A2B1C1	A3B1C1	**C1**
	A1B1C2	A2B1C2	A3B1C2	
	A1B1C3	A2B1C3	A3B1C3	
	A1B1C4	A2B1C4	A3B1C4	
	A1B1C5	A2B1C5	A3B1C5	
B2	A1B2C1	A2B2C1	A3B2C1	**C2**
	A1B2C2	A2B2C2	A3B2C2	
	A1B2C3	A2B2C3	A3B2C3	
	A1B2C4	A2B2C4	A3B2C4	
	A1B2C5	A2B2C5	A3B2C5	
B3	A1B3C1	A2B3C1	A3B3C1	**C3**
	A1B3C2	A2B3C2	A3B3C2	
	A1B3C3	A2B3C3	A3B3C3	
	A1B3C4	A2B3C4	A3B3C4	
	A1B3C5	A2B3C5	A3B3C5	
B4	A1B4C1	A2B4C1	A3B4C1	**C4**
	A1B4C2	A2B4C2	A3B4C2	
	A1B4C3	A2B4C3	A3B4C3	
	A1B4C4	A2B4C4	A3B4C4	
	A1B4C5	A2B4C5	A3B4C5	
B5	A1B5C1	A2B5C1	A3B4C1	**C5**
	A1B5C2	A2B5C2	A3B4C2	
	A1B5C3	A2B5C3	A3B4C3	
	A1B5C4	A2B5C4	A3B4C4	
	A1B5C5	A2B5C5	A3B4C5	

LEGEND

Material:	Impact mass:	Inbound velocity:
A1 = EPS 62.95 kg/m^3	B1 = 3.59kg	C1 = 1.0 m/s
A2 = EPS 83.46 kg/m^3	B2 = 4.09 kg	C2 = 2.0 m/s
A3 = EPS 100.12 kg/m^3	B3 = 4.59 kg	C3 = 3.0 m/s
	B4 = 5.09 kg	C4 = 4.0 m/s
	B5 = 5.59 kg	C5 = 5.0 m/s

Table 3 Cross-sectional research design for expanded polypropylene.

	A1	A2	A3	
B1	A1B1C1	A2B1C1	A3B1C1	**C1**
	A1B1C2	A2B1C2	A3B1C2	
	A1B1C3	A2B1C3	A3B1C3	
	A1B1C4	A2B1C4	A3B1C4	
	A1B1C5	A2B1C5	A3B1C5	
B2	A1B2C1	A2B2C1	A3B2C1	**C2**
	A1B2C2	A2B2C2	A3B2C2	
	A1B2C3	A2B2C3	A3B2C3	
	A1B2C4	A2B2C4	A3B2C4	
	A1B2C5	A2B2C5	A3B2C5	
B3	A1B3C1	A2B3C1	A3B3C1	**C3**
	A1B3C2	A2B3C2	A3B3C2	
	A1B3C3	A2B3C3	A3B3C3	
	A1B3C4	A2B3C4	A3B3C4	
	A1B3C5	A2B3C5	A3B3C5	
B4	A1B4C1	A2B4C1	A3B4C1	**C4**
	A1B4C2	A2B4C2	A3B4C2	
	A1B4C3	A2B4C3	A3B4C3	
	A1B4C4	A234C4	A3B4C4	
	A1B4C5	A2B4C5	A3B4C5	
B5	A1B5C1	A2B5C1	A3B4C1	**C5**
	A1B5C2	A2B5C2	A3B4C2	
	A1B5C3	A2B5C3	A3B4C3	
	A1B5C4	A2B5C4	A3B4C4	
	A1B5C5	A2B5C5	A3B4C5	

LEGEND

Material:	Impact mass:	Inbound velocity:
A1 = EPP 44.53 kg/m^3	B1 = 3.59 kg	C1 = 1.0 m/s
A2 = EPP 83.94 kg/m^3	B2 = 4.09 kg	C2 = 2.0 m/s
A3 = EPP 117.09 kg/m^3	B3 = 4.59 kg	C3 = 3.0 m/s
	B4 = 5.09 kg	C4 = 4.0 m/s
	B5 = 5.59 kg	C5 = 5.0 m/s

Table 4 Cross-sectional research design for vinyl nitrile.

	A1	A2	A3	
B1	A1B1C1	A2B1C1	A3B1C1	**C1**
	A1B1C2	A2B1C2	A3B1C2	
	A1B1C3	A2B1C3	A3B1C3	
	A1B1C4	A2B1C4	A3B1C4	
	A1B1C5	A2B1C5	A3B1C5	
B2	A1B2C1	A2B2C1	A3B2C1	**C2**
	A1B2C2	A2B2C2	A3B2C2	
	A1B2C3	A2B2C3	A3B2C3	
	A1B2C4	A2B2C4	A3B2C4	
	A1B2C5	A2B2C5	A3B2C5	
B3	A1B3C1	A2B3C1	A3B3C1	**C3**
	A1B3C2	A2B3C2	A3B3C2	
	A1B3C3	A2B3C3	A3B3C3	
	A1B3C4	A2B3C4	A3B3C4	
	A1B3C5	A2B3C5	A3B3C5	
B4	A1B4C1	A2B4C1	A3B4C1	**C4**
	A1B4C2	A2B4C2	A3B4C2	
	A1B4C3	A2B4C3	A3B4C3	
	A1B4C4	A2B4C4	A3B4C4	
	A1B4C5	A2B4C5	A3B4C5	
B5	A1B5C1	A2B5C1	A3B4C1	**C5**
	A1B5C2	A2B5C2	A3B4C2	
	A1B5C3	A2B5C3	A3B4C3	
	A1B5C4	A2B5C4	A3B4C4	
	A1B5C5	A2B5C5	A3B4C5	

LEGEND

Material:
A1 = VN 602
A2 = VN 600
A3 = VN 740

Impact mass:
B1 = 3.59 kg
B2 = 4.09 kg
B3 = 4.59 kg
B4 = 5.09 kg
B5 = 5.59 kg

Inbound velocity:
C1 = 1.0 m/s
C2 = 1.5 m/s
C3 = 2.0 m/s
C4 = 2.5 m/s
C5 = 3.0 m/s

3.6 ANALYSIS

3.6.1 STRESS STRAIN CURVES

From the stress-strain curve the elastic modulus and the compressive yield point were determined. The stress (σ_e) at a particular point was calculated using the load (P) and the samples original cross-sectional area (A_0):

$$\sigma_e = P/A_0$$

(Roylance, 2001)

The strain (ε_e) was calculated using displacement (d) and the samples original length (L_o):

$$\varepsilon_e = d/L_0$$

(Roylance, 2001)

Compressive yield is described as the ability of the material to resist crushing from vertical pushing forces (ASTM International: D 1621-04a, 2004). This value was determined just prior the start of the plateau/functional phase of the stress-strain curve using an off-set technique. The yield is the stress required to initiate plastic deformation of the material samples. It is at this point, which permanent deformation occurs and is often referred to as the upper load limit. The elastic modulus was calculated as the slope between two manually selected points on the linear section of the curve prior the plateau phase. For the particular samples investigated an obvious yield point was not noted, therefore, a parallel line to the modulus line was drawn at a chosen offset of 0.2%, a common offset value for plastics (Hibberler, 1991). The point at which the offset line and test curve intersected was defined as the yield point (Instron, 2007).

3.6.2 IMPACT VELOCITY

Impact velocity was calculated using the Fastcam 512 PCI high speed camera by manually calculating distance over time. The high speed camera recorded at 2000 frames per second. Using the video images in Photron Motion Tool Suite Analysis, the impact velocity was calculated by manually tracking 5 frames immediately preceding the impact of each trial. A small reflective marker on the impactor is used to track the video images frame by frame. Using 5 frames, the time interval was calculated using the following technique:

$$1 \text{ second}/2000 \text{ frames} \times 5 \text{ frames} = 0.0025 \text{ seconds}$$

When the tracking was complete, the time data recorded in Photron Motions Tool Suite during the tracking was exported to Excel. Using the calculated thickness of the material samples a distance was found between the 5 frames. This is done by tracking a point on the impact mass from the start to the finish of the selected frames. For example:

$$0.010 \text{ metres} / 0.0025 \text{ seconds} = 4.0 \text{ m/s}$$

Therefore, the inbound velocity found immediately preceding the impact was 4.0 m/s for the example given.

3.6.3 LINEAR ACCELERATION

The impact data was collected and viewed using the computer software programs Photron Motion Analysis Suite and BioProc2. BioProc2 is designed for data processing, analyzing, and displaying (Robertson, 2007). The sampling rate was 20 000 Hertz and a low pass Butterworth filter of 1000 Hertz was used to filter all data, which is the standard cut-off frequency used on the monorail drop system. Low-pass Butterworth filters are commonly used in biomechanics-related research (Manal & Rose, 2003). Force data was then converted into accelerations (g) using the formula, $F = ma$. Force time graphs were generated using tab files created in BioProc2 exported to Microsoft Excel and the maximum force observed during the impact was recorded as peak force.

3.6.4 IMPULSE

Impulse (I) is the integral of force (F) with respect to impact time (t) (Gordon et al., 2006).

$$I = \int F dt$$

(Gordon et al., 2006)

BioProc2 was also used to calculate impulse for all trials. Impulse was recorded during the analysis for peak force, which was filtered at 1000 Hertz. An impulse threshold of 25 Newtons was used to register the start of the impact and the end of signal registered when zero Newtons was reached. This threshold value was slightly greater than the magnitude of noise and variance recorded by the system prior the impact and therefore helped isolate the digital impact data during analysis.

CHAPTER 4. RESULTS

4.1 QUASISTATIC RESULTS

Table 5 Mean and standard deviation test results for VN, EPS, and EPP subjected to quasistatic compression testing.

Material	Elastic Modulus (N/mm^2)	0.2% offset load (N) [Compressive load at yield point]	0.2% offset stress (N/mm^2) [Compress stress at yield point]
VN 602	1.51 (0.15)	90.38 (4.69)	0.0336 (0.002)
VN 600	2.55 (0.74)	135.53 (26.12)	0.049 (0.0092)
VN 740	9.82 (0.27)	390.49 (9.64)	0.133 (0.0064)
EPS 62.95 kg/m^3	16.56 (3.61)	782.60 (56.04)	0.41 (0.034)
EPS 83.46 kg/m^3	23.68 (5.10)	1255.15 (6.47)	0.63 (0.0058)
EPS 100.12 kg/m^3	25.37 (3.77)	1505.35 (10.33)	0.79 (0.015)
EPP 44.53 kg/m^3	2.49 (0.23)	234.40 (16.81)	0.095 (0.0091)
EPP 83.94 kg/m^3	8.14 (1.55)	835.61 (19.67)	0.41 (0.01)
EPP 117.09 kg/m^3	15.19 (3.39)	1252.72 (74.88)	0.58 (0.027)

Table 5 displays the mean results with standard deviations for each material subjected to quasistatic testing at a strain rate of 100 mm/min. The elastic modulus increased for each material with increasing material density, as well as the compressive load and stress at the yield point increased with increasing material density. EPS was able to withstand the greatest force values during dynamic testing and had the highest elastic modulus and yield values compared to EPP and VN. The stress versus strain graphs can be found in appendix C.

4.2 DYNAMIC IMPACT RESULTS

For each material type a three-way Analysis of Variance was conducted to determine the effects that material density, inbound velocity, and head mass had on the energy attenuation properties of foams by observing the peak linear acceleration and impulse transmitted through the material upon impact. The dependent variables peak linear acceleration and impulse were analyzed using separate tests because the variables were not completely independent from one another. A bivariate Pearson's Correlation revealed a strong positive relationship between acceleration and impulse for EPS ($r = 0.868$, $p < 0.001$), EPP ($r = 0.852$, $p < 0.001$), and VN (0.766, $p < 0.001$).

There were three densities of each material, five inbound velocities, and five drop masses, which gave a total of 75 possible impact conditions for each material. It was hypothesized that significant differences in peak linear acceleration and impulse would be observed throughout the different impact conditions and an alpha level of 0.05 was used as the significance level.

If significant main effects were found in the previous analysis the partial correlation test was used to determine if linear associations existed between the dependent variables and independent variables. A partial correlation test was chosen to mask the influence of the independent variables not being analyzed so the effects of one independent variable on the dependent variables could be determined. Bivariate correlations were then conducted for impact mass and density at each impact condition to look for trends in the data.

4.3 EXPANDED POLYSTYRENE

4.3.1 ANALYSIS OF VARIANCE

The mean linear acceleration with standard deviation measurements are shown in the table below for each condition EPS samples were impacted.

Table 6 Mean peak linear acceleration (g) and standard deviation (SD) measurements for EPS 62.95, 83.46. and 100.12 kg/m^3 across five impact masses (3.59, 4.09, 4.59, 5.09, and 5.59 kg) and five inbound velocities (1.0, 2.0, 3.0, 4.0, and 5.0 m/s), where n = 5 and N = 360.

		Peak Linear Acceleration (g)					
Mass	Velocity	EPS 62.95 kg/m^3		EPS 83.46 kg/m^3		EPS 100.12 kg/m^3	
(kg)	(m/s)	Mean	SD	Mean	SD	Mean	SD
3.59	1.0	23.54	1.49	34.90	2.83	36.22	1.08
	2.0	31.12	0.90	43.51	0.56	49.08	2.03
	3.0	43.54	0.93	53.48	0.80	61.11	0.92
	4.0	74.71	1.67	73.17	2.53	80.41	1.51
	5.0	175.38	13.25	119.00	6.23	117.17	3.38
4.09	1.0	21.73	0.67	31.41	1.54	32.78	1.63
	2.0	27.25	2.09	40.43	1.38	44.59	0.78
	3.0	43.27	0.53	51 62	2.15	57.98	2.11
	4.0	89.01	5.51	75.16	0.73	80.69	1.38
	5.0	189.81	14.02	134.82	3.80	131.15	3.89
4.59	1.0	19.63	0.94	26.94	1.57	28.78	1.03
	2.0	26.19	1.53	37.10	1.27	41.25	1.35
	3.0	41.72	0.73	46.48	0.90	52.75	1.16
	4.0	140.75	20.50	86.14	2.57	89.71	1.56
	5.0	234.63	6.25	186.14	11.40	156.22	4.27
5.09	1.0	17.63	0.64	26.56	1.04	28.56	1.08
	2.0	25.40	1.01	34.05	0.92	38.07	0.97
	3.0	42.65	1.66	47.44	2.23	51.73	0.97
	4.0	212.59	21.74	111.22	3.85	102.86	2.87
	5.0			219.85	7.65	187.69	10.58
5.59	1.0	16.87	0.61	23.75	0.91	26.06	1.07
	2.0	23.09	0.87	32.21	1.27	35.54	0.75
	3.0	43.16	1.29	43.98	0.97	49.56	0.89
	4.0	226.42	13.43	115.90	8.87	103.07	3.35
	5.0					177.49	8.14

Note: Blank spaces indicate testing was not conducted.

As well, the mean impulse and standard deviations are provided for each impact condition for ESP in table 7.

Table 7 Mean impulse and standard deviation (SD) for EPS 62.95, 83.46, and 100.12 kg/m3 across five impact masses (3.59, 4.09, 4.59, 5.09, and 5.59 kg) and five inbound velocities (1.0, 2.0, 3.0, 4.0, and 5.0 m/s), where n = 5 and N = 360.

		Impulse (N·s)					
Mass	**Velocity**	**EPS 62.95 kg/m³**		**EPS 83.46 kg/m³**		**EPS 100.12 kg/m³**	
(kg)	**(m/s)**	**Mean**	**SD**	**Mean**	**SD**	**Mean**	**SD**
3.59	1.0	5.83	0.24	5.63	0.41	5.38	0.28
	2.0	9.26	0.32	9.19	0.27	9.26	0.31
	3.0	13.20	0.50	12.79	0.04	12.90	0.35
	4.0	17.42	0.53	17.04	0.47	16.83	0.17
	5.0	21.84	0.28	21.78	0.66	20.97	0.03
4.09	1.0	6.22	0.22	6.37	0.42	6.19	0.09
	2.0	10.01	0.30	11.09	0.39	10.35	0.27
	3.0	15.56	0.38	15.17	0.43	14.93	0.12
	4.0	20.32	0.24	19.94	0.12	19.81	0.16
	5.0	26.27	0.77	24.88	0.38	24.47	0.06
4.59	1.0	6.83	0.23	6.91	0.33	6.73	0.44
	2.0	11.80	0.44	11.62	0.21	11.61	0.22
	3.0	16.88	0.14	16.49	0.04	16.55	0.19
	4.0	24.63	0.72	23.78	0.18	23.62	0.25
	5.0	32.01	0.67	29.08	0.23	28.74	0.43
5.09	1.0	7.60	0.52	7.67	0.24	7.61	0.29
	2.0	12.76	0.25	12.67	0.09	12.65	0.29
	3.0	18.81	0.21	18.51	0.16	18.74	0.26
	4.0	28.60	0.29	27.81	0.26	27.39	0.39
	5.0	7.68	0.18	32.52	0.30	32.07	0.20
5.59	1.0	13.85	0.59	8.38	0.42	8.50	0.10
	2.0	21.37	0.59	13.91	0.22	14.02	0.43
	3.0	30.88	0.61	20.41	0.24	20.30	0.21
	4.0			30.01	0.21	29.33	0.08
	5.0					33.82	0.08

Note: Blank spaces indicate testing was not conducted.

The hypotheses that significant differences in peak linear acceleration and impulse would be observed throughout the different impact conditions were supported for expanded polystyrene. There were significant main effects for material density on peak linear acceleration ($F(2, 288) = 367.24$, $p < 0.05$) and impulse ($F(2, 288) = 98.89$, $p < 0.05$). As well, significant main effects were found for head mass on peak linear acceleration ($F(4, 288) = 302.76$, $p<0.05$) and impulse ($F(4, 288) = 5795.876$, $p<0.05$) and finally, significant main effects were found for inbound velocity on peak linear acceleration ($F(2, 288) = 8285.97$, $p<0.05$) and impulse ($F(2, 288) = 41285.35$, $p<0.05$).

Significant two-way interactions between head mass and inbound velocity were found for peak linear interactions ($F(16, 288) = 212.76$, $p<0.05$) and impulse (($F(16, 288) = 30.49$, $p<0.05$). Significant two-way interactions were found between impact mass and density on peak linear acceleration ($F(8, 288) = 54.62$, $p<0.05$) and impulse ($F(8, 288) = 4.22$, $p<0.05$), and between inbound velocity and density for peak linear acceleration ($F(8, 288) = 378.87$, $p<0.05$) and impulse ($F(8, 288) = 30.49$, $p<0.05$). Significant three-way interaction for peak linear acceleration ($F(29, 288) = 32.28$, $p<0.05$) and impulse ($F(29, 288) = 4.77$, $p<0.05$) were found between all of the independent variables; impact mass, inbound velocity, and density.

For EPS, the mean and standard deviation for peak linear acceleration and impulse was 74.25 g +/- 58.62 and 16.89 N·s +/- 8.10, respectively. The estimated marginal mean and standard deviation for peak linear acceleration was 74.25 g +/- 0.291 respectively and the 95% confidence interval was 73.68 g to 74.82. The estimated marginal mean and standard deviation for impulse was 16.89 N·s +/- 0.291 respectively and the 95% confidence interval was 16.86 N·s to 16.93 N·s. The three-way ANOVA revealed the observed power for all main effects and interactions for peak linear acceleration computed were 1.0, meaning there was a 100% chance of finding significant differences between each group in any particular sample with the same sample size. The observed powers for impulse were also all 1.0, except for the two-way interaction between impact mass and density which was 0.994.

Due to mechanical limitations, testing was discontinued when a material reached force values above 15000 N. Therefore, there were missing values for ESP 62.95 kg/m^3 when tested at 5.0 m/s using a 5.09 kg and 5.59 kg impact mass. As well, there were missing data for EPS 83.46 kg/m^3 when tested at 5.0 m/s using a 5.59 kg impact mass. This means a total of 15 impact conditions could not be tested for EPS. These missing values were not replaced for statistical analysis.

An assumption associated with the analysis of variance statistical test is that the error variances of the dependent variables were equal across the groups investigated. The Levene's test of equality of variances; however, revealed that the mean peak linear acceleration and mean impulse were not homogenous across groups ($F(71, 288) = 9.84$, $p<0.05$) and ($F(71, 288) = 2.91$, $p<0.05$). Further analysis of the data revealed a positive kurtosis for peak linear acceleration and a negative kurtosis for impulse, 0.692 and -0.948, respectively. As well, peak linear acceleration and impulse were positively skewed, 1.325 and 0.400, respectively. The kurtosis values are within +/- 1 and the skewness values fell between +/- 2, both of which display normality in the distribution of data (George & Mallery, 2007). Thus, all the data were accepted as normally distributed and despite Levene's test showing heterogeneity across groups, the ANOVA test was used.

The effect size indicates how much of the total variance is explained by each main effect and interaction. In regard to the main effects on peak linear acceleration, inbound velocity was the greatest for EPS, with 99.1% of the total dispersion being explained by its effect in a sample size of 360. Next, impact mass had a moderately high effect size of 80.8% and material density had moderate effect size of 71.8%. The two-way interactions between velocity and impact mass (92.2%) and velocity and density (91.3%) revealed very high significance and the interaction between density and impact mass showed a small 60.3% effect size. Finally, the three-way interactions revealed a 76.5% chance of finding an interaction effect on peak linear acceleration in a sample of 360.

In regards to main effects on impulse, inbound velocity was again the greatest with a 99.8% effect size. Impact mass was next at 98.8% and density had a very low effect size of 40.7%. In regards to the two-way interactions on predicting impulse, impact mass and velocity was the greatest at 96.3%, followed by density and velocity (45.9%) and density and impact mass (10.5%). Finally, the three-way interactions revealed a 32.5% chance of finding an interaction effect on impulse in a sample of 360.

Post hoc testing for impact mass was conducted separately for each combination of material density and velocity using the Bonferroni Test, which assumes homogeneity of variance across means. The Levene's test of equality of variances revealed that the mean linear acceleration and mean impulse were homogenous across groups at each combination of density and velocity ($p > 0.05$). Figure 20 displays the peak linear acceleration results for impact mass at each density for each inbound velocity.

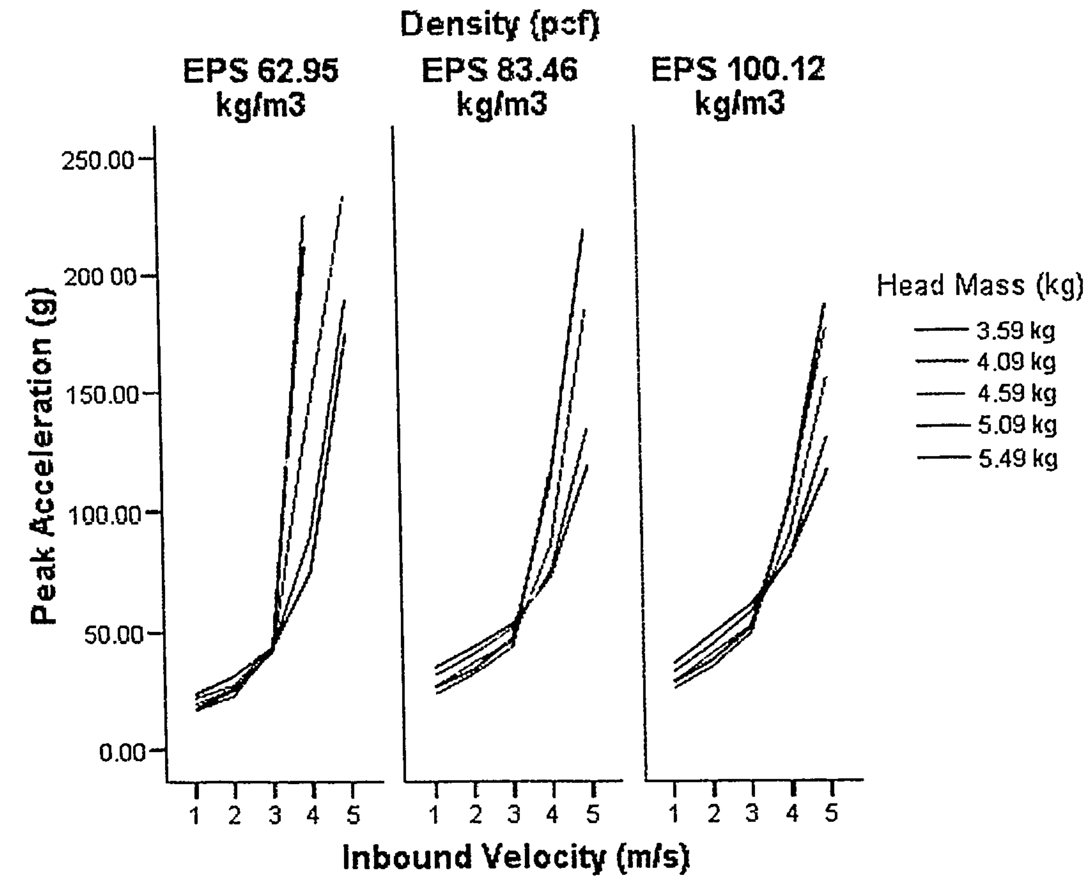

Figure 20 Peak linear acceleration results for EPS 62.95, 83.46, and 100.12 kg/m^3 at velocity 1.0, 2.0, 3.0, 4.0, and 5.0 m/s for each impact mass.

Impact mass was shown to have a significant main effect on peak linear accelerations. The majority of the results were significantly different between impact masses; however, there were some conditions which were not significantly different, such as EPS 62.95 kg/m^3 between 3.59 kg and 4.09 kg at 1.0, 3.0, 4.0, and 5.0 m/s. This can be noted by their close proximity in the first column of the above figure. It should also be pointed out that at 3.0 m/s for EPS 62.95 kg/m^3 each of the impact masses performed insignificantly different ($p > 0.05$). The graphs were intersecting due to the interaction between inbound velocity and impact mass. There were significant peak acceleration differences between 3.59 kg and 4.59 kg, 3.59 kg, and 5.09 kg, 3.59 kg and 5.59 kg, 4.09 kg and 5.09 kg, and 4.09 kg and 5.59 kg at 3.0 m/s for EPS 83.46 kg/m^3 and EPS 100.12 kg/m^3. All of the possible combinations of impact mass are present in table 8 and interactions are "boxed" where significant differences in peak linear acceleration occur.

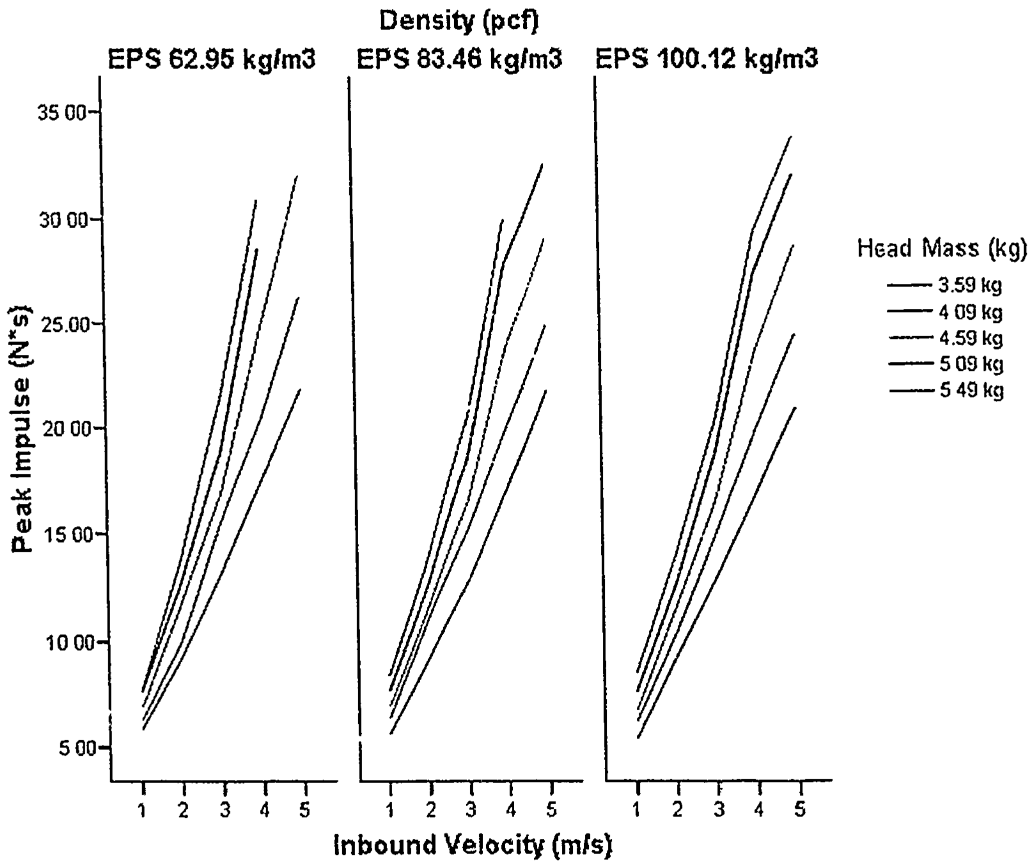

Figure 21 Peak impulse results for EPS 62.95, 83.46, and 100.12 kg/m^3 at velocity 1.0, 2.0, 3.0, 4.0, and 5.0 m/s for each impact mass.

Figure 21 displays that impact mass had a significant effect of impulse measurements for nearly all conditions. Post hoc testing using the Bonferroni test revealed that significant differences were observed for 130 of the 141 comparisons between impact masses. All possible combinations of mass are within each box in table 8 below. Boxed squares represent significant differences in mean peak linear acceleration and an asterisk represents significant differences in impulse between the corresponding masses, where:

M1 = 3.59 kg
M2 = 4.09 kg
M3 = 4.59 kg

M4 = 5.09 kg
M5 = 5.59 kg

Table 8 Significant differences in mean peak linear acceleration (squares ([M] – [M]) and impulse (asterisk(*)) between impact mass (M1 to M5) for EPS 62.95, 83.46, and 100.12 kg/m³ at velocity 1.0, 2.0, 3.0, 4.0, and 5.0 m/s, $p<0.05$.

Material	1.0 m/s	2.0 m/s	3.0 m/s	4.0 m/s	5.0 m/s
EPS 62.95 kg/m³	[M1] - M2 - [M3] * - [M4] * - [M5] * [M2] - [M3] - [M4] * - [M5] * [M3] - [M4] * - [M5] * [M4] - M5	[M1] - [M2] - [M3] * - [M4] * - [M5] * [M2] - M3 * - [M4] * - [M5] * [M3] - M4 * - [M5] * [M4] - M5 *	[M1] - M2 * - M3 * - M4 * - M5 * [M2] - M3 * - M4 * - M5 * [M3] - M4 * - M5 * [M4] - M5 *	[M1] - M2 * - [M3] * - [M4] * - [M5] * [M2] - [M3] * - [M4] * - [M5] * [M3] - [M4] * - [M5] * [M4] - M5 *	[M1] - M2 * - [M3] * [M2] - [M3] *
EPS 83.46 kg/m³	[M1] - [M2] - [M3] * - [M4] * - [M5] * [M2] - [M3] - [M4] * - [M5] * [M3] - M4 - [M5] * [M4] - M5	[M1] - [M2] - [M3] * - [M4] * - [M5] * [M2] - [M3] - [M4] * - [M5] * [M3] - M4 * - M5 * [M4] - M5 *	[M1] - M2 * - [M3] * - [M4] * - [M5] * [M2] - [M3] * - [M4] * - [M5] * [M3] - M4 * - M5 * [M4] - [M5] *	[M1] - M2 * - [M3] * - [M4] * - [M5] * [M2] - [M3] * - [M4] * - [M5] * [M3] - [M4] * - [M5] * [M4] - M5 *	[M1] - [M2] * - [M3] * - [M4] * - [M5] * [M2] - [M3] * - [M4] * - [M5] * [M3] - [M4] *
EPS 100.12 kg/m³	[M1] - [M2] * - [M3] * - [M4] * - [M5] * [M2] - [M3] - [M4] * - [M5] * [M3] - M4 * - [M5] * [M4] - [M5] *	[M1] - [M2] * - [M3] * - [M4] * - [M5] * [M2] - [M3] * - [M4] * - [M5] * [M3] - [M4] * - [M5] * [M4] - M5 *	[M1] - [M2] * - [M3] * - [M4] * - [M5] * [M2] - [M3] * - [M4] * - [M5] * [M3] - M4 * - [M5] * [M4] - M5 *	[M1] - [M2] * - [M3] * - [M4] * - [M5] * [M2] - [M3] * - [M4] * - [M5] * [M3] - M4 * - [M5] * [M4] - M5 *	[M1] - [M2] * - [M3] * - [M4] * - [M5] * [M2] - [M3] * - [M4] * - [M5] * [M3] - [M4] * - [M5] * [M4] - M5 *

Note: Blank spaces indicate testing was not conducted.

Post hoc testing using the Bonferroni test was also conducted to determine whether significant differences between velocities existed at each impact mass and material density. Peak linear acceleration measurements were significantly different between 131 out of 141 comparisons and impulse measurements were all significantly different between all inbound velocities. Significant differences were not found for peak linear accelerations between 1.0 and 2.0 m/s for EPS 83.46 kg/m^3 at all five inbound masses. Significant differences were not observed between 1.0 and 2.0 m/s and 2.0 and 3.0 m/s for EPS 83.46 kg/m^3 at 4.59 kg, as well as between 1.0 and 2.0 m/s for EPS 83.46 kg/m^3 at 5.09 kg and 5.59 kg and EPS 110.12 kg/m^3 at 5.09 kg.

Post hoc testing was also conducted to determine which conditions of material density differed significantly. Significant differences in peak linear acceleration were noted between EPS 62.95 and EPS 100.12 kg/m^3 at all impact conditions (mass cross velocity). EPS 83.46 and 100.12 kg/m^3 did not differ significantly at the following conditions:

3.59 kg at 1.0 and 4.0 m/s,

4.09 kg at 1.0, 4.0, and 5.0 m/s,

4.59 kg at 1.0 and 4.0 m/s,

5.09 kg at 4.0 m/s,

5.59 kg at 5.0 m/s.

In addition, peak linear acceleration between EPS 62.95 and EPS 83.46 kg/m^3 did not differ significantly when impacted using 3.59 kg at 4.0 m/s and 5.59 kg at 3.0 m/s. Finally, post hoc testing for material density revealed that impulse differed significantly for 33 out of 75 combinations. The following graph displays the outcomes for each density across inbound velocity for each impact mass.

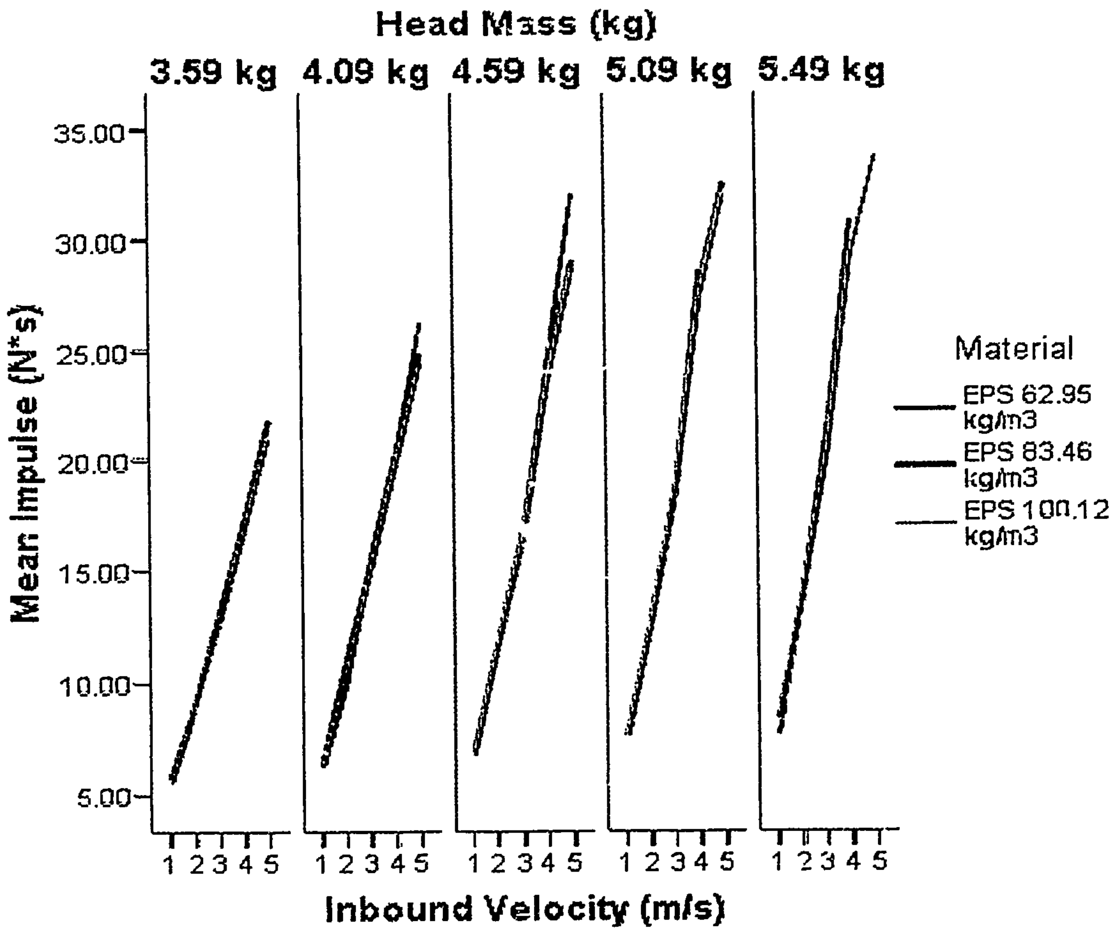

Figure 22 Mean impulse results for EPS 62.95, 83.84, 100.12 kg/m^3 at veloc'ty 1.0, 2.0, 3.0, 4.0, and 5.0 m/s for each impact mass.

Figure 22 displays that the impulse results for each density were very similar for the majority of conditions, indicating that density was a poor predictor for impulse. The change in density did not have an effect on impulse. As a reminder, the effect size for density was only 40.7%.

4.2.2 CORRELATIONS

A partial correlation test revealed that inbound velocity was positively correlated to both acceleration ($r = 0.841$, $p<0.05$) and impulse ($r = 0.893$, $p<0.05$), when controlling for material density and impact mass. This indicates that inbound velocity had a strong linear relationship to both dependent variables. Impact mass produced a small positive relationship between acceleration ($r = 0.201$, $p<0.05$) and large positive relationship with impulse ($r = 0.846$, $p<0.05$), when controlling for inbound velocity and material density. Finally, material density produced a non-linear negative relationship between acceleration (r -0.129, $p<0.05$) and impulse ($r = -0.095$, $p<0.05$). The results are presented in the table below.

Table 9 EPS partial correlation results for each independent variable on the dependent variable, with significance level (N = 360).

	Acceleration (g)		Impulse (N·s)	
	Correlation	Significance	Correlation	Significance
Inbound Velocity (m/s)	0.841	0.000	0.974	0.000
Impact Mass (kg)	0.201	0.000	0.846	0.000
Material Density (kg/m^3)	-0.129	0.015	-0.095	0.073

The figure below was created to display the trend impact mass had on peak linear accelerations at each inbound velocity and material density.

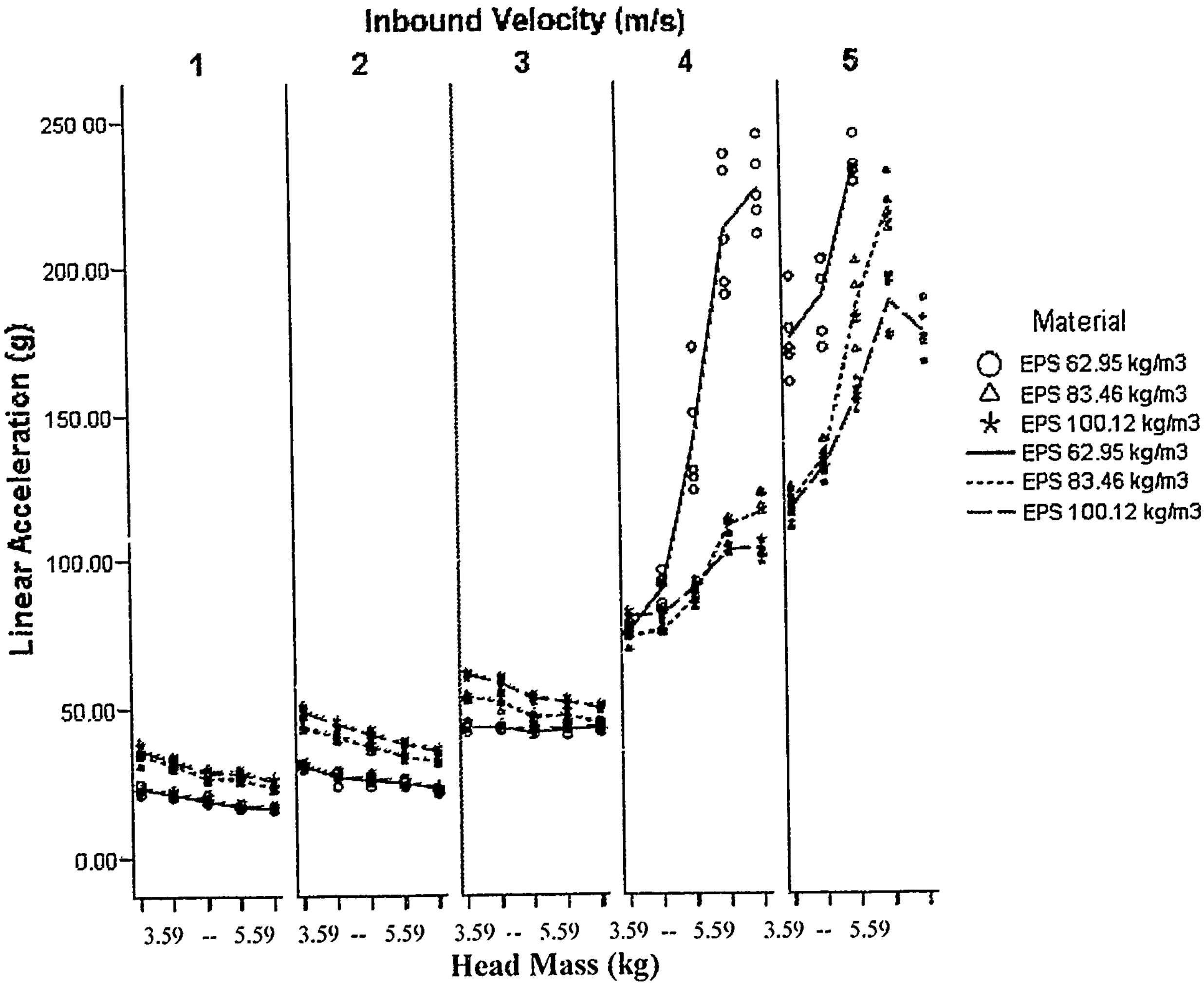

Figure 23 Peak linear acceleration results with interpolation line for EPS 62.95, 83.46, and 100.12 kg/m^3 for increasing impact mass (1-5) at each inbound velocity.

Further investigations using bivariate correlation tests were conducted to determine the relationship between impact mass, acceleration, and impulse for each material density and inbound velocity. The results for acceleration (g) and impulse (N·s) are presented in tabular format below and all results were found to be significant, $p<0.05$.

Table 10 Bivariate correlation results for impact mass, acceleration (g), and impulse (N·s) at each material density and inbound velocity.

Material (kg/m^3)	1.0 m/s		2.0 m/s		3.0 m/s		4.0 m/s		5.0 m/s	
	g	N·s	g	N·s	g	N·s	g	N·s	g	N·s
EPS 62.95	-0.939	0.917	-0.872	0.971	-0.165	0.987	0.952	0.991	0.886	0.989
EPS 83.46	-0.906	0.943	-0.967	0.975	-0.878	0.994	0.933	0.995	0.968	0.994
EPS 100.12	-0.927	0.972	-0.968	0.985	-0.940	0.995	0.930	0.994	0.915	0.990

Overall, a strong negative linear correlation between impact mass and acceleration were found for each density at velocities 1.0, 2.0, and 3.0 m/s, except for EPS 62.95 kg/m^3 at 3.0 m/s. Conversely, at 4.0 m/s and 5.0 m/s a strong positive correlation was found for impact mass. Impulse was strongly and positively correlated to impact mass at all conditions.

Bivariate correlations were not conducted for inbound velocity as there was a strong positive and linear relationship to both acceleration and impulse in the partial correlation. Density however, was analyzed at each impact condition (mass and velocity) and the results are presented below. Not all results were found significant.

Table 11 Bivariate correlation results for material density on acceleration (g) and impulse (N·s) at each impact mass and inbound velocity for EPS.

Mass	1.0 m/s		2.0 m/s		3.0 m/s		4.0 m/s		5.0 m/s	
	g	N s	g	N s	g	N s	g	N·s	g	N s
3.59 kg	0.870	-0.541	0.965	0.000	0.991	-0.335	0.651	-0.532	-0.845	-0.654
4.09 kg	0.891	-0.052	0.942	0.255	0.964	-0.643	-0.532	-0.758	-0.857	-0.826
4.59 kg	0.922	-0.129	0.950	-0.263	0.980	-0.586	0.878	-0.768	-0.912	-0.968
5.09 kg	0.925	-0.045	0.966	-0.223	0.925	-0.042	-0.875	-0.842	-0.89	-0.695
5.59 kg	0.942	-0.769	0.952	0.173	0.871	-0.733	-0.899	-0.879		

Note: Blank spaces indicate testing was not conducted.

From table 11, it is noted that inbound velocity was positively and linearly correlated to acceleration at 1.0 m/s, 2.0 m/s, and 3.0 m/s. At 4.0 m/s and 5.0 m/s, however inbound velocity revealed strong negative relationships between peak linear acceleration. Impulse showed weak correlations to density throughout most of conditions suggesting that density was not a good predictor for impulse. Explanations regarding these trends are in chapter 6.

4.4 EXPANDED POLYPROPYLENE

4.4.1 ANALYSIS OF VARIANCE

The mean linear acceleration with standard deviation measurements are shown in the table below for each condition EPP samples were impacted.

Table 12 Mean peak linear acceleration (g) and standard deviation measurements for EPP 44.53, 83.94, and 117.09 kg/m^3 across five impact masses (3.59, 4.09, 4.59, 5.09, and 5.59 kg) and five inbound velocities (1.0, 2.0, 3.0, 4.0, and 5.0 m/s), where n = 5 and N = 315.

		Peak Linear Acceleration (g)					
Mass	Velocity	EPP 44.53 kg/m^3		EPP 83.94 kg/m^3		EPP 117.09 kg/m^3	
(kg)	(m/s)	Mean	SD	Mean	SD	Mean	SD
3.59	1.0	11.87	0.51	24.53	0.87	32.47	0.72
	2.0	19.59	0.28	34.12	1.24	48.82	1.72
	3.0	55.05	2.93	42.38	0.87	56.02	1.96
	4.0			64.26	4.49	69.84	1.58
	5.0			150.22	4.25	119.51	1.67
4.09	1.0	11.12	0.38	23.24	1.34	31.26	1.19
	2.0	20.33	0.76	31.33	0.73	44.94	1.04
	3.0	68.55	7.79	40.78	0.92	53.46	1.48
	4.0			77.52	5.31	72.76	1.61
	5.0			182.16	12.25	116.91	3.80
4.59	1.0	9.63	0.29	21.77	1.16	26.48	1.08
	2.0	20.25	0.60	27.70	0.63	41.25	0.98
	3.0	82.05	4.85	38.28	0.68	47.36	1.46
	4.0			104.41	7.23	82.13	4.41
	5.0					159.02	1.67
5.09	1.0	8.92	0.17	19.20	0.56	26.37	0.88
	2.0	20.90	0.54	26.23	0.40	35.89	1.18
	3.0	108.14	12.06	37.56	0.89	46.34	1.01
	4.0			148.12	18.17	105.73	7.48
	5.0					202.16	14.34
5.59	1.0	8.11	0.31	18.03	0.87	24.11	1.37
	2.0	21.33	0.45	24.30	0.59	34.41	0.62
	3.0	128.17	10.10	37.71	1.21	44.79	1.52
	4.0			168.18	20.54	109.53	12.56
	5.0					212.87	13.63

Note: Blank spaces indicate testing was not conducted.

As well, the mean impulse and standard deviations are provided for each impact condition for EPP in table 13.

Table 13 Mean impulse (N s) and standard deviation measurements for EPS 44.53, 83.94, and 117.09 kg/m^3 across five impact masses (3.59, 4.09, 4.59, 5.09, and 5.59 kg) and five inbound velocities (1.0, 2.0, 3.0, 4.0, and 5.0 m/s), where n = 5 and N = 315.

		Impulse (N·s)					
Mass	Velocity	EPP 44.53 kg/m^3		EPP 83.94 kg/m^3		EPP 117.09 kg/m^3	
(kg)	(m/s)	Mean	SD	Mean	SD	Mean	SD
3.59	1.0	6.47	0.43	5.85	0.13	5.99	0.12
	2.0	10.47	0.34	10.04	0.10	10.09	0.10
	3.0	15.56	0.26	14.27	0.11	14.47	0.11
	4.0	20.44	0.27	18.69	0.30	18.79	0.32
	5.0			23.96	0.09	23.92	0.27
4.09	1.0	7.22	0.46	6.77	0.08	6.86	0.25
	2.0	12.48	0.20	11.57	0.13	11.77	0.17
	3.0	18.43	0.15	16.58	0.09	16.61	0.35
	4.0			22.25	0.14	22.10	0.14
	5.0			27.48	0.15	27.08	0.15
4.59	1.0	7.73	0.25	7.31	0.08	7.28	0.22
	2.0	13.82	0.18	12.79	0.11	12.87	0.17
	3.0	20.46	0.10	18.38	0.06	18.44	0.08
	4.0			25.83	2.11	26.06	0.17
	5.0					31.39	0.45
5.09	1.0	8.67	0.09	8.20	0.14	8.32	0.13
	2.0	15.52	0.07	14.11	0.07	14.24	0.02
	3.0	23.47	0.51	20.66	0.20	20.68	0.40
	4.0			31.01	0.07	30.51	0.07
	5.0					35.81	0.30
5.59	1.0	9.50	0.12	8.81	0.13	8.92	0.10
	2.0	17.10	0.17	15.50	0.16	15.64	0.11
	3.0	25.33	0.10	22.66	0.08	22.51	0.07
	4.0			33.43	0.12	33.03	0.32
	5.0					37.86	0.31

Note: Blank spaces indicate testing was not conducted.

The hypotheses that significant differences in peak linear acceleration and impulse would be observed throughout the different impact conditions were supported for EPP. There were significant main effects for material density on peak linear acceleration ($F(2, 252) = 401.54$, $p<0.05$) and impulse ($F(2, 252) = 348.84$, $p<0.05$). Significant main effects were found for head mass on peak linear acceleration ($F(4, 252) = 284.71$, $p<0.05$) and impulse ($F(4, 252) = 5901.62$, $p<0.05$) and finally, significant main effects were found for inbound velocity on peak linear acceleration ($F(2, 252) = 4613.92$, $p < 0.05$) and impulse ($F(2, 252) = 34187.12$, $p < 0.05$).

Significant two-way interactions between head mass and velocity were found for peak linear interactions ($F(16, 252) = 119.59$, $p<0.05$) and impulse (($F(16, 252) = 389.15$, $p<0.05$). Significant two-way interactions were found between impact mass and density for peak linear acceleration ($F(8, 252) = 33.12$, $p<0.05$) and impulse ($F(8, 252) = 6.51$, $p<0.05$), and between velocity and density for peak linear acceleration ($F (8, 252) = 401.13$, $p<0.05$) and impulse ($F (8, 252) = 33.19$, $p<0.05$). As well, a significant three-way interaction for peak linear acceleration ($F (29, 252) = 16.61$, $p<0.05$) and impulse ($F (29, 252) = 1.72$, $p<0.05$) were found between all of the independent variables; impact mass, inbound velocity, and material.

For EPP, the mean and standard deviation for peak linear acceleration and impulse was 63.03 g +/- 53.36 and 17.30 N·s +/- 8.28 respectively. The estimated marginal mean and standard deviation for peak linear acceleration was 63.03 g +/- 0.348 g and the 95% confidence interval was 62.34 to 63.72. The estimated marginal mean and standard deviation for impulse was 17.30 N·s +/- 0.019; therefore, the 95% confidence interval was 17.27 to 17.34. The three-way ANOVA revealed the observed power for all main effects and interactions for peak linear acceleration computed were 1.0 and the observed powers for impulse were all 1.0, except for the three-way interaction between impact mass, density, and velocity which was 0.967.

Due to mechanical limitations, testing was discontinued when a material reached force values above 15 000 N. Therefore, there were missing data for EPP 44.53 kg/m^3 when tested at 5 m/s using all impact masses. There was also missing data for EPP 44.53 kg/m^3 at 4 m/s using impact masses of 4.09, 4.59, 5.09, and 5.49 kg. For EPP 83.94 kg/m^3 there were missing values at 5 m/s using 4.59, 5.09, and 5.59 kg impact masses and finally, EPP 117.09 kg/m^3 had no missing data.

The Levene's test of equality of variances however, revealed that the peak linear acceleration and impulse were not homogenous across groups ($F(71, 252) = 6.00$, $p<0.05$) and ($F(71, 252) = 4.87$, $p<0.05$). Further analysis of the data revealed a positive kurtosis for peak linear acceleration and a negative kurtosis for impulse, 0.822 and -0.504 respectively. As well, peak linear acceleration and impulse were positively skewed, 1.326 and 0.566 respectively. The kurtosis values are within +/- 1 and the skewness values fall between +/- 2, both of which display normality in the distribution of data (George & Mallery, 2007). Thus, all the data was treated as normally distributed and despite Levene's test showing heterogeneity across groups, the ANOVA test was used.

In regards to main effects on peak linear acceleration for EPP, inbound velocity was the greatest, with a 98.7% chance of finding this effect to be significant in a sample of 360. Next, impact mass had a high effect size of 81.9% and material density had a 76.1% chance of finding the effect to be significant. The two-way interactions between velocity and impact mass (88.4%) and velocity and density (91.8%) revealed very high effect sizes and the interaction between density and impact mass showed a small 15.3% effect size. Finally, the three-way interactions revealed a low 58.1% chance of finding an interaction effect on peak linear acceleration in a sample of 315.

In regards to main effects on impulse, inbound velocity was again the greatest with a 99.8% chance of finding significance for EPP. Impact mass was next at 98.9% and density had a lower effect size of 73.5%. In regards to the two-way interaction, on predicting impulse, impact mass and velocity was the greatest at 96.1% and density and impact mass (17.1%) and density and velocity (48.0%) were much lower. Finally, the three-way interactions revealed a low 12.5% chance of finding an interaction effect on impulse in a sample of 315.

Again, post hoc testing for impact mass was conducted separately for each combination of material density and velocity using the Bonferroni Test, which assumes homogeneity of variance across means. The Levene's test of equality of variances revealed that the mean linear acceleration and mean impulse were homogenous across groups at each combination of density and velocity ($p > 0.05$). Figure 24 displays the peak linear acceleration results for impact mass at each density and inbound velocity.

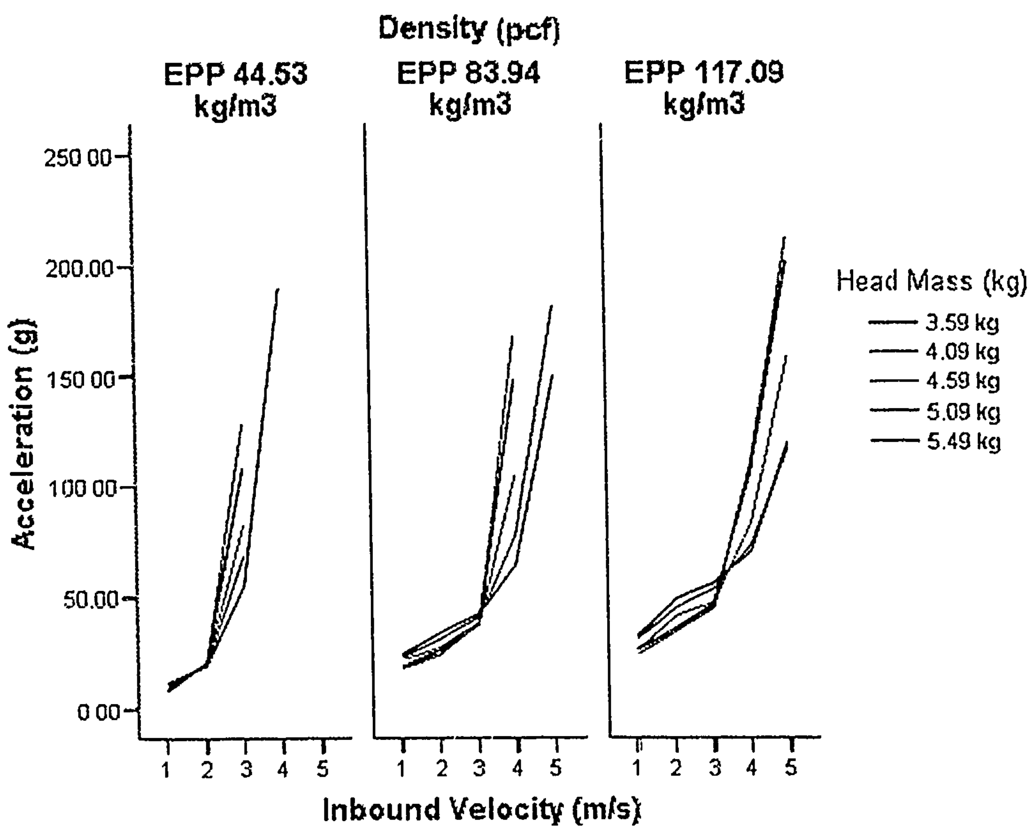

Figure 24 Peak linear acceleration results for each impact mass for EPP 44.53, 83.94, and 117.09 kg/m^3 at velocity 1.0, 2.0, 3.0, 4.0, and 5.0 m/s.

Impact mass was shown to have a significant main effect on peak linear accelerations and impulse for EPP at the three material densities. In particular, all impact masses produced significantly different results for EPP 83.94 kg/m^3 at 1.0 m/s and EPP 117.09 kg/m^3 at 2.0

m/s. This can be observed in figure 25 above. Significant differences in peak linear acceleration were always observed between 3.59 and 5.09 kg and 3.59 and 5.59 kg. Generally, where the curves do not overlap in the figure is where significant differences were found. It is noted that the curves in column one are shorter because the testing resulted in force values greater than 15000 N and was therefore stopped.

.

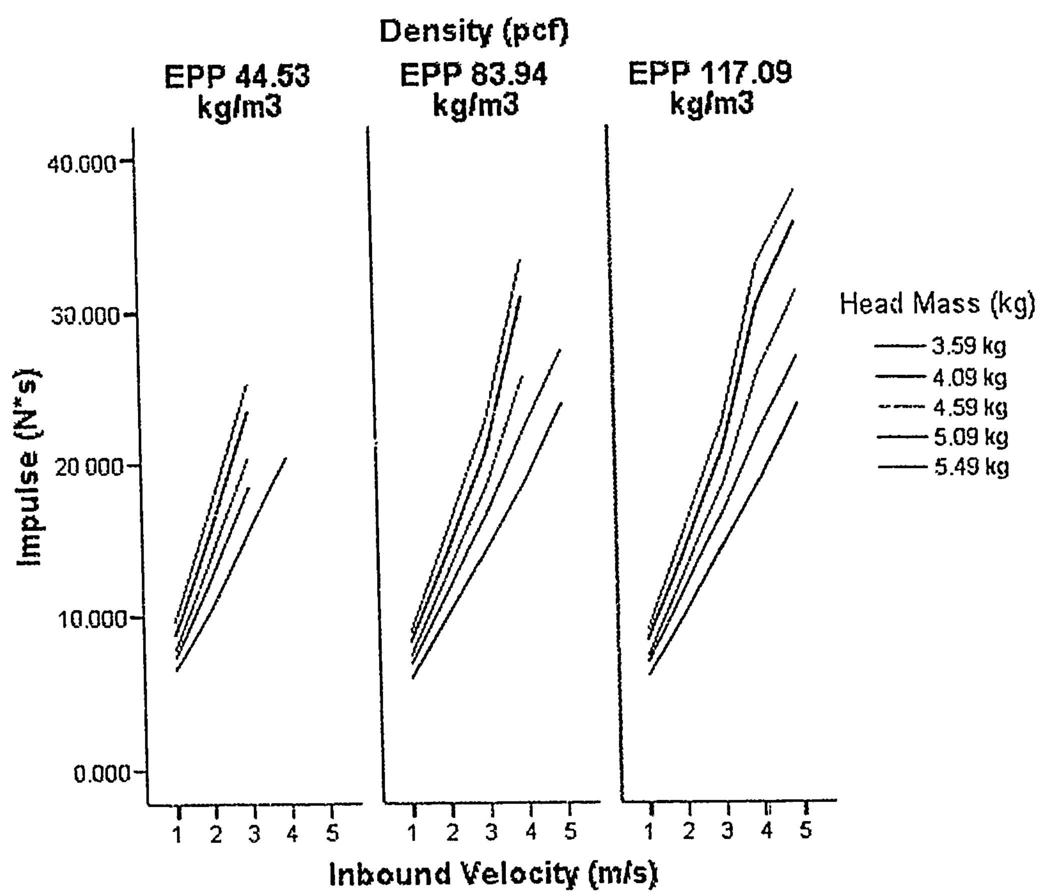

Figure 25 Peak impulse results for each impact mass using EPP 44.53, 83.94, and 117.09 kg/m^3 and velocity 1.0, 2.0, 3.0, 4.0, and 5.0 m/s.

Figure 25 displays that impact mass had a significant effect on impulse measurements for EPP. Post hoc testing using the Bonferroni test revealed that significant differences in impulse were observed for 119 of the 121 comparisons between impact masses at each material density and inbound velocity. The two non-significant findings for impulse were between 4.09 and 4.59 kg and between 5.09 and 5.59 kg for EPP 44.53 at 1 m/s. Table 14 highlights where significant differences in peak linear acceleration and impulse occurred between each impact mass at each velocity and density. The material density is defined for each row and the inbound velocity for each column. All possible combinations of mass with velocity and density are within each box. Boxed squares represent significant differences in mean peak linear acceleration and an asterisk represents significant differences in impulse between the corresponding masses, where:

M1 = 3.59 kg
M2 = 4.09 kg
M3 = 4.59 kg
M4 = 5.09 kg
M5 = 5.59 kg

Table 14 Significant differences for EPP for mean peak linear acceleration (squares ([M_] – [M_]) and impulse (*) between variable impact mass and inbound velocity, where $p<0.05$.

Material	1.0 m/s	2.0 m/s	3.0 m/s	4.0 m/s	5.0 m/s
EPP 62.95 kg/m^3	[M1] - [M2] * - [M3] * - [M4] * - [M5] * [M2] - [M3] - [M4] * - [M5] * [M3] - [M4] * - [M5] * [M4] - [M5]	[M1] - M2* - M3 * - [M4] * - [M5] * [M2] - M3 * - M4 * - M5 * [M3] - M4 * - M5 * [M4] - M5 *	[M1] - M2 * - [M3] * - [M4] * - [M5] * [M2] - M3 * - [M4] * - [M5] * [M3] - [M4] * - [M5] * [M4] - [M5]*		
EPP 83.46 kg/m^3	[M1] - M2* - [M3] * - [M4] * - [M5] * [M2] - M3* - [M4] * - [M5] * [M3] - [M4]* - [M5] * [M4] - M5*	[M1] - [M2] * - [M3] * - [M4] * - [M5] * [M2] - [M3]* - [M4] * - [M5] * [M3] - [M4] * - [M5] * [M4] - [M5] *	[M1] - [M2] * - [M3] * - [M4] * - [M5] * [M2] - [M3] * - [M4] * - [M5] * [M3] - M4 * - [M5] * [M4] - [M5] *	[M1] - M2 * - [M3] * - [M4] * - [M5] * [M2] - [M3] * - [M4] * - [M5] * [M3] - [M4] * - [M5] * [M4] - M5 *	[M1] - [M2] *
EPP 100.12 kg/m^3	[M1] - M2 * - [M3] * - [M4] * - [M5] * [M2] - [M3]* - [M4] * - [M5] * [M3] - [M4] * - [M5] * [M4] - [M5] *	[M1] - M2 * - [M3] * - [M4] * - [M5] * [M2] - [M3] * - [M4] * - [M5] * [M3] - M2 * - [M5] * [M4] - [M5] *	[M1] - M2 * - [M3] * - [M4] * - [M5] * [M2] - [M3] * - [M4] * - [M5] * [M3] - M4 * - M5 * [M4] - M5 *	[M1] - M2 * - M3 * - [M4] * - [M5] * [M2] - M3 * - [M4] * - [M5] * [M3] - [M4] * - [M5] * [M4] - M5 *	[M1] - M2 * - [M3] * - [M4] * - [M5] * [M2] - [M3] * - [M4] * - [M5] * [M3] - [M4] * - [M5] * [M4] - M5 *

*Blank spaces indicate testing was not conducted.

Post hoc testing using the Bonferroni test was also conducted to determine where significant differences between velocities existed at each impact mass and material density. Peak linear acceleration measurements were significantly different for nearly all inbound velocities, except between 1.0 and 2.0 m/s for EPP 44.53 kg/m^3 at 3.59 kg. Significant differences were not observed between 1.0 and 2.0 m/s and 2.0 and 3.0 m/s for EPP 83.94 kg/m^3 at 4.59, 5.09, and 5.59 kg and EPP 117.09 kg/m^3 at 3.59, 5.09, and 5.59 kg. Impulse was found to be significantly different between all inbound velocities at each impact condition.

Post hoc testing using the Bonferonni test revealed significant differences for peak linear acceleration between each material density at all combinations of inbound velocities and impact masses, except for four conditions. Non-significant differences were noted between EPP 44.53 kg/m^3 and EPP 117.09 kg/m^3 at 3.0 m/s using 3.59 kg. In addition, no significant differences were found between EPP 83.94 kg/m^3 and EPP 117.09 kg/m^3 at 3.0 m/s using 4.59 and 5.09 kg, as well as at 4.0 m/s using 3.59 kg. Using impulse as the dependent variable, significant differences were generally not observed across EPP 83.94 kg/m^3 and EPP 117.09 kg/m^3 at each inbound velocity and impact mass. EPP 44.53 kg/m^3 was generally significantly different than EPP 83.94 kg/m^3 and EPP 117.09 kg/m^3 for each condition. The figure below displays the outcomes for each density across inbound velocity and impact mass.

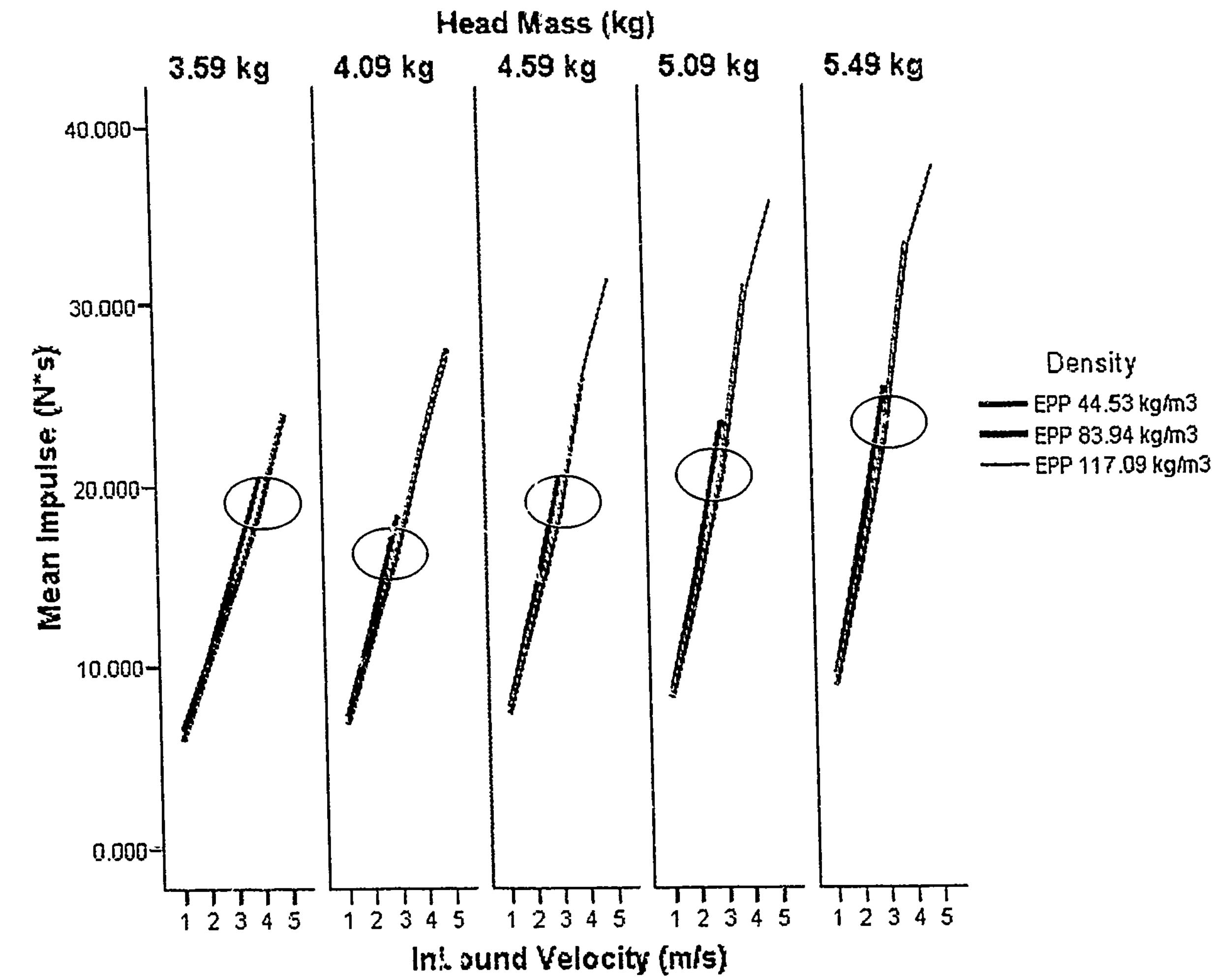

Figure 26 Peak impulse results for EPP 44.53, 83.94, and 117.09 kg/m^3 at velocity 1.0, 2.0, 3.0, 4.0, and 5.0 m/s for each impact mass.

When two curves overlapped, significant differences were not observed. EPP 44.53 was always significantly different than the other two densities for each impact mass at 3.0 m/s. This is pointed out by the circles in the figure.

4.4.2 CORRELATIONS

A partial correlation test revealed that inbound velocity was positively correlated to both acceleration ($r = 0.843$, $p<0.05$) and impulse ($r = 0.973$, $p<0.05$), when controlling for material density and impact mass. This indicates that inbound velocity had a strong linear relationship to both dependent variables. Impact mass produced a small positive relationship between acceleration (r = 0.191, p<0.05) and large positive relationship with impulse (r = 0.862, p<0.05), when controlling for inbound velocity and material density. Finally, material density produced a non-linear negative relationship between acceleration (r -0.075, p<0.05) and impulse (r = -0.148, p<0.05). The results are presented in the table below.

Table 15 EPP partial correlation results for each independent variable on the dependent variable, with significance level (N = 315).

	Acceleration (g)		Impulse (N·s)	
	Correlation	Significance	Correlation	Significance
Inbound Velocity (m/s)	0.843	0.000	0.973	<0.0005
Impact Mass (kg)	0.191	0.000	0.862	<0.0005
Material Density (kg/m^3)	-0.075	0.094	-0.148	0.004

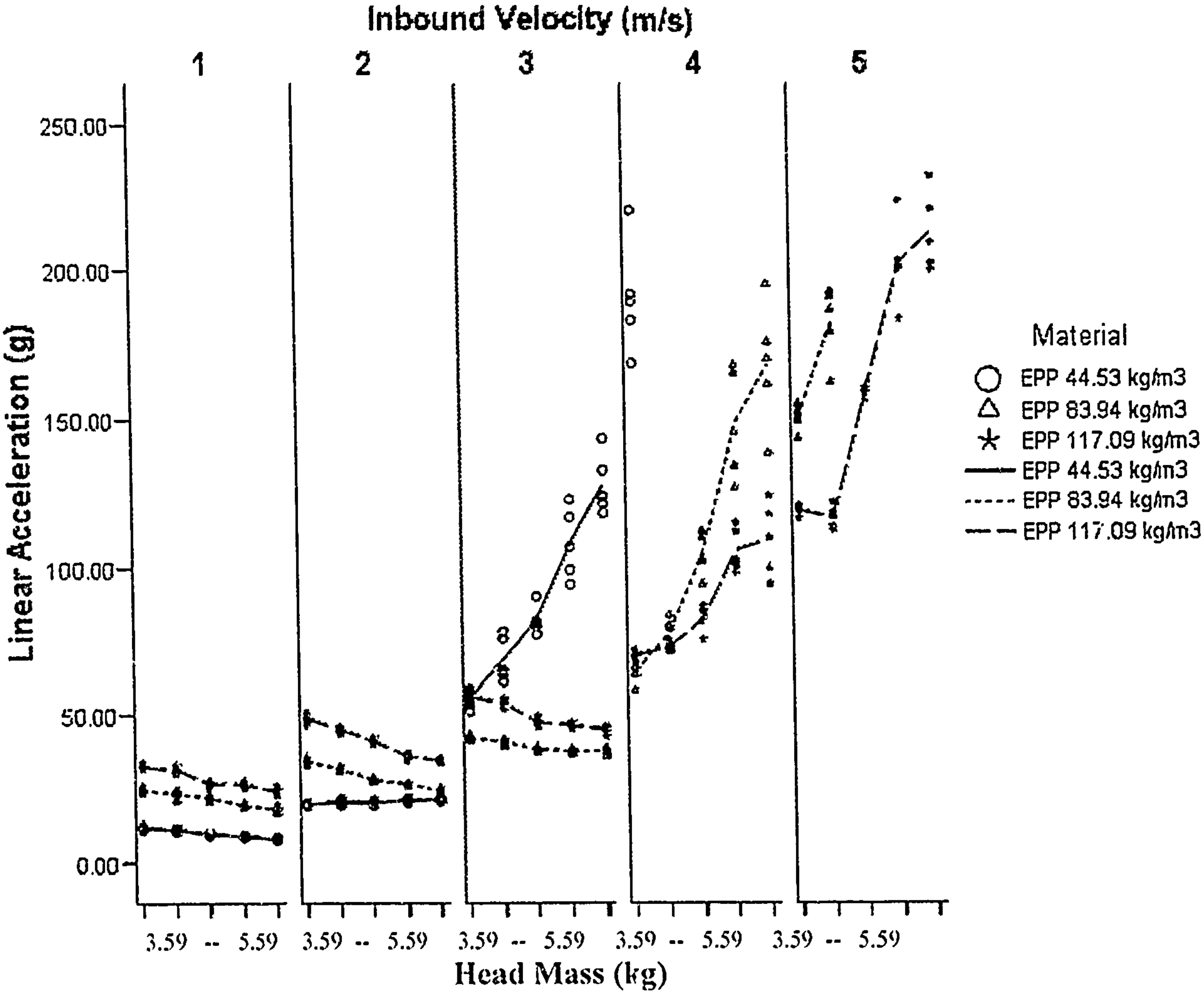

Figure 27 Peak linear acceleration results with interpolation lines for EPP 44.53, 83.94, and 117.09 kg/m^3 across impact mass (1=3.59 kg and 5=5.59 kg) at each inbound velocity.

Further investigations using bivariate correlation tests were conducted to determine the relationship between impact mass, acceleration, and impulse for each material density and inbound velocity. The results for acceleration (g) and impulse (N·s) are presented in tabular format below and all results were found to be significant, $p<0.05$.

Table 16 Partial correlation results for impact mass, acceleration (g), and impulse (N·s) at each material density and inbound velocity.

Material (kg/m^3)	1.0 m/s		2.0 m/s		3.0 m/s		4.0 m/s		5.0 m/s	
	G	N·s	g	N·s	g	N·s	g	N·s	g	N·s
EPP 44.53	-0.969	0.963	0.740	0.995	0.955	0.995				
EPP 83.94	-0.931	0.992	-0.969	0.998	-0.853	0.999	0.946	0.983	0.890	0.998
EPP 117.09	-0.920	0.983	-0.972	0.997	-0.917	0.997	0.898	0.996	0.940	0.993

Note: Blank spaces indicate testing was not conducted.

Overall, a strong negative correlation between impact mass and acceleration were found for each density of EPP at 1.0 m/s and strong positive correlations were found for impact mass at 4.0 and 5.0 m/s for each density of EPP. Impulse was strongly and positively correlated to impact mass at all conditions.

Similar to EPS, bivariate correlations were not conducted for inbound velocity as it was shown there was a strong positive and linear relationship to both acceleration and impulse in the partial correlation. Density however, was analyzed at each impact condition (mass and velocity) and the results are presented below. All results were found to be significant, $p<0.05$, except for three cases, which are indicated with an asterisk.

Table 17 Partial correlation results for material density, acceleration (g), and impulse (N·s) at each impact mass and inbound velocity for EPP.

Mass (kg)	1.0 m/s		2.0 m/s		3.0 m/s		4.0 m/s		5.0 m/s	
	g	N·s	g	N·s	g	N·s	g	N·s	g	N·s
3.59	0.989	-0.542	0.996	-0.585	0.061*	-0.759	-0.833	-0.798	-0.983	-0.12*
4.09	0.987	-0.472	0.995	-0.698	-0.510	-0.836	-0.562	-0.515	-0.970	-0.830
4.59	0.962	-0.679	0.983	-0.797	-0.744	-0.851	-0.901	0.860*		
5.09	0.992	-0.625	0.980	-0.819	-0.788	-0.835	-0.863	-0.971		
5.59	0.982	-0.741	0.950	-0.809	-0.822	-0.888	-0.888	-0.681		

* Not significant at the 0.05 level.
Note: Blank spaces indicate testing was not conducted.

From table 17, it is noted that inbound velocity was positively and linearly correlated to acceleration at 1.0 and 2.0 m/s; however, it was negatively correlated to acceleration at 3.0, 4.0, and 5.0 m/s, excluding the three non-significant values. Impulse showed mostly strong linear correlations to material density throughout the conditions.

4.5 VINYL NITRILE RESULTS

4.5.1 ANALYSIS OF VARIANCE

The mean linear acceleration with standard deviation measurements are shown in the table below for each condition VN samples were impacted.

Table 18 Mean peak linear acceleration (g) and standard deviation measurements for vinyl nitrile 602, 600, and 740 across five impact masses (3.59, 4.09, 4.59, 5.09, and 5.59 kg) and five inbound velocities (1.0, 1.5, 2.0, 2.5, and 3.0 m/s), where $n = 5$ and $N = 375$.

		Peak Linear Acceleration (g)					
Mass	Velocity	VN 602		VN 600		VN 740	
(kg)	(m/s)	Mean	SD	Mean	SD	Mean	SD
3.59	1.0	10.17	0.59	11.99	0.92	19.84	1.32
	2.0	11.75	0.58	13.91	0.62	25.11	1.36
	3.0	16.24	0.20	17.09	0.49	28.17	3.11

	4.0	29.93	0.69	30.01	3.57	31.15	3.42
	5.0	54.12	2.89	42.80	4.27	31.96	1.18
4.09	1.0	9.39	0.46	10.98	1.41	20.17	1.67
	2.0	11.13	0.48	12.97	0.46	24.95	1.87
	3.0	16.48	0.63	17.20	0.55	28.92	0.95
	4.0	33.35	0.66	26.72	0.61	32.67	1.11
	5.0	62.13	1.85	51.48	8.32	33.21	2.01
4.59	1.0	7.99	0.63	9.42	1.00	16.93	1.75
	2.0	9.97	0.28	11.63	0.52	21.63	0.93
	3.0	16.66	0.80	16.60	1.24	24.03	2.19
	4.0	38.26	1.66	31.79	3.40	25.66	1.27
	5.0	81.96	1.67	54.10	2.92	29.55	1.25
5.09	1.0	7.06	0.48	8.26	0.57	15.46	1.24
	2.0	9.64	0.29	10.70	0.39	19.67	1.71
	3.0	18.54	0.80	16.97	1.42	21.83	1.75
	4.0	40.80	2.19	32.28	1.67	24.96	2.44
	5.0	83.34	3.11	61.17	2.99	29.95	0.28
5.59	1.0	6.96	0.17	8.82	0.54	15.42	1.36
	2.0	10.95	0.25	11.42	0.13	18.95	1.94
	3.0	19.51	0.72	17.04	0.94	20.93	1.05
	4.0	39.67	2.45	30.51	0.73	26.84	0.77
	5.0	93.80	3.28	63.02	3.67	30.25	1.21

As well, the mean impulse and standard deviations are provided for each impact condition for VN in table 19.

Table 19 Mean impulse (N·s) and standard deviation measurements for vinyl nitrile 602, 600, and 740 across five impact masses (3.59, 4.09, 4.59, 5.09, and 5.59 kg) and five inbound velocities (1.0, 1.5, 2.0, 2.5, and 3.0 m/s), where n = 5 and N = 375.

		Impulse (N·s)					
Mass	Velocity	VN 602		VN 600		VN 740	
(kg)	(m/s)	Mean	SD	Mean	SD	Mean	SD
3.59	1.0	5.64	0.66	5.29	0.52	5.05	0.26
	2.0	7.88	0.40	7.94	0.51	7.02	0.16
	3.0	9.94	0.68	9.38	0.23	8.78	0.41
	4.0	12.32	0.32	12.25	0.34	10.64	0.14
	5.0	14.95	0.08	14.61	0.34	12.70	0.05
4.09	1.0	6.15	0.27	6.15	0.75	5.97	0.34
	2.0	8.75	0.94	8.51	0.69	7.92	0.30
	3.0	11.67	0.56	11.26	0.50	10.01	0.36
	4.0	14.70	0.11	13.84	0.26	12.89	0.42
	5.0	17.41	0.06	17.00	0.30	14.73	0.15
4.59	1.0	7.21	0.68	6.59	0.39	100.12	0.05

	2.0	10.18	0.73	9.33	0.35	8.39	0.10
	3.0	12.78	0.40	12.83	0.81	11.00	0.02
	4.0	16.53	0.06	15.71	0.30	13.96	0.10
	5.0	19.37	0.13	18.67	0.10	16.69	0.21
5.09	1.0	7.53	0.43	7.70	0.35	7.21	0.35
	2.0	10.89	0.24	10.27	0.45	9.55	0.44
	3.0	14.62	0.11	13.79	0.41	12.47	0.49
	4.0	18.77	0.12	17.85	0.16	16.05	0.17
	5.0	21.82	0.07	21.09	0.05	18.66	0.36
5.59	1.0	8.36	0.04	8.36	0.61	7.42	0.14
	2.0	12.74	0.29	12.56	0.69	11.03	0.06
	3.0	16.09	0.19	15.38	0.43	13.49	0.07
	4.0	20.27	0.15	19.05	0.57	17.50	0.23
	5.0	23.66	0.12	22.90	0.58	20.51	0.21

The hypotheses that significant differences in peak linear acceleration and impulse would be observed throughout the different impact conditions were supported for vinyl nitrile. There were significant main effects for material density on peak linear acceleration ($F(2, 300) = 259.19$, $p<0.05$) and impulse ($F(2, 300) = 700.79$, $p<0.05$). Significant main effects were found for head mass on peak linear acceleration ($F(4, 300) = 18.46$, $p<0.05$) and impulse ($F(4, 300) = 2477.85$, $p<0.05$) and finally, significant main effects were found for inbound velocity on peak linear acceleration ($F(2, 300)$ 5690.55, $p<0.05$) and impulse ($F(2, 300) = 10610.68$, $p<0.05$).

Significant two-way interactions between head mass and velocity were found for peak linear interactions ($F(16, 300) =229.97$, $p<0.05$) and impulse (($F(16, 300) = 10610.6$, $p<0.05$). As well, significant two-way interactions were found between impact mass and density for peak linear acceleration ($F(8, 300) =73.16$, $p<0.05$) and impulse ($F(8, 300) = 6.64$, $p<0.05$), and between velocity and density for peak linear acceleration ($F(8, 300) = 904.41$, $p<0.05$) and impulse ($F(8, 300) = 33.85$ $p<0.05$). As well, a significant three-way interaction for peak linear acceleration ($F(29, 300) = 63.41$. $p<0.05$) and impulse (F (29,

300) = 1.50, $p<0.05$) were found between all of the independent variables; impact mass, inbound velocity, and density.

For VN, the mean and standard deviation for peak linear acceleration and impulse was 26.36 g +/- 18.26 g and 12.46 N·s +/- 4.73 respectively. The estimated marginal mean and standard deviation for peak linear acceleration was 26.36 g +/- 0.10 g and the 95% confidence interval was 26.16 to 26.56. The estimated marginal mean and standard deviation for impulse was 12.46 N·s +/- 0.02; therefore, the 95% confidence interval was 12.42 to 12.49. The three-way ANOVA revealed the observed power for all main effects and interactions for peak linear acceleration computed were 1.0 and the observed powers for impulse were all 1.0, except for the three-way interaction between impact mass, density, and velocity which was 0.986. There were no missing data for VN 600, 602, or 740.

The Levene's test of equality of variances however, revealed that the mean peak linear acceleration and mean impulse were not homogenous across groups ($F(74, 300) = 4.97$, $p<0.05$) and ($F(74, 252) = 4.13$, $p<0.05$). Further analysis of the data revealed a positive kurtosis for peak linear acceleration and a negative kurtosis for impulse, 3.08 and -0.716 respectively. As well, peak linear acceleration and impulse were positively skewed, 1.733 and 0.413 respectively. The kurtosis values are not within +/- 2; however the skewness falls between +/- 2, displaying normality in the distribution of data (George & Mallery, 2007). The ANOVA test was decided to be used due to its robustness.

In regards to main effects on peak linear acceleration for EPP, inbound velocity was the greatest, with a 98.7% chance of finding this effect to be significant in a sample of 375. Next, material density had a high effect size of 63.3% and impact mass had only a 19.8% chance of finding the effect to be significant. The two-way interactions between velocity and density (96.0%) revealed high significance and the interactions between density and impact mass (66.1%) and velocity and impact mass (76.4%) showed a lower chance. Finally, the three-way interactions revealed a low 64.1% chance of finding an interaction effect on peak linear acceleration in a sample of 375.

In regards to main effects on impulse, inbound velocity was again the greatest with a 99.3% chance of finding significance. Impact mass was next at 97.1% and density had a lower effect size of 82.4%. In regards to the two-way interactions on predicting impulse, impact mass and velocity was the greatest at 812% and density and impact mass (15.1%) and density and velocity (47.4%) were much lower. Finally, the three-way interactions revealed a low 13.8% chance of finding an interaction effect on impulse in a sample of 375.

Again, post hoc testing for impact mass was conducted separately for each combination of material density and velocity using the Bonferroni Test, which assumes homogeneity of variance across means. The Levene's test of equality of variances revealed that the mean linear acceleration and mean impulse were homogenous across groups at each combination of density and velocity ($p > 0.05$). Figure 28 displays the peak linear acceleration results for impact mass at each density for each inbound velocity.

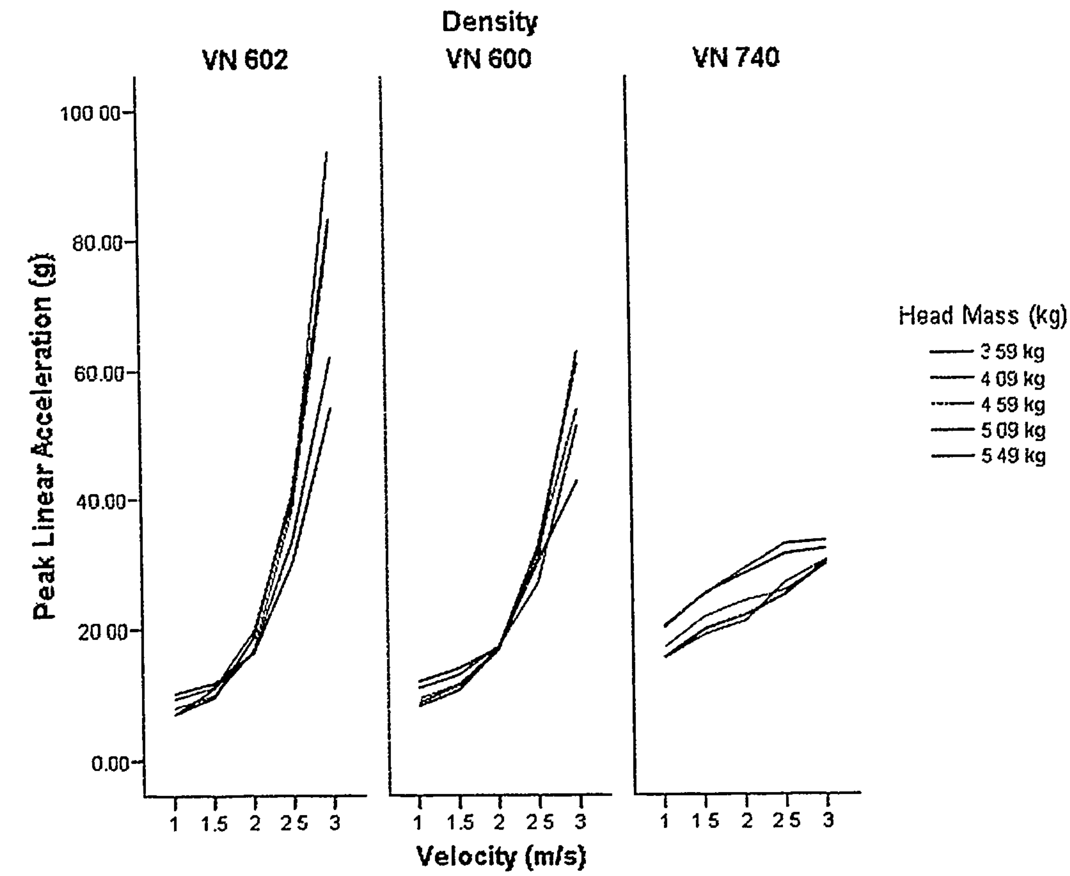

Figure 28 Mean peak linear acceleration results for each impact mass using VN 602, VN 600, and VN 740 at velocity 1.0, 2.0, 3.0, 4.0, and 5.0 m/s.

Impact mass was shown to have a significant main effect on peak linear accelerations and impulse for VN at the three material densities. Significant differences for peak linear acceleration however, were only found for 85/150 possible interactions of impact mass. Where these differences occur is highlighted in table 5.16. Observing the figure above displays the results for impact mass at each velocity. For example, VN 740 revealed significant differences between 4.09 and 5.09 kg and 4.09 and 5.59 kg for each inbound velocity. Also, 3.59 kg differed significantly from 5.09 and 5.59 kg at each inbound velocity for VN 602.

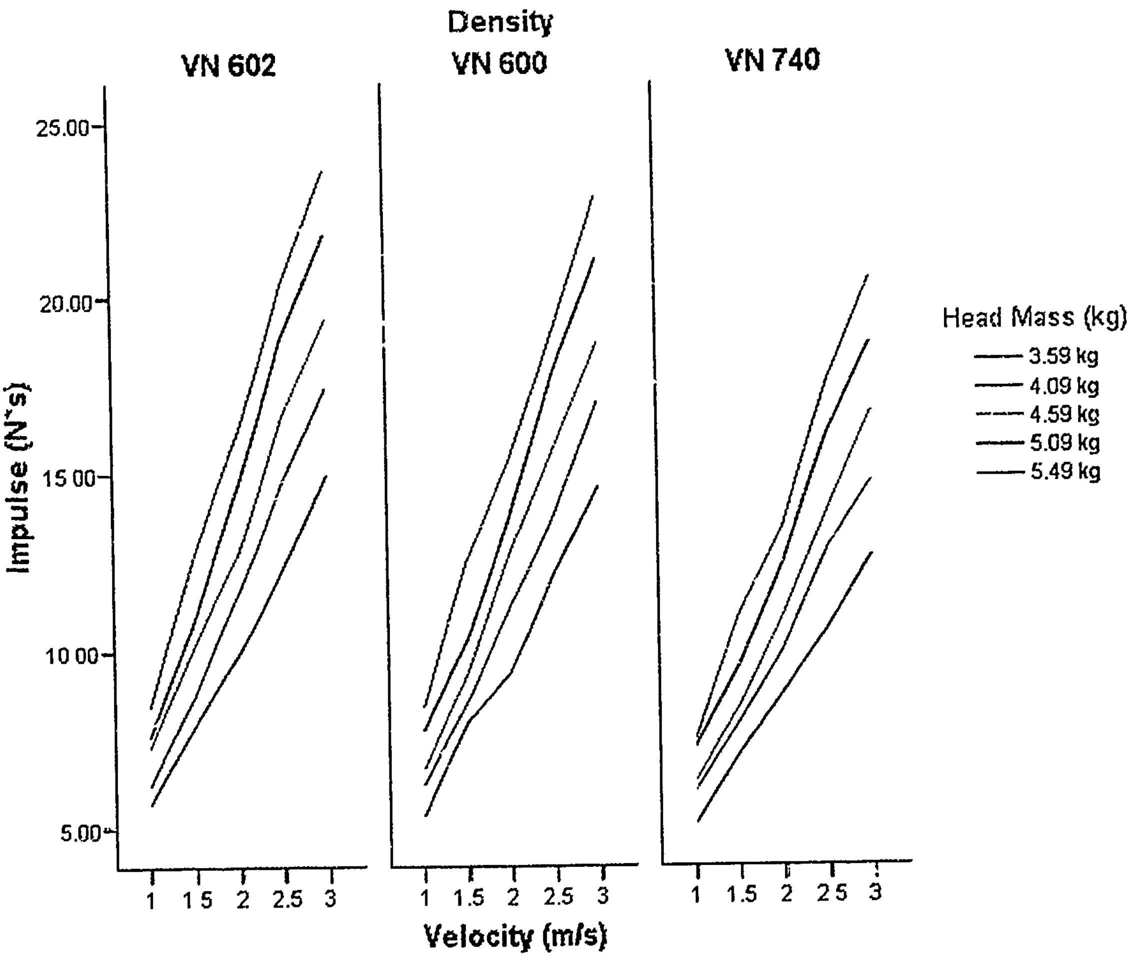

Figure 29 Mean impulse results for each impact mass using VN 602, VN 600, and VN 740 and velocity 1.0, 2.0, 3.0, 4.0, and 5.0 m/s.

Figure 29 displays that impact mass had a significant effect on impulse measurements. Post hoc testing using the Bonferroni test revealed that significant differences in impulse were observed for 134 of the 150 comparisons between impact masses at each material density and inbound velocity. The non-significant findings for impulse were between impact masses that were closest in mass; for example, between 3.59 kg and 4.09 kg at 1 and 1.5 m/s for VN 602 and VN 600. Table 4.16 highlights where significant differences in peak linear acceleration and impulse occurred between each impact mass at each velocity and density. Boxed squares represent significant differences in mean peak linear acceleration and an asterisk represents significant differences in impulse between the corresponding masses, where:

M1 = 3.59 kg
M2 = 4.09 kg
M3 = 4.59 kg
M4 = 5.09 kg
M5 = 5.59 kg

Table 20 Significant differences for VN for mean peak linear acceleration (squares ([M] – [M]) and impulse (*) between variable impact mass and inbound velocity, where $p<0.05$.

Material	1 m/s	1.5 m/s	2 m/s	2.5 m/s	3 m/s
VN 602	[M1] - M2 - [M3] * - [M4] * - [M5] * [M2] - [M3] * - [M4] * - [M5] * [M3] - M4 - [M5] * M4 - M5	[M1] - M2 - [M3] * - [M4] * - [M5] * [M2] - [M3] * - [M4] * - M5 * [M3] - M4 - [M5] * [M4] - [M5] *	[M1] - M2 * - M3 * - [M4] * - [M5] * [M2] - M3 * - [M4] * - [M5] * [M3] - [M4] * - [M5] * M4 - M5 *	[M1] - M2 * - [M3] * - [M4] * - [M5] * [M2] - [M3] * - [M4] * - [M5] * M3 - M4 * - M5 * M4 - M5 *	[M1] - [M2] * - [M3] * - [M4] * - [M5] * [M2] - [M3] * - [M4] * - [M5] * [M3] - M4 * - [M5] * [M4] - [M5] *
VN 600	[M1] - M2 - [M3] * - [M4] * - [M5] * [M2] - M3 - [M4] * - [M5] * M3 - M4 * - M5 * M4 - M5	[M1] - [M2] - [M3] * - [M4] * - [M5] * [M2] - [M3] - [M4] * - [M5] * [M3] - [M4] - M5 * M4 - M5 *	[M1] - [M2] * - [M3] * - [M4] * - [M.] * [M2] - [M3] * - [M4] * - [M5] * [M3] - [M4] - M5 * M4 - M5 *	M1 - M2 * - M3 * - M4 * - M5 * [M2] - [M3] * - [M4] * - M5 * M3 - M4 * - M5 * M4 - M5 *	[M1] - M2 * - [M3] * - [M4] * - [M5] * [M2] - M3 * - M4 * - [M5] * M3 - M4 * - M5 * M4 - M5 *
VN 740	[M1] - M2 * - M3 * - [M4] * - [M5] * [M2] - M3 - [M4] * - [M5] * M3 - M4 * - M5 * M4 - M5	[M1] - M2 * - [M3] * - [M4] * - [M5] * [M2] - [M3] - [M4] * - [M5] * M3 - M4 * - M5 * M4 - M5 *	[M1] - M2 * - [M3] * - [M4] * - [M5] * [M2] - M3 * - [M4] * - [M5] * M3 - M4 * - M5 * M4 - M5 *	[M1] - M2 * - [M3] * - [M4] * - [M5] * [M2] - [M3] * - [M4] * - [M5] * M3 - M4 * - M5 * M4 - M5 *	M1 - M2 * - M3 * - M4 * - M5 * [M2] - [M3] * - [M4] * - [M5] * M3 - M4 * - M5 * M4 - M5 *

Post hoc testing using the Bonferroni test was also conducted to determine whether significant differences between velocities existed at each impact mass and material density. Peak linear acceleration measurements were significantly different for nearly all inbound velocities, except between velocities close in value. Inbound velocities 1.0 and 1.5 m/s were not significantly different for VN 602 at 3.59, 4.09, 4.59, and 5.09 kg, as well as for VN 600 at all five impact masses. As well, peak linear acceleration was not significantly different between 1.5 and 2.0 m/s for VN 600 at 3.39, 4.09, and 4.59 kg, as well as VN 740 at 3.59, 4.59, 5.09, and 5.59 kg. Finally, significant differences were not found between 2.0 m/s and 2.5 m/s for VN 740 at 3.59, 4.59, and 5.09 kg and between 2.5 and 3.0 m/s for VN 740 at 3.59 and 4.09 kg. Impulse was found to be significantly different between all inbound velocities at each impact condition.

Post hoc testing using the Bonferonni test revealed significant differences for peak linear acceleration across material density for 60 out of 75 impact conditions. VN 602 and VN 600 were not significantly different at velocities 2.5 and 3.0 m/s at 3.59 kg, 1.0 and 2.0 m/s for 4.09 and 5.09 kg, 1.0 m/s and 2.0 m/s for 4.59 kg, and finally for 1.5 m/s at 5.59 kg. VN 602 and VN 740 were not significantly different at 2.5 m/s for 3.59 and 4.09 kg, as well as at 2.0 m/s for 5.59 kg. Finally, VN 600 and VN 740 were found significantly different at all conditions except for 3.59 kg at 1.0 m/s. Using impulse as the dependent variable, significant differences were not observed between VN 602 and VN 600 at 3.59 kg for each inbound velocity; as well, at 4.09 kg for 1.0, 1.5, and 2 m/s. Except for three conditions, impulse results for VN 740 was significantly different than VN 602 at all impact masses and inbound velocities. Differences were not observed for impulse at 3.59 kg for 1.0 and 1.5 m/s, 4.09 kg for 1.5 m/s, and 5.09 kg for 1.0 m/s between the aforementioned two materials. Finally, analysis between VN 600 and VN 740 showed that significant differences for impulse were found for nearly all conditions except for 3.59 kg at 1.0 and 2 m/s, 4.09 kg at 1.5 m/s, 4.59 kg at 1.0 m/s, and 5.09 kg at 1.0 and 1.5 m/s. The figure below displays the impulse results for each material density across inbound velocity for each impact mass.

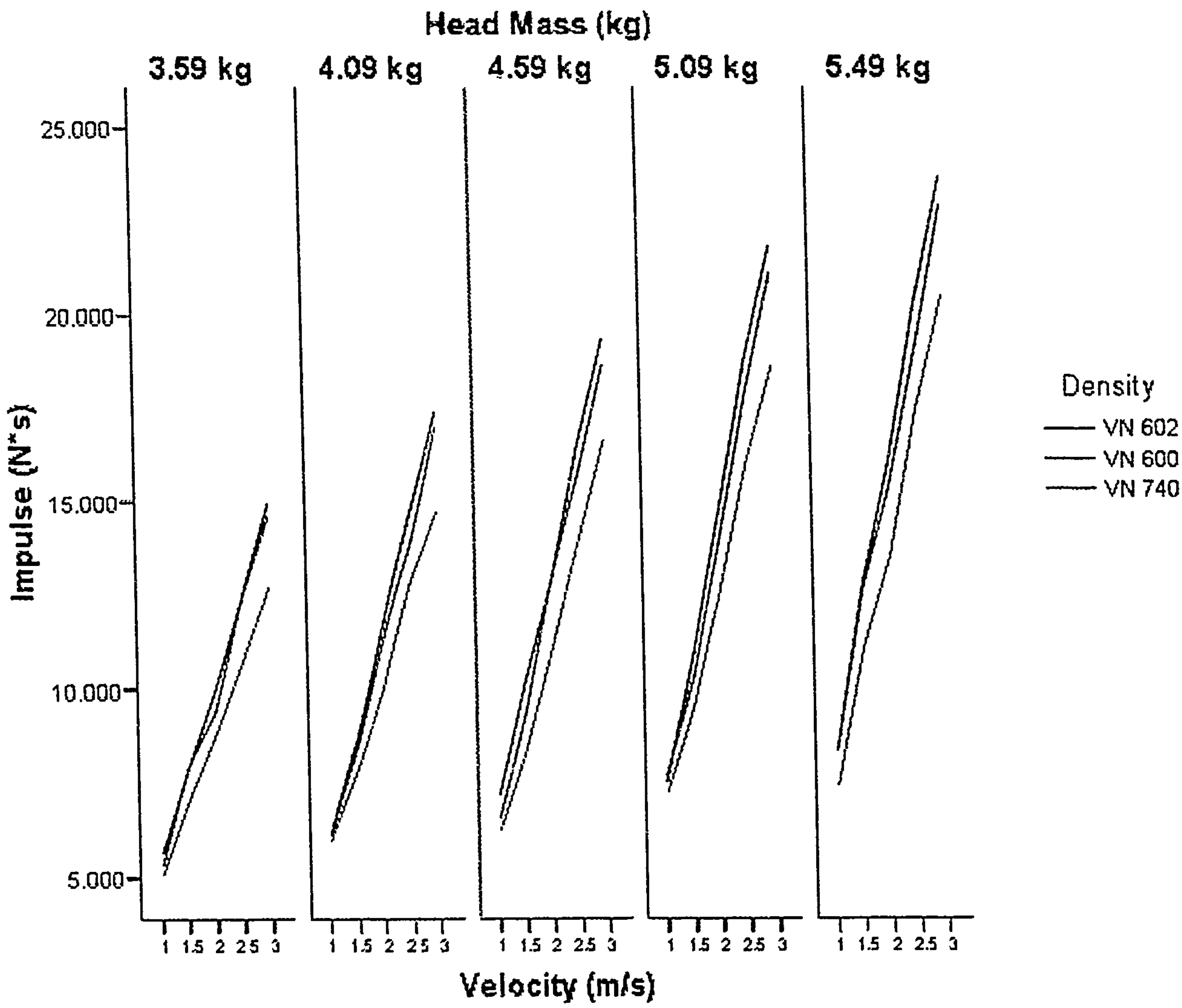

Figure 30 Peak impulse results for VN 602, VN 600, and VN 740 at velocity 1.0, 1.5, 2.0, 2.5, and 3.0 m/s for each impact mass.

Figure 31 below is a close-up for the effects of 3.59 kg on impulse at each of the inbound velocities tested. A strong linear relationship between inbound velocity and impulse is evident in both figures.

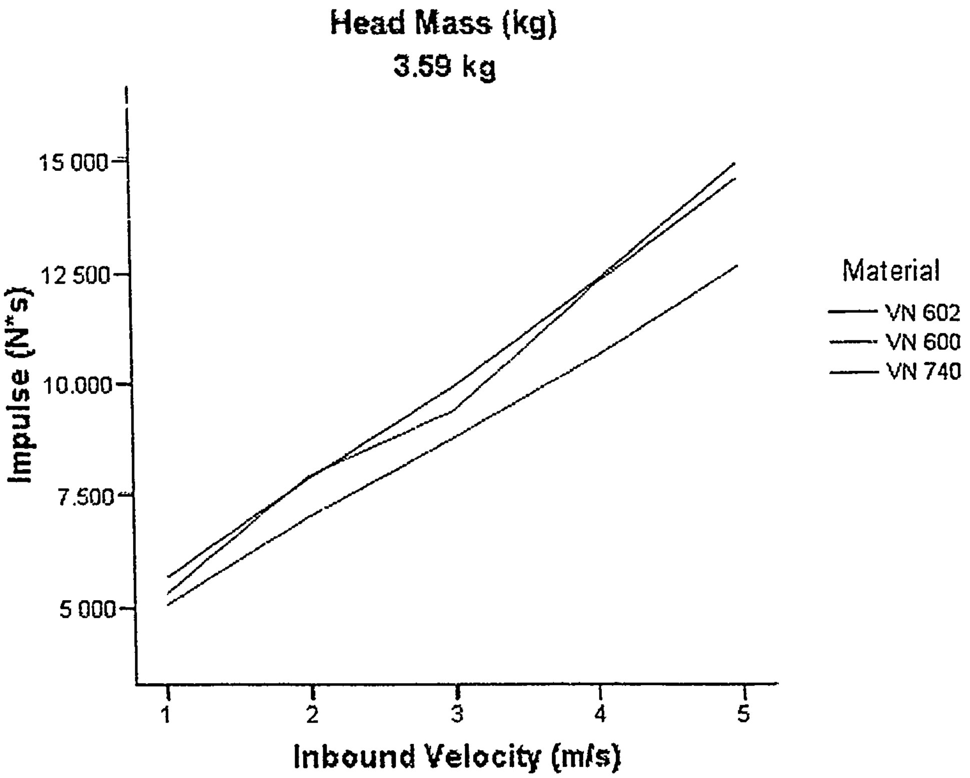

Figure 31 Peak impulse results for VN 602, VN 600, and VN 740 at velocity 1.0, 1.5, 2.0, 2.5, and 3.0 m/s for 3.59 kg.

4.5.2 CORRELATIONS

A partial correlation test revealed that inbound velocity was positively correlated to both acceleration ($r = 0.780$, $p<0.05$) and impulse ($r = 0.976$, $p<0.05$), when controlling for material density and impact mass. Impact mass produced a small positive relationship between acceleration ($r = 0.073$, $p<0.05$) and large positive relationship with impulse ($r = 0.908$, $p<0.05$), when controlling for inbound velocity and material density. Finally, material density produced a non-linear negative relationship between acceleration ($r = -0.173$, $p<0.05$) and negative relationship between impulse ($r = -0.619$, $p<0.05$). The results are presented in the table below.

Table 21 VN partial correlation results for each independent variable on the dependent variable, with significance level (N = 375).

	Acceleration (g)		Impulse (N·s)	
	Correlation	Significance	Correlation	Significance
Inbound Velocity (m/s)	0.780	<0.0005	0.976	<0.0005
Impact Mass (kg)	0.073	<0.0005	0.908	<0.0005
Material Density (kg/m^3)	-0.173	<0.0005	-0.619	<0.0005

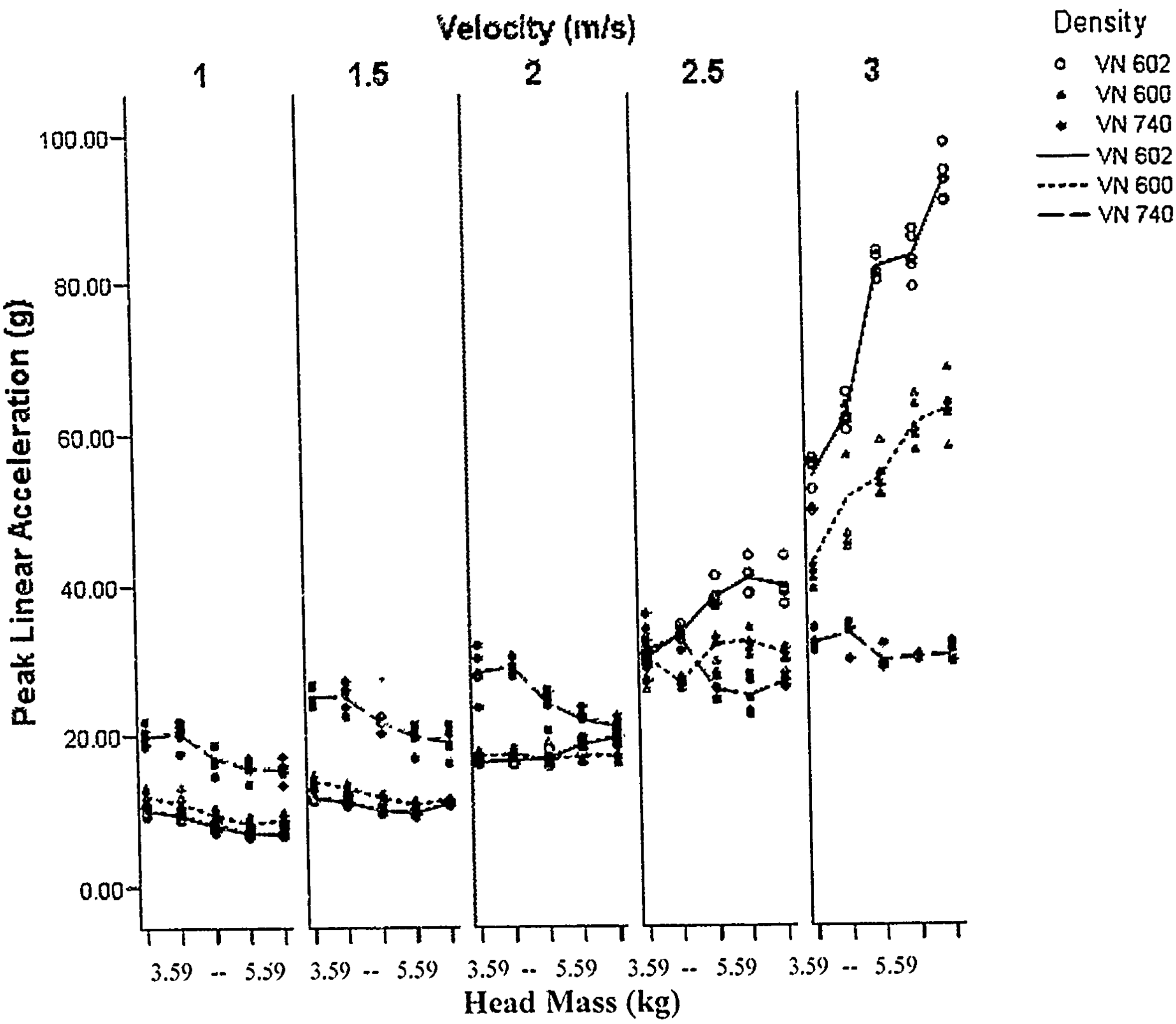

Figure 32 Acceleration results with interpolation lines for VN 602, 600, and 740 for increasing impact mass (1-5) at each inbound velocity.

Further investigations using bivariate correlation tests were conducted to determine the relationship between impact mass, acceleration, and impulse for each material density and inbound velocity. The results for acceleration (g) and impulse (N·s) are presented in tabular format below and all results were found to be significant, $p<0.05$.

Table 22 Partial correlation results for impact mass, acceleration (g), and impulse (N·s) at each material density and inbound velocity.

Material	1.0 m/s		1.5 m/s		2.0 m/s		2.5 m/s		3.0 m/s	
	g	N·s	g	N·s	g	N·s	g	N·s	g	N·s
VN 602	-0.794	0.905	-0.369	0. 946	0.850	0.962	0.868	0.996	0.958	0.999
VN 600	-0.789	0.908	-0.836	0.918	-0.053	0.971	0.322	0.989	0.838	0.993
VN 740	-0.918	0.905	-0.512	0.946	-0.850	0.982	0.868	0.996	0.958	0.999

Overall, negative correlations between impact mass and acceleration were found for each density of VN at 1 m/s and strong positive correlations were found for impact mass at 5 m/s for each density of VN. Impulse was strongly and positively correlated to impact mass at all conditions.

Similar to EPS and EPP, bivariate correlations for inbound velocity were not conducted as it was shown there was a strong positive and linear relationship to both acceleration and impulse in the partial correlation. Density however, was analyzed at each impact condition (mass and velocity) and the results are presented below. All results were found to be significant, $p<0.05$).

Table 23 Partial correlation results for material density, acceleration (g), and impulse (N·s) at each impact mass and inbound velocity for VN.

Mass	1.0 m/s		2.5 m/s		2.0 m/s		2.5 m/s		3.0 m/s	
(kg)	g	N•s	g	N•s	g	N•s	g	N•s	g	N•s
3.59	0.921	-0.469	0.922	-0.645	0.859	-0.742	0.188	-0.840	-0.957	-0.912
4.09	0.900	-0.164	0.908	-0.472	0.885	-0.821	-0.090	-0.943	-0.996	-0.957
4.59	0.897	-0.692	0.919	-0.866	0.803	-0.749	-0.928	-0.968		
5.09	0.906	-0.326	0.892	-0.843	-0.566	-0.927	-0.959	-0.976		
5.59	0.931	-0.701	0.859	-0.813	-0.322	-0.944	-0.940	-0.959		

From table 23, it is noted that inbound velocity was positively linearly correlated to acceleration at 1.0 and 1.5 m/s; however, it was negatively correlated to acceleration at 3.0 m/s. Impulse showed strong negative correlations to material density at 2.0, 2.5, and 3.0 m/s.

CHAPTER 5. DISCUSSION

Severe and mild head injuries have shown links to poor cognitive, psychosocial, and neurological outcomes, demonstrating a need for protection for both high and low impact energies (Barth et al., 2002). As mentioned previously, all helmet testing protocols and standards require helmets to be impacted from a pre-defined height/inbound velocity using a specific impact mass, both of which significantly affect the total energy involved during an impact. This study has demonstrated that this difference in energy induced by both a variety of headform masses and inbound velocity significantly affected the performance of the materials tested.

Similar trends were found between EPS, EPP, and VN throughout the analysis for peak linear acceleration and impulse. Inbound velocity had the strongest relationship with the dependent variables, followed by impact mass for EPS and EPP and material density for VN. The fact that velocity had a greater influence on material performance compared to impact mass was not surprising considering the inbound velocity range was relatively much larger compared to the range of impact masses. In real life head mass changes by only a few kilograms; whereas, inbound velocity can change dramatically from one hit to the next.

Nevertheless, both variables influenced the performance of the single- and multi-impact materials tested and therefore need to be considered in helmet testing standards.

Taking into consideration the effect strength of inbound velocity it becomes easy to recognize the limitations of the ASTM International standard for ice hockey helmets. This particular standard requires helmets to be tested from just one impact velocity of 4.5 ± 0.09 m/s using either a 3.1, 4.1, 4.7, or 5.6 kg headform mass (ASTM International, F1045-06). It has been stated that helmet standards which involve high-energy impacts of 40-60 J to prevent cranial fractures and severe concussions are not designed to ensure the same degree of protection at low- and medium-energy impacts (Hoshizaki, 1995). For reference, a five kilogram headform mass impacted at 4.5 m/s would result in an impact energy of 50.6 Joules (J). Since materials incorporated in helmets function within a limited energy range it is evident that helmets designed to pass one inbound velocity are jeopardizing player's safety during impacts which fall outside of the testing parameters.

Correlation analysis revealed that the interaction between impact mass, inbound velocity, and material density were consistent at 1.0, 2.0 and 3.0 m/s; however, at 4.0 and 5.0 m/s the interactions inversed for EPS and EPP. VN did not show this trend. Looking at EPS and EPP, an impact mass of 3.59 kg at 1.0 m/s produced significantly higher peak linear accelerations compared to 5.59 kg; however, at 5.0 m/s the lower impact mass produced significantly lower peak linear accelerations than the higher impact mass. For EPS and EPP the point at which the relationship between the three predictor variables inversed was the performance threshold of the material. After the threshold point, the material failed or bottomed out upon impact. EPS 62.95 kg/m^3 for example, the threshold is evident at 3.0 m/s where the different impact masses did not produce significantly different results in peak linear acceleration. This suggests that this density performed optimally for the greatest range of impact masses at 3.0 m/s.

In regards to vinyl nitrile, this switch in trend was not observed for VN 740. as mechanical failure was not achieved for all of the inbound velocities. Vinyl nitrile is a multi-impact material and therefore does not require mechanical destruction to attenuate energy. Unlike EPS, VN attenuates energy by pushing air out of the foam cells and does not require damaging the structure of cell walls to do so. The quasi-static and dynamic testing revealed that VN had lower yield values compared the EPP and EPS, which were stiffer materials that could withstand higher impact forces. The low yield point for VN made it a better material at attenuating energy through the range of impact masses chosen and resulted in significantly lower peak accelerations compared to EPP and EPS throughout the lower inbound velocities.

Significant two- and three-way interactions were found between all of the independent variables, which were primarily the result of the unpredictable energy attenuation results at the higher inbound velocities. Two-way interactions occurred when the effect of one variable were not consistent across the levels of the second variable and the three-way interaction occurred when the interaction between two variables were not consistent across the third variable (George & Mallery, 2006). Inbound velocity had the greatest influence on the interaction effects. When the foam samples were impacted outside of their performance range, bottoming-out occurred resulting in unpredictable energy attenuation results, causing an interaction effect. For example, the mass by density interaction at 1.0 m/s for EPS was not the same as the mass by density interaction at 4.0 m/s. For following figure displays this interaction effect.

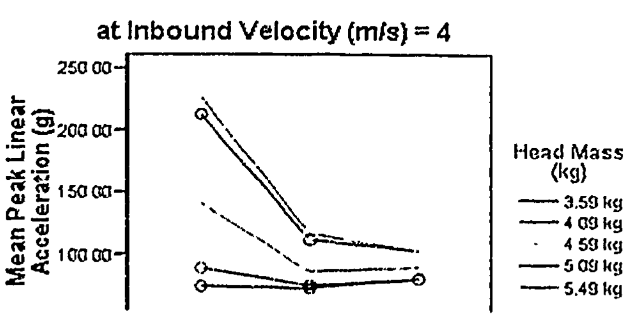

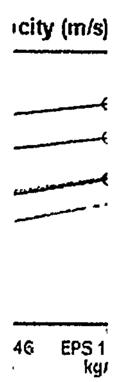

Figure 33 EPS plot graphs displaying the three-way interaction effect of head mass by density across two inbound velocities, 1.0 m/s and 4.0 m/s.

In figure 33, it can be seen that at 1.0 m/s the mean peak linear accelerations had increased for each head mass as material density increased. At 4.0 m/s however, the samples began to bottom-out and the higher material density resulted in lower mean peak linear accelerations displaying a three-way interaction effect.

The figures below highlight the robustness of VN 740 at attenuating energy through the lowest and highest impact masses tested.

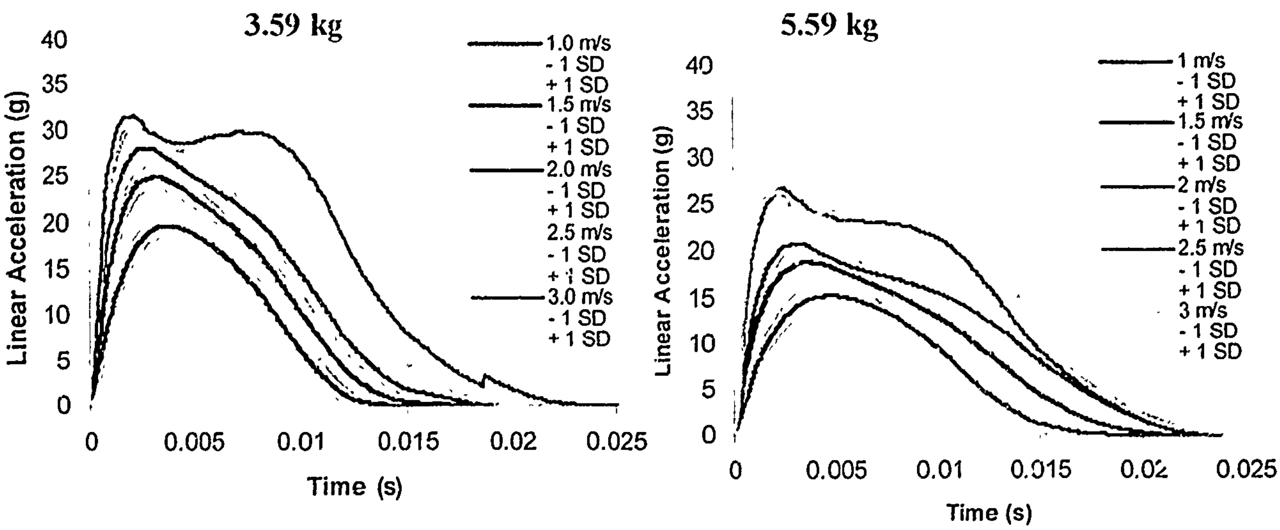

Figure 34 Linear acceleration time curves of VN 740 at all inbound velocities for 3.59 kg and 5.59 kg.

VN 740 was able to attenuate the impact energy efficiently across the lowest and highest impact mass and throughout each inbound velocity tested. If testing was continued at higher velocities, failure would inevitably be seen and the effect of impact mass would most likely be teased out. Although it is difficult to see in these figures, post-hoc testing had revealed significant differences in peak linear acceleration between 3.59 kg and 5.59 kg at all of the inbound velocities shown, except 3.0 m/s.

Regardless of the peak acceleration output, head mass caused the performance of each material to differ significantly, which was illustrated comparing impulses. In figure 34 for example, it can be seen that the peak linear acceleration for impact mass was not statistically different for EPS 62.95 kg/m^3 when tested at 3.0 m/s; however, impulse was. Comparisons to EPS 100.12 kg/m^3; however, displays an example where both peak linear acceleration and impulse changed significantly. The partial correlation analysis found the impulse difference across impact mass was linear for both densities, where a greater head mass produced a larger impulse, suggesting an increased risk of head injury. The relationship between inbound velocity and impulse was also positive and linear. Overall, regardless of the peak acceleration output, each head mass caused the performance of the material to differ significantly.

The following graphs illustrate the outcome of the two EPS densities at 3.0 m/s and show that even when peak linear accelerations did not change, impulses did.

a) **EPS 62.95 kg/m^3** b) **EPS 100.12 kg/m^3**

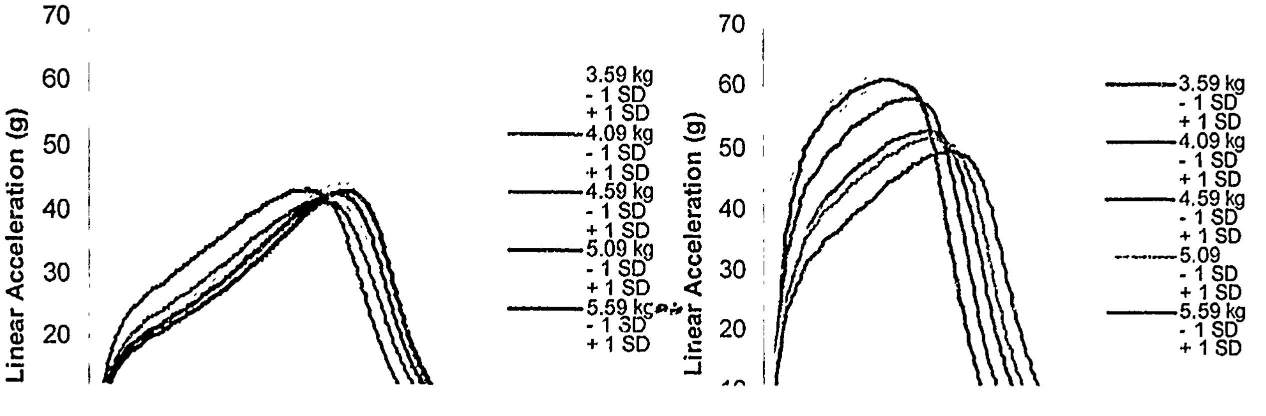

Figure 35 Linear acceleration time trace with standard deviations for EPS 62.95 kg/m^3 and EPS 100.12 kg/m^3 for each impact mass at 3.0 m/s.

The front end of the curves in figure 34 represents the linear elastic phase of the material. At approximately 0.001 seconds the slope of the curves decreased indicating the material's yield point or breaking point during the dynamic impacts. This was controlled by air trapped within the cell walls of the foam (Landro et al., 2001). The larger impact energy caused the material to compress more forcefully resulting in a lower yield point; whereas, the lower impact mass was able to succumb to significantly greater accelerations before compressing, but bottomed out earlier than the heavier impact masses. In terms of impulse, inbound velocity and impact mass had a very large effect size for EPP, EPS, and VN, indicating a very strong relationship between these two predictor variables on impulse.

Overall, inbound velocity had the strongest effect on peak linear acceleration: 98.7% for EPP. The fo'lowing graph is shown to represent the effect that inbound velocity had on material performance.

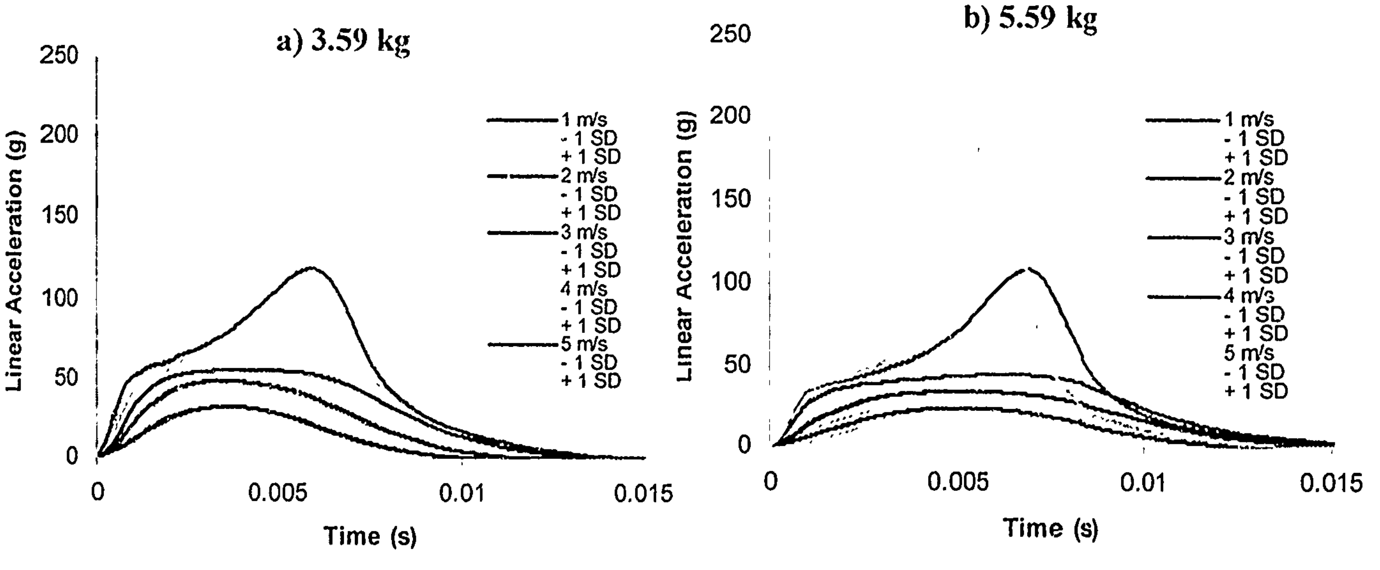

Figure 36 Linear acceleration time curves for impacts conducted on EPP 117.09 kg/m^3 at all inbound velocities using a 3.59 kg and 5.59 kg impact mass.

Acceleration and impulse increased significantly with increasing inbound velocity. At lower inbound velocities, the impact energy was too low to cause mechanical compression of the material, which minimized the energy attenuated from the impact and therefore the efficiency of the material. This was evident by the lack of yield point and short plateau phase. At 4.0 m/s however, EPP 117.09 kg/m^3 performed optimally, which was indicated by a long plateau in the acceleration-time curve immediately following the yield point. At 5.0 m/s, the sharp spike in the both curves represents complete densification and failure of the material. Overall, all results have indicated that the performance of the polymeric materials tested were significantly affected by the impact energy, where inbound velocity had the largest influence on this change.

In addition to mass and velocity, the density of the materials resulted in variable attenuation characteristics during both dynamic and quasistatic testing. The quasistatic compression results were consistent with the findings of Ivarsson et al. (2003) and Subhash et al.(2006), who revealed that as foam density increased, the Young's modulus and yield stresses and strains increased as well. Essentially, the denser the material the greater the forces it could withstand. The hypothesis that material density would significantly affect the performance of the material during an impact was supported for the present study.

The effects of head mass are consistent with findings of Queen, Weinhold, Kirkendall, and Yu (2003), who found that a decrease in head mass resulted in an increase in linear and angular head accelerations during a head impact in soccer heading. This study investigated linear and angular head accelerations during soccer heading in children using two neck stiffness conditions and three head masses designed to represent a range of child head masses. The results for each head mass on linear accelerations as a function of velocity are shown below.

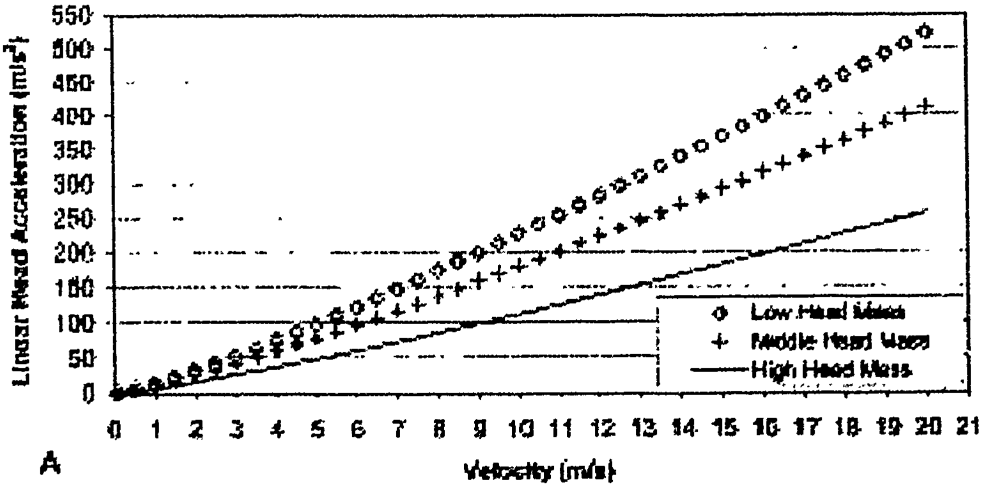

Figure 37 The effect head mass on linear head accelerations (Queen et al, 2003).

This study demonstrated that changes in head mass had substantially increased the impact variables that are linked to an increase risk of head injury. The lower head mass produced higher linear head accelerations than the higher head masses for each inbound velocity shown. Their focus was on the effect of ball properties during soccer heading and they used relative ball-to-head contact velocities to show the influence of head mass.

Another supporting study conducted by Kleiven and Holst (2002) investigated the consequence of head size following trauma to the head using finite elements modeling. Their study revealed that variation in head size altered the outcome of an impact and offered insight into future investigations. Kleiven and Holst (2002) compared intracranial stresses, such as maximal shear strain and the HIC for different head sizes. They found that HIC increased with decreasing head size; however, the intracranial stresses decreased with decreasing head size for a given acceleration pulse. It was therefore concluded that the HIC, which incorporates acceleration, was not an appropriate predictor for the risk of injury based on the assumption that intracranial responses of the brain tissue were a better indicator of head injury. The headforms used in the present study were not biofidelic, which was a delimitation stated in the introduction of this paper. Kleiven and Holst (2002) support the findings associated with the present study, but suggest that further investigation regarding the physiological responses for variable head mass should be considered.

As mentioned in the literature review, it was proposed in 1995 that the SNELL Memorial Foundation standard for bicycle helmets should incorporate a headform drop mass of 3.9 kg in their testing standards for children's helmets. Currently, the SNELL standards use a 5 kg drop mass for testing children and adult helmets, providing assurance that the helmets which pass the impact requirements on the largest appropriate headform would also meet those requirements when tested on the smaller headforms. In October 2007 however, the Snell Memorial Foundation released a draft standard for protective headgear for use in children's motor sport helmets, which is to be implemented in 2010. The major changes in this standard include using variable head mass as outlined by the International Standards Organization. For example, they've added a 3.1, 3.6, 4.1, and a 4.7 kg headform to their testing protocols (Snell Memorial Foundation M2010, 2007). Helmets which met the performance requirements on a particular headform may now fail when tested on a lighter, smaller headform, since it may result in increased peak accelerations and exceed the peak criterion. Although this change is for motorcycle helmets and not for bicycle helmets, this indicates a change in the right direction.

The results of this study regarding the effects of mass and velocity are not limited to football, hockey, and bicycling. In motor sports; as mentioned, there are currently no helmets or helmet standards specifically designed to protect children. Thus, children under the age of 6 years use adult helmets which do not account for children's unique anatomy (Arbogast et al., 2003). It is important to increase our understanding regarding what needs to be considered when developing a helmet standard for children who wish to pursue such sports.

CHAPTER 6. CONCLUSIONS, CONTRIBUTIONS, and FUTURE WORK

6.1 CONCLUSION

Overall, the hypotheses of this study were supported. Head mass, inbound velocity, and material density had a significant effect on the performance of single- and multi-impact polymeric materials incorporated in sporting helmets.

6.2 CONTRIBUTIONS

This study was the first to relate the effect of impact mass on the energy attenuation performance of sporting helmets. It has successfully shown that the effects of impact mass and inbound velocity were significant for several densities of both single- and multi-impact polymeric materials. It demonstrated the profound differences that low and high head mass can have on the risk of injury and suggests that helmets must be designed using parameters specific for the intended impact range of the user. These data also underscores the importance of all helmet standards to adopt variable impact mass and velocity into their testing protocols to help better protect our children.

6.3 FUTURE WORK

Impact mass in this study was designed to represent head mass and excluded the influence of the rest of the human body during impact. Studies conducted on animals have suggested that children's necks require less force to be injured during a head impact, subsequently putting children at an increased risk of a brain injury (Arbogast et al., 2003). Future studies on the influence of neck stiffness in young children for determining the risk of head injury would provide insight into how material performance is influenced by this variable and if neck compliance should be incorporated in testing standards.

For the purpose of this study all materials were tested separate from the helmet. A future study should apply a similar methodology using a full helmet to check for generalizeability of the results to helmet application. As well, the variables peak linear acceleration and impulse were chosen to represent the risk of head injury. As suggested by Kleiven and Holst (2002), investigation into the effects of variable head mass on the intracranial response during impacts could lead to stronger conclusions relating to the risk of head trauma.

Finally, using the results of this research, it can be inferred that new helmet technology should be engineered to function effectively for variable impact energies in order to increase the safety range that new helmets could optimally function. Thus, data taken from this study can help scientists design a safer and more specialized helmet for its intended user.

REFERENCES

Arbogast, K.B., Margulies, S.S., Patlak, M., Fenner, H., & Thomas. D.J. (2003). Differences in injury patterns between children and adults. Summary of a conference held at The Children's Hospital of Philadelphia, PA on March 31st, 2003. Retrieved May 25th, 2007 from http://www.smf.org/articles/pdf/choptrauma.pdf.

ASTM International: D 1621-04a (2004). Standard test method for compressive properties of rigid cellular plastics. American Society for Testing Materials (ASTM) Standards.

ASTM International: F 1045-06 (2006). Standard Performance Specification for Ice Hockey Helmets. PA, USA.

Avalle, M., Belingardi, G., & Montanini, R. (2001). Characterization of polymeric structural foams under compressive impact loading by means of energy-absorption diagram. *International Journal of Impact Engineering*, 25, 455-472.

Barth, J.T., Freeman, J.R., Broshek, D.K., & Varney, R.N. (2001). Acceleration-deceleration sport-related concussion: The gravity of it all. *Journal of Athletic Training*, 36, 253-256.

Bauer HH4000 Helmet. Top quality hockey helmets for the ultimate in safety and comfort. Retrieved May 20th, 2007 from http://www.oceanhockey.com/IBS/SimpleCat/Shelf/ASP/Hierarchy/0J.html.

Becker, E.B. (1998). Helmet development and standards. *Snell Memorial Foundation*, North Highlands, CA, USA. Retrieved November 15th, 2006 from http://www.smf.org/articles/helmet_development.html.

Becker, E.B. (2000). Snell's response to CSA child helmet standard. Snell Memorial Foundation, Inc. Retrieved November 5th, 2006 from http://www.smf.org/articles/csa.html.

Bicycle Helmet Safety Institute (2006). A comparison of bicycle helmet standards. Retrieved November 15ht, 2006 from http://www.helmets.org/stdcomp.html.

Cadex. (2006a). Half Magnesium K1A Headform. Retrieved August 13th, 2007 from http://www.cadexinc.com/Impact/halfMagnesium.html.

Cadex (2006b). Impact Machine Uniaxle. Retrieved August 13th, 2007 from http://www.cadexinc.com/Impact/impactMachineUniAxle.html.

Cadex (2006c). Calibration. Retrieved August 13th, 2007 http://www.cadexinc.com/Impact/calibration.html.

Camacho, D.L.A., Nightingale, R.W., & Myers, B.S. (2001). The influence of surface padding properties on head and neck injury risk. *Journal of Biomechanical Engineering*, 123, 432-439.

Canadian Institute for Health Information (2006). Head injuries in Canada: A decade of change (1994-1995 to 2003-2004). August 2006.

CAN/CSA-D113.2-M89 Cycling Helmets. A National Standard of Canada (Reaffirmed 2004). May 1996.

Cass, D.T. & Gray A.J. (1989). Pediatric bicycle injuries. *Australian and New Zealand Journal of Surgery*, 59, 719-724.

Coleman, F. (2006). Calibration certificate. ICP 203B Force Sensor. PCB Piezotronics. New York, USA.

Curnow, W.J. (2003). The efficacy of bicycle helmets against brain injury. *Accident Analysis and Prevention*, 35, 287-292.

Depreitere, B., Van, L.C., Maene, S., Plets, C., Vander S.J., & Van Audekercke, R. (2004). Bicycle-related head injury: a study of 86 cases. *Accident Analysis and Prev. .tion,* 36(4), 561-567.

DICK's Sporting Goods, (2007). Helmet components. Retrieved January 20th, 2007 from http.//www.dickssportinggoods.com/sm-football-helmet-buyers-guide--bg-222807.html.

Gadd, C.W. (1966). Use of a weighted-impulse criterion for estimating injury hazard. Research Laboratories, General Motors Corp.

Gefen, A., Gefen, N., Zhu, Q., Raghupathi, R., & Margulies, S.S. (2003). Age-dependent changes in material properties of the brain and braincase of the rat. *Journal of Neurotrauma*, 20, 1163-1177.

George, D. & Mallery, P. (2006). SPSS for Windows Step-by-Step: A Simple Guide and reference, 14.0 update (7th Edition). Allyn & Bacon Publisher.

Gillette, M.L., Neidig, H.A., Spencer, J.N.(1999). Determining density. Chemical Education Resources, Inc. Pennsylvania, USA.

Goldsmith, W. & Plunkett, J. (2004). A biomechanical analysis of the causes of traumatic brain injury in infants and children. The American Journal of Forensic Medicine and Pathology, 25, 89-100.

Gordon, K.E., Dooley, J.M., & Wood, E.P. (2006). Descriptive epidemiology of concussion. *Pediatric Neurology*, 34, 376-378.

Heh, S. & Stadnik, A.G. (1997). Discussion of special provisions for helmets for children ages 1-5, Test headform mass and peak-g. Consumer Product Safety Commission, Memorandum.

Hibberler, R.C. (1991). Mechanics of Materials. Section 3.3 Stress-strain behaviour of ductile and brittle materials. Macmillan Publishing Company, New York, USA.

Hoshizaki, T.B. & Brien, S.E. (2004). The science and design of head protection in sport. *Neurosurgery*, 55, 956-967.

Hui, S.K. & Yu, T.X. (2002). Modeling of the effectiveness of bicycle helmets under impact. *International Journal of Mechanical Sciences*, 44, 1081-1100.

International Organization for Standardization, (ISO) 3386/1. Polymeric materials, cellular flexible – Determination of stress-strain characteristic in compression – Part 1: Low-density materials. Switzerland, 1986.

Instron (2007). Instron Bluehill Calculations Reference, Reference Manual – Software, Revision A M12-15346-EN, (Help V 2.5).

Instron (1997). 5560 Series Table Model Testing Systems. Available online at http://www.instron.us/wa/products/universal_material/5560.aspx (Accessed 15 January 2008).

ISO TC 83/SC 5N (2006). Working Draft ISO/EN 10256 Head and face protection for use in ice hockey. Standards Council of Canada, Ottawa, Canada.

ISO 3386/1, (1986). Polymeric materials, cellular flexible – Determination of stress-strain characteristic in compression – Part 1: Low-density materials. UDC 687-405.8:620.173.

Ivarsson, J., Viano, D.C., Lövsund, & Parnaik, Y. (2003). Head kinematics in mini-sled tests of foam padding: Relevance of linear responses from free motion headform (FMH) testing to head angular responses. *Journal of Biomechanical Engineering*, 125, 523-532.

Johnson, E.A.C. & Young, P.G. (2005). On the use of a patient-specific rapid prototyped model to simulate the response of the human head to impact and comparison with analytical and finite element models. *Journal of Biomechanics*, 38, 39-45.

King A.I., Ruan, J.S., Zhou, C., Hardy, W.N., & Khalil, T.B. (1995). Recent advances in biomechanics of head injury research. *Journal of Neurotrauma*, 12, 651–58.

Kleiven, S. & Holst, H.V. (2002). Consequences of head size following trauma to the human head. *Journal of Biomechanics*, 35, 153-160.

Landro, L.D., Sala, G., & Olivieri, D. (2002). Deformation mechanisms and energy absorption of polystyrene foam for protective helmets. *Polymer Testing*, 21, 217-228.

Liu, D., Chang, C.Y., Chin-Ming, F. & Shu-Lin, H. (2003). Influence of environmental factors on energy absorption degradation of polystyrene foam in protective helmets. *Engineering Failure Analysis*, *10*, 581-591.

Manal, K. & Rose, W. (2003). A general solution for the time delay introduced by a low-pass Butterworth digital filter: An application to musculoskeletal modeling. *Journal of Biomechanics*, 40, 678 – 681.

Martin, R.B., Liptai, L., Yerby, S., Williams, K.R. (1994). The relationship between mass and acceleration for impacts on padded surfaces. *Journal of Biomechanics*, 27, 361-364.

McHenry, B.G. (2004). Head injury criterion and the ATB. Presented at the 2004 ATB Users' Conference. McHenry Software, Inc.

McIntosh, A., & McCrory, P. (2000). Impact energy attenuation performance of football headgear. *British Journal of Sports Medicine*, 34, 337-341.

McIntosh, A., McCrory, P., & Finch, C.F. (2006). Performance enhanced headgear: a scientific approach to the development of protective headgear. *British Journal of Sports Medicine*, 38, 46-49.

Mills, N.J. & Gilchrist, A. (1991). The effectiveness of foams in bicycle and motorcycle helmets. *Accident Analysis and Prevention*, 23, 153-165.

Mills, N.J. & Gilchrist, A. (2003). Reassessing bicycle helmet impact protection. 2003 International IRCOBI Conference on the biomechanics of impacts, 1-12.

Model 203B ICP. Dynamic Force Sensor Installation and Operating Manual. PCB Piezotronics Force/Torque Division. PCB Piezotronics, Inc. New York, USA.

Model 484B Dual Mode ICP Power Unit. Dynamic Force Sensor Installation and Operating Manual. PCB Piezotronics Line Powered ICP Sensor Signal Conditioner. PCB Piezotronics, Inc. New York, USA.

Model 354M37 ICP Accelerometer Installation and Operating manual. PCB Piezotronics sensors for acceleration, shock, vibration, dynamic strain, impact hammers, piezoelectric actuators. PCB Piezotronics, Inc. New York, USA.

Model 394C06. Hand-Held Shaker Installation and Operation Manual. PCB Piezotronics Vibration Division. PCB Piezotronics, Inc. New York, USA.

Myers, B. (1997). An evaluation of a helmet standard for children. Report to the U.S. Consumer Product Safety Commission.

Myers, B.S. & Nightingale, R.W. (1997). The dynamics of head and neck impact and its role in injury prevention and the complex clinical presentation of cervical spine injury. *Proceedings of the 1997 International IRCOBI Conference on the Biomechanics of Impact*, 15-33.

Newman, J. (2006). A proposal for ASTM F08-53's consideration – A new severity index NSI for helmet impact assessment. NBEC, Edmonton, Canada, 1-9.

Newman, J.A., Beusenberg, M.C., Shewchenko, N., Withnall, C., & Fournier, E. (2004). Verification of biomechanical methods employed in a comprehensive study of mild traumatic brain injury and the effectiveness of American football helmets. *Journal of Biomechanics*, 38, 1469-1481.

Noakes, T.D. (1995). Fatal cycling injuries. *Sports Medicine*, 20, 348-362.

NOCSAE 001-06m07 (2007). National Operating Committee on Standards for Athletic Equipment (2006). Standard drop test method and equipment used in evaluating the performance characteristics of protective headgear. *NOCSAE DOC (ND) 001-06m07.*

NOCSAE 002-98m05 (2005). National Operating Committee on Standards for Athletic Equipment (2006). Standard performance specification for newly manufactured football helmets. *NOCSAE DOC (ND) 002-98m05.*

Ommaya, A.K., Goldsmith, W., & Thibault, L. (2002). Biomechanics and neuropathology of adult and paediatric head injury. *British Journal of Neurosurgery,* 16, 220-242.

Patel, D.R., Shivdasani, V., & Baker, R.J. (2005). Management of sport-related concussion in young athletes. *Sports Medicine*, 35, 671-684.

Post, A. (2006). Chamber research protocol. Ottawa: School of Human Kinetics, University of Ottawa.

Queen, R.M., Weinhold, P.S., Kirkendall, D.T., & Yu, B. (2003). Theoretical study of the effect of ball properties on impact force in soccer heading. Medicine & Science in Sports & Exercise, 35 (12), 2069-2076.

Rensselaer Polytechnic Institute (2005). Bike Safety. Retrieved May 20th, 2007 from http://www.rpi.edu/dept/public_safety/safety/bike.html.

Robertson, D.G.E. (2007). BioProc2 Data Processing System. Version 2.39. Retrieved October 13th, 2007 from http://www.health.uottawa.ca/biomech/csb/software/bioproc2.htm.

Robertson, D.G.E., Caldwell, G.E., Hamill, J., Kamen, G., & Whittlesey, S.N. (2004). *Research methods in biomechanics*. Champaign Il: Human Kinetics.

Roylance, D. (2001). Stress-strain curves. Department of Materials Science and Engineering Massachusetts Institute of Technology, Cambridge, MA.

Shulmeister, V., Van der Burge M.W.D., Van der Giessen, E., & Marissen, R. (1998). A numerical study of large deformations of low-density elastomeric open-cell foams. *Mechanics of Materials*, 30, 125-140.

Snell Memorial Foundation (2000). 1995 Standard for Protective Equipment, 1998 Revision. For use in Bicycling. North Highlands, CA.

Snell Memorial Foundation M2010 (2007). Draft 2010 standard for protective headgear. For use with motorcycles and other motorized vehicles. Special Note to Helmet Users. Retreived May 16, 2008 from http://www.smf.org/standards/m/2010/m2010_final.htm.

Snyder, R.G. (1976). Human Impact Tolerance. Highway Safety Research Institute, The University of Michigan.

Song, B., Chen, W.W., Dou, S., Winfree., N.A., & Kang, J.H. (2005). Strain-rate effects on elastic and early cell-collapse responses of a polystyrene foam. *International Journal of Impact Engineering,* 31, 509-521.

Stevenson, T.A. (1998). Consumer Product Safety Commission, 16 CFR Part 1203, Safety Standard for Bicycle Helmets: Final Rule. *Federal Register Part II*, 63, 1-37.

Subhash, G., Liu, Q., & Gao, X.L. (2006). Quasistatic and high strain rate uniaxial compressive response of polymeric structural foams. *International Journal of Impact Engineering*, 32, 1113-1126.

Thom, D.R., (2007). Comparison tests of motorcycle helmets qualified to international standards. *Collision and Injury Dynamics*. California, USA.

Todd, B.A., Smith, S.L., Vongpaseuth, T. (1998). Polyurethane foams: Effects of specimen size when determining cushioning stiffness. *Journal of Rehabilitation Research and Development*, 35, 219-224.

Towner, E., Dowswell, T., Burkes, M., Dickinson, H., John, T., & Hayes, M. (2006). Bicycle helmets: review of effectiveness (No.30). Bicycle helmet standards. Retrieved January 30th, 2007 from http://www.dft.gov.uk/pgr/roadsafety/research/rsrr/theme1 /bicyclehelmetsreviewofeffect4726?page=6#1013.

Townsend, B. (2002). The physics of car collisions, how they work and how to avoid them. Effects of Collisions on People. Retrieved May 15th, 2007 from http://ffden-2.phys.uaf.edu/211_fall2002.web.dir/Ben_Townsend/Collisionsandpeople.htm.

Viot, P., Beani, F., & Lataillade, J.L. (2005). Polymeric foam behavior under dynamic compressive loading. *Journal of Materials Science*, 40, 5829-5837.

Yu-Hallada, L.C., Kuczynski, E., & Weierstall, M. (1998). Polyurethane: The material of choice for occupant protection and energy management. *Journal of Cellular Plastic*, 34, 272-287.

Zhang, J., Kikuchi, N., Li, V., Yees, A., & Nusholtz, G. (1998). Constitutive modeling of polymeric foam material subjected to dynamic crash loading. *International Journal of Engineering*, 21, 369-386.

Zhang, L., Yang, K., King, A. (2004). A proposed injury threshold for mild traumatic brain injury. *Journal of Biomechanical Engineering*, 126, 226-236.

APPENDIX

APPENDIX A: EQUIPMENT

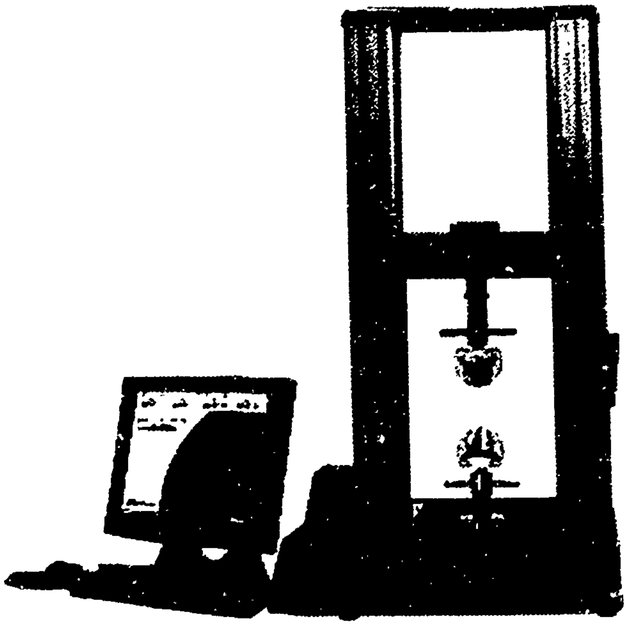

Figure 38 Instron 5560 Series material testing machine used to test compressive characteristics of foam samples (Instron, 1997).

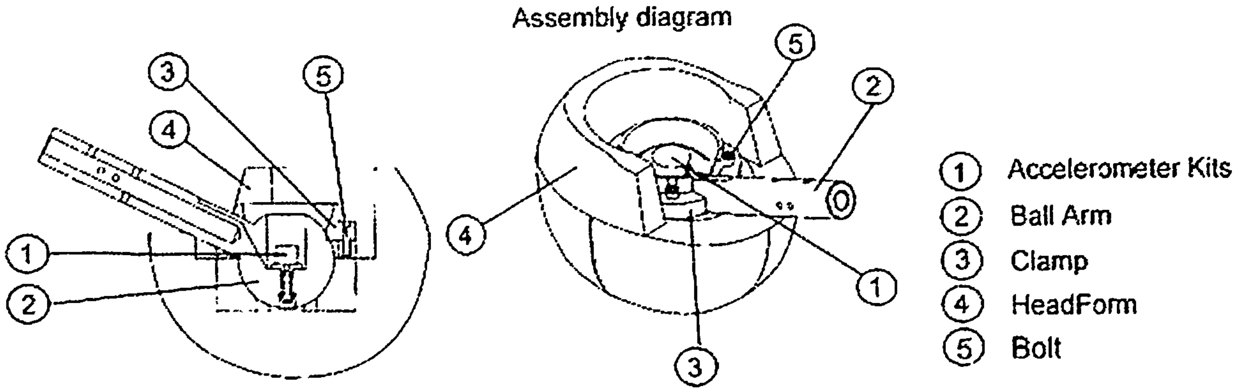

Figure 39 The Half Magnesium K1Aa showing the accelerometer location, ball arm, clamp, and attachment bolts (Cadex, 2006a).

APPENDIX B: MATERIAL SPECIFICATIONS

Table 24 The final density report provided by Polymos for each sheet of EPS molded.

EPS

PPX number	Thickness (in")	Material	Material Grade	Final density (pcf)	2" diam. Discs.
74	1	EPS	S7354	3.92	No
75	1	EPS	S7354	3.93	No
76	1	EPS	S7354	3.98	Yes
77	1	EPS	S7354	3.99	Yes
78	1	EPS	S7354	4.00	Yes
79	1	EPS	S7354	4.02	Yes
80	1	EPS	S7354	4.02	Yes
81	1	EPS	S7354	3.81	Yes
82	1	EPS	S7354	3.86	Yes
83	1	EPS	S7354	3.87	Yes
84	1	EPS	S7354	3.88	Yes
86	1	EPS	S7354	5.14	No
87	1	EPS	S7354	5.12	No
88	1	EPS	S7354	5.09	Yes
89	1	EPS	S7354	5.18	Yes
90	1	EPS	S7354	5.26	Yes
91	1	EPS	S7354	5.21	Yes
92	1	EPS	S7354	5.23	Yes
93	1	EPS	S7354	5.25	Yes
94	1	EPS	S7354	5.32	Yes
95	1	EPS	S7354	5.22	Yes
96	1	EPS	S7354	5.27	Yes
98	1	EPS	S7354	6.06	No
99	1	EPS	S7354	6.20	No
100	1	EPS	S7354	6.19	Yes
101	1	EPS	S7354	6.18	Yes
102	1	EPS	S7354	6.23	Yes
103	1	EPS	S7354	6.21	Yes
104	1	EPS	S7354	6.23	Yes
105	1	EPS	S7354	6.26	Yes
106	1	EPS	S7354	6.25	Yes
107	1	EPS	S7354	6.32	Yes
108	1	EPS	S7354	6.35	Yes

Table 25 The final density report provided by Polymos for each sheet of EPP molded.

EPP

PPX number	Thickness (in")	Material	Material Grade	Final density (pcf)	2" diam. Discs.
2	1	EPP	5615	2.71	No
3	1	EPP	5615	2.71	No
4	1	EPP	5615	2.73	Yes
5	1	EPP	5615	2.81	Yes
6	1	EPP	5615	2.85	Yes
7	1	EPP	5615	2.85	Yes
8	1	EPP	5615	2.88	Yes
9	1	EPP	5615	2.88	Yes
10	1	EPP	5615	2.89	Yes
11	1	EPP	5615	2.58	Yes
12	1	EPP	5615	2.71	Yes
26	1	EPP	5637	5.75	No
27	1	EPP	5637	5.71	No
28	1	EPP	5637	5.66	Yes
29	1	EPP	5637	5.67	Yes
30	1	EPP	5637	5.69	Yes
31	1	EPP	5637	5.64	Yes
32	1	EPP	5637	5.57	Yes
33	1	EPP	5637	5.64	Yes
34	1	EPP	5637	5.71	Yes
35	1	EPP	5637	5.68	Yes
36	1	EPP	5637	5.65	Yes
218	1	EPP	5442	7.25	No
219	1	EPP	5442	7.30	No
220	1	EPP	5442	7.29	Yes
221	1	EPP	5442	7.37	Yes
222	1	EPP	5442	7.32	Yes
223	1	EPP	5442	7.34	Yes
224	1	EPP	5442	7.35	Yes
225	1	EPP	5442	7.31	Yes
226	1	EPP	5442	7.33	Yes
227	1	EPP	5442	7.32	Yes
228	1	EPP	5442	7.30	Yes

Table 26 Average thickness and standard deviation (cm) of 20 samples of each material density.

	Average thickness (cm)	Standard Deviation (cm)
EPS 62.95 kg/m^3	2.562	0.0543
EPS 83.46 kg/m^3	2.541	0.0495
EPS 100.12 kg/m^3	2.587	0.0518
VN 602	2.591	0.0129
VN 600	2.588	0.0246
VN 740	2.589	0.0284
EPP 44.53 kg/m^3	2.551	0.0656
EPP 83.94 kg/m^3	2.593	0.0669
EPP 117.09 kg/m^3	2.542	0.0579

APPENDIX C: MATERIAL SPECIFICATIONS

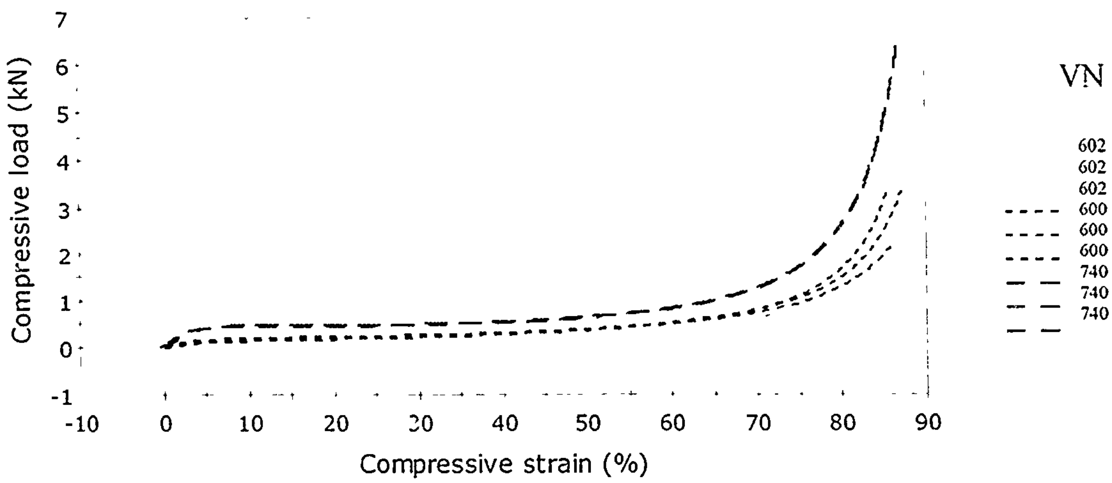

Figure 40 Quasistatic stress (compressive load kN) versus strain (%) results for vinyl nitrile 602, 600, and 740.

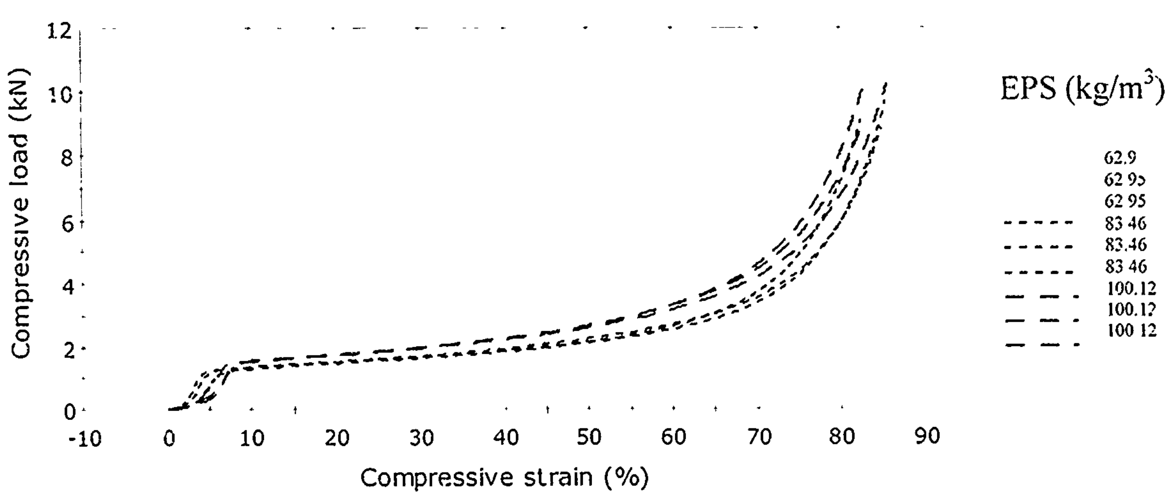

Figure 41 Quasistatic stress (compressive load kN) versus strain (%) results for expanded polystyrene 62.95, 83.46, 100.12 kg/m^3.

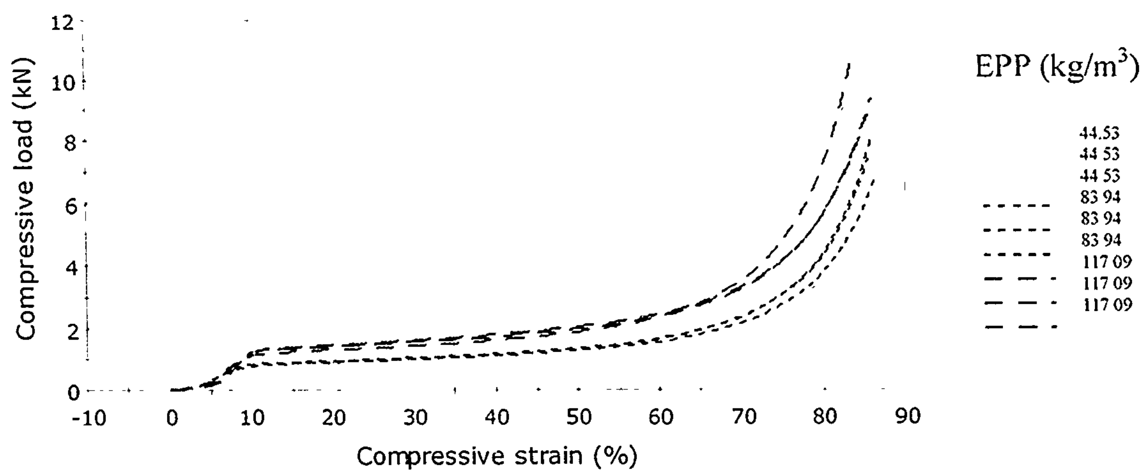

Figure 42 Quasistatic stress (compressive load kN) versus strain (%) results for expanded polypropy .ene 44.53, 83.94, 117.09 kg/m^3.